APPLICATIONS OF NEW PULSE NMR TECHNIQUES IN CHEMISTRY: TWO-DIMENSIONAL NMR SPECTROSCOPY

by

SUBRAMANIAM SUKUMAR

B.Sc. (Hons.), University of Ceylon, Colombo, Sri-Lanka, 1975

M.Sc., Dalhousie University, Halifax, Canada, 1977

THESIS SUBMITTED IN PARTIAL FULFILMENT OF

THE REQUIREMENTS FOR THE DEGREE OF

DOCTOR OF PHILOSOPHY

in

THE FACULTY OF GRADUATE STUDIES

(Department of Chemistry)

We accept this thesis as conforming
to the required standard

THE UNIVERSITY OF BRITISH COLUMBIA

February, 1981

In presenting this thesis in partial fulfilment of the requirements for an advanced degree at the University of British Columbia, I agree that the Library shall make it freely available for reference and study. I further agree that permission for extensive copying of this thesis for scholarly purposes may be granted by the head of my department or by his or her representatives. It is understood that copying or publication of this thesis for financial gain shall not be allowed without my written permission.

Department of CHEMISTRY

The University of British Columbia
2075 Wesbrook Place
Vancouver, Canada
V6T 1W5

Date 19th, February, 1981.

ABSTRACT

The potential of three recently developed techniques, proton 2D J-. ^{13}C- ^{1}H chemical shift correlation- and proton zero-quantum transition (ZQT)-spectroscopy, for resolving and assigning complex proton spectra has been evaluated. The main part of this work describes the features of proton 2D J spectroscopy and related experiments and includes discussions on the optimum methods for displaying the spectra and efficient methods for the processing of data. It is shown that phase-sensitive cross-sections offer a convenient and practical method for these purposes. Proton 2D J spectra can also provide effectively the equivalent of broad band homonuclear and heteronuclear decoupling, thus distinguishing between these different scalar couplings.

Assignment techniques based on 2D NMR spectroscopy have many advantages over conventional assignment techniques such as double resonance. Thus, the combination of proton 2D J spectroscopy and ^{13}C- ^{1}H shift correlation spectroscopy is a powerful tool for studying complex molecules.

A preliminary study is described, in which ZQT (2D) spectroscopy is used to assign the proton spectrum of a model compound.

A new method (spin-echo absorption spectroscopy) for obtaining high-resolution absorption mode proton spectra from biological samples is demonstrated, using some model systems, including a preliminary study on red-blood cells. This approach can be incorporated into a new concept, "integrated NMR experiments".

Most of the discussions in this thesis are aimed towards practicing chemists who are interested in the analysis of complex organic molecules and in the efficient methods for performing 2D NMR experiments.

TABLE OF CONTENTS

LIST OF TABLES

LIST OF FIGURES

LIST OF COMPOUNDS

1. α,β-xylose
2. α,cyclodextrin
3. dextran T-10
4. β-methyl xylopyranoside
5. α,β-glucose
6. trideuteriomethyl 2,3,4,6-tetra-O-trideuterioacetyl-α-D-glucopyranoside
7. 2,3,4-tri-O-acetyl-6-deoxy-α-D-glucopyranosyl 3,4,di-O-acetyl-1,6-dideoxy-β-D-fructofuranoside
8. uridine
9. α,β cellobiose
10. 1',4,6,6'-tetrachloro -1',4,6,6'-tetradeoxy-galacto-sucrose tetramesylate
11. furoic acid
12. 5,epi-sisomycin
13. 1,2,3,4,7,7-hexachloro-6-exo-fluoro-bicyclo[2.2.1] hept-2-ene
14. 3,4,6-tri-O-acetyl-2-deoxy-2-fluoro-β-D-glucopyranosyl fluoride
15. 4,4-dideuterio-2-oxo-2-phenoxy-5-phenyl-1,3,2-dioxaphosphorinane
16. diphenyl-1,1,1-trifluoro-isopropyl-phosphate

- diethyl malonate

ACKNOWLEDGEMENTS

It is a pleasure to thank Drs. G. Pouzard and G.A. Morris for many helpful discussions, on various aspects of NMR spectrscopy. The work on ZQT spectroscopy and on red blood cell work was done in collaboration with Dr. G. Pouzard and Mr. R. Snoek respectively, to both of whom I am greatly indebted. The experience and knowledge of Ms. T. Markus, H. Chow and J. Sallos of the Electronics group at the U.B.C. Chemistry department who helped to construct and maintain the spectrometer used in most part of this work is greatly appreciated. My thanks also reach out to the many friends who have contributed to the completion of this thesis, either directly or indirectly, and made by stay in Vancouver so memorable.

Finally, I wish to thank my director, Professor L.D. Hall, for providing an excellent opportunity and encouragement to work in a new area of science, which made the current work so interesting and worthwhile.

CHAPTER I

INTRODUCTION

1.1 Background

Since the original work of Bloch et al. (1-3) and of Purcell et al. (4) in 1946, nuclear magnetic resonance (NMR) spectroscopy has developed and diversified into widely differing fields including physics, chemistry, biology and medicine. Chemists (and some biochemists) generally have been involved in studies of the structural and chemical properties of molecules using high resolution (5,6) and more recently solid state NMR techniques, whereas NMR imaging (7) and "topical magnetic resonance" (TMR) (8) are some of the latest techniques to become available for cell biologists, physiologists and physicians. The rapid progress of NMR spectroscopy in these many different areas can be attributed mainly to the development of multipulse Fourier transform NMR techniques, of magnets which operate at very high ("super-conducting") magnetic fields, and of advances in (mini-)computer technology and the associated data storage systems. As a result, it is now possible to perform routinely rather sophisticated NMR experiments which include both hardware and software operations automated under computer control. In addition to these capabilities the advent of new experimental concepts, such as two-dimensional (2D) NMR spectroscopy (9,10) has provided the chemist, for example, with methods for studying structures of a molecular complexity, which only a few years ago would have been regarded as essentially impossible.[1]

The first commercial high resolution NMR spectra were available around 1956, and prior to 1966 most spectra were obtained in the continuous wave (CW) mode. Much of the early developments and research involved multiple resonance studies of protons and understanding connectivity relationships between the energy levels of spin systems (11). This proved to be a valuable tool for

[1] Some typical examples are considered in Chapters III and IV

assigning spectra but the major limitations in those days were the relatively low sensitivity (signal to noise ratio) of NMR spectroscopy and the complications arising from overlapping signals in proton NMR spectra. Presently, the commercial availability of superconducting magnets which operate at fields equivalent to a resonance frequency of up to 600 MHz for protons have considerably eased both problem of signal overlap and sensitivity.

The development by Cooley and Tukey (12) in 1965 of a fast Fourier transform algorithm, ideal for use with a minicomputer, and the subsequent introduction of pulsed Fourier transform (FT) technique into NMR spectrosocpy by Ernst and Anderson (13) in 1966 has had a substantial impact in chemistry, particularly in organic chemistry. Besides facilitating numerous proton NMR experiments, the increased efficiency of this method has opened many new avenues of research, including studies of low sensitive nuclei such as carbon-13, and of multipulse FTNMR spectroscopy.

The measurement of high resolution NMR spectra using the continuous wave (CW) or "slow-passage" method involves the slow variation of either the frequency or field such that the resonance absorption of radiofrequency (RF) energy by each group of equivalent nuclei is measured individually, to yield the NMR spectrum. In contrast, in the basic pulsed Fourier transform technique a strong radiofrequency pulse is applied such that it excites all nuclei simultaneously. The response, or the free induction decay (FID) signal, which is measured as a function of time, contains all the (resonant) frequency information of the nuclei influenced by the pulse, and can be viewed in frequency space after Fourier transformation. The resulting spectrum is identical to that obtained by the CW method and represents a plot of signal intensity versus frequency.

In view of the importance of the pulsed FT technique, both to NMR spectroscopy in general and to the work of this thesis in particular, a brief discussion of this method is given in the next section. This will familiarize the reader with the basic concepts and nomenclature used in pulsed FTNMR spectroscopy, which are often referred to in subsequent chapters in the context of spin-echo and 2D Fourier transform spectroscopy. As will be seen there are two different models (the classical magnetization vector model and the quantum mechanical description) which are commonly used to explain FTNMR experiments; these will be briefly reviewed in the next section, mainly from an experimental chemist's point of view, without indulging into mathematical details.

1.2 Pulsed Fourier transform NMR spectroscopy

Pulsed Fourier transform NMR spectroscopy involves study of the responses from suitable magnetic nuclei to pulses of radiofrequency energy. The classical magnetization vector model provides a simple and convenient picture for understanding some of the basic features of these experiments. In this model, the effect of RF pulses on an ensemble of nuclear "spins" which have been subjected to a static magnetic magetic field (B_o) are described in terms of the behaviour of a macroscopic or net magnetization vector $\underset{\sim}{M}$. At equilibrium this can be represented as a vector precessing at a characteristic (Larmor) frequency and aligned along the direction of the field B_o (Fig. 1.1). At equilibrium the x and y components of the magnetization will be effectively zero due to precession of $\underset{\sim}{M}$ about z, but the z component will be finite since its magnitude does not vary with time.

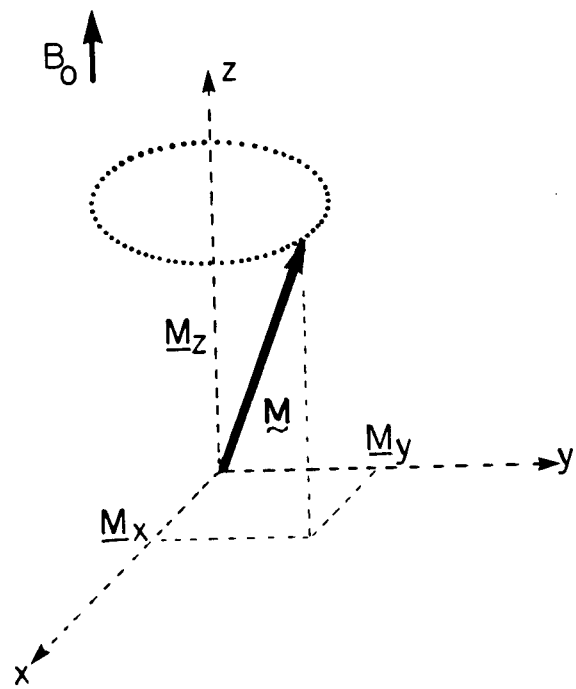

Figure 1.1: The magnetization of a set of equivalent nuclei in a magnetic field B_o are represented by a (macroscopic) vector $\underset{\sim}{M}$ which precesses about z at its characteristic Larmor frequency. At any instant, $\underset{\sim}{M}$ can be represented by its components in the x, y and z directions, indicated by M_x, M_y and M_z respectively.

It is generally more convenient to visualize the behaviour of individual sets of equivalent nuclei in multipulse NMR experiments in terms of their individual magnetization components in a "rotating reference frame". In this model, the x and y coordinates represented in Fig. 1.1 are assumed to be rotating about the z axis at the transmitter frequency of the spectrometer and in the same sense as the nuclear precession. The new coordinates are now defined as x', y' and z', and in this reference frame the applied RF field (usually along the x' direction) appears to be fixed. The effect of an RF pulse on a spin system at equilibrium is to rotate ("flip") the total magnetization vector from its position along z' through an angle α' ($= 2\pi\alpha$), about the direction of the pulse as shown in Figure 1.2A. The flip angle α' is given by

$$\alpha' = \gamma B_1 t_\alpha \text{ (radians)} \qquad [1.1]$$

where γ = gyromagnetic ratio (rad. s^{-1}gauss^{-1}); B_1 = magnetic induction of the RF pulse (gauss); t_α = pulse duration. Given that both γ and B_1 are held constant, and that the NMR receiver system is designed to detect the component of magnetization along the y axis, it follows that the amplitude of the detected signal is a function of the duration of the RF pulse, varying in a sinusoidal fashion. Thus, $\alpha = 90^\circ$ corresponds to the flip of $\underline{M}_z$, onto the +y' direction and corresponds to the maximum observable signal; in contrast, $\alpha = 270^\circ$ leaves $\underline{M}_z$, along the -y' axis and produces a minimum (negative) signal. Zero values correspond to the initial state ($\alpha = 0^\circ$ or 360°) and the "inverted" state ($\alpha = 180^\circ$), when the magnetization lies along the longitudinal axis (Fig. 1.2A).

Although this classical vector model in the rotating reference frame usually suffices for a qualitative understanding of many pulsed NMR

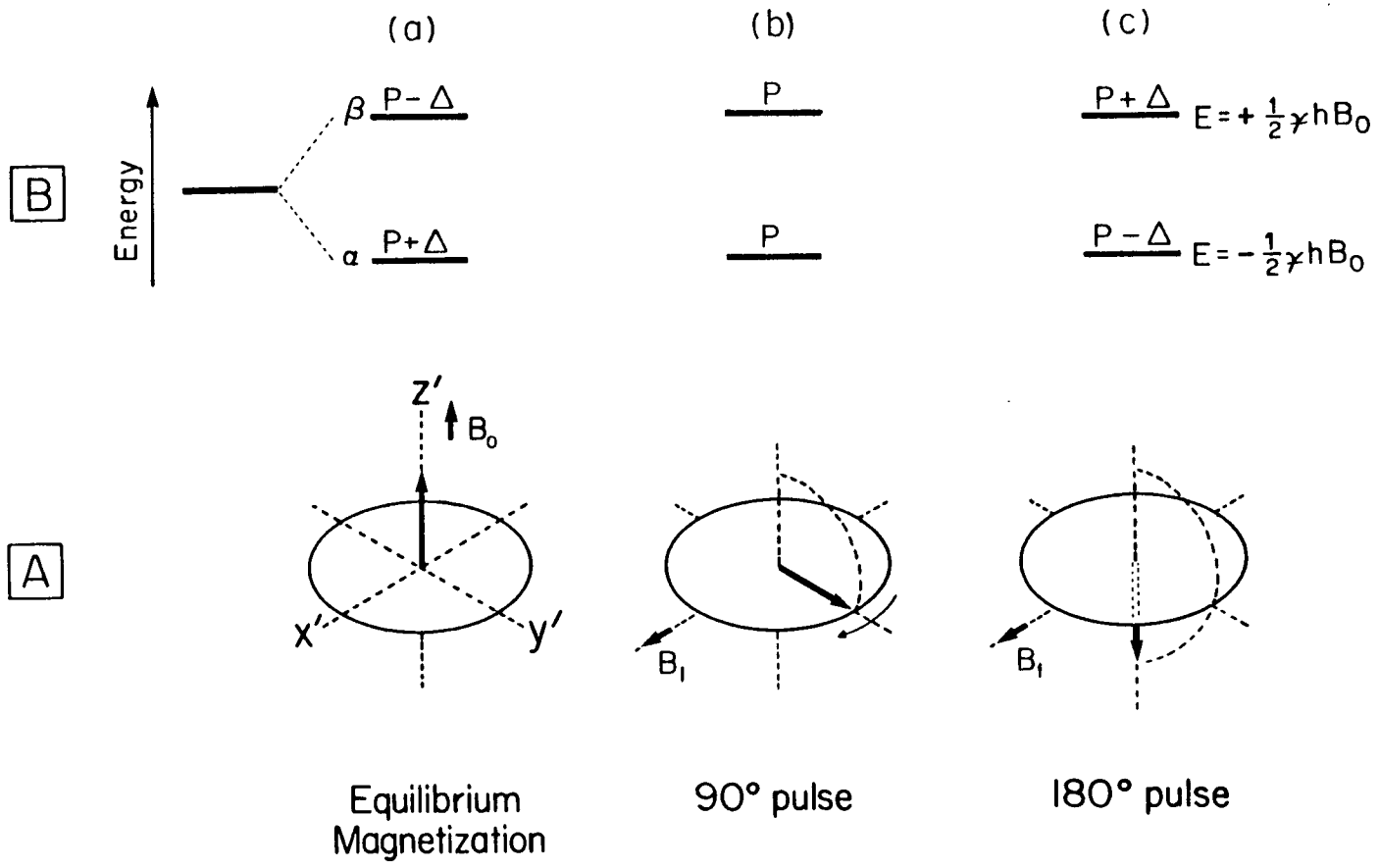

Figure 1.2: (A) The magnetization vector model in the rotating reference frame and (B) the energy level representation, to illustrate the effect of 90° and 180° pulse on a spin 1/2 system ΔP represents the spin population difference between the two levels. $\nu = \gamma/2\pi$

experiments from an application chemist's point of view, it is inadequate for a more detailed understanding of, for example, spectral analysis or time dependent phenomena, for which purposes the quantum mechanical model is used. In this latter model, each magnetic nucleus is considered to be associated with discrete energy levels. For example, a spin ½ nucleus (such as ^{1}H or ^{13}C) in a magnetic field is represented by two energy levels, which correspond effectively to the direction of the nuclear moment being oriented "parallel" or "anti-parallel" to the magnetic field; these are generally referred to as the α- and β-states respectively (Fig. 1.2B). The energies of these states are given by

$$E = \frac{-1}{2\pi}\gamma h m B_o \qquad [1.2]$$

where h = Planck's constant (erg. s) and m = $\pm$½, corresponding to the α- and β-states respectively. The energy difference between the levels is therefore,

$$\Delta E = \frac{1}{2\pi}\gamma h B_o \qquad [1.3]$$

In accordance with Planck's law, absor tion (or resonance) is established by providing the system an RF energy equal to,

$$\Delta E = h\nu_o = \frac{1}{2\pi}\gamma h B_o \qquad [1.4]$$

hence,

$$\nu_o = \frac{1}{2\pi}\gamma B_o \qquad [1.6]$$

Equation [1.6] refers to the resonance condition and corresponds to the resonance frequency or Larmor precession frequency.

For an ensemble of equivalent nuclei, the "spins" are distributed between the energy levels according to Boltzmann's law; the spin population ratio between the lower (n_l) and upper (n_u) level is given by[1]

$$\frac{n_l}{n_u} = \exp\left[\frac{2\Delta E}{kT}\right] \simeq 1 + \frac{2\Delta E}{kT} \qquad [1.7]$$

k = Boltzmann's constant (erg deg.$^{-1}$)

The maximum observable magnetization or NMR signal intensity will be proportional to the excess spin population $2\Delta P$ in Figure 1.2B.

Two equivalent, but rather simple models were presented above; the classical vector model is associated with the effect of magnetizations in the rotating reference frame and the simple quantum mechanical model is associated with spins, and their distribution or transitions within the energy levels. The various features involved in pulsed NMR are now explained in terms of both these models.

A 90^{o} pulse equalizes the spin population between two levels ("saturation") corresponding to an optimum absorption of energy and hence a maximum signal intensity. A 180^{o} pulse, on the other hand, reverses the equilibrium Boltzmann distribution (a transformation which is referred to as going to a negative spin-temperature); in the rotating frame, a 90^{o} pulse represents a transfer of the total magnetization onto the y' plane, hence corresponds to a maximum signal; in contrast, the 180^{o} pulse transfers the M_z, magnetization onto the -z' direction and therefore does not induce an NMR signal in the receiver coil (cf. Figs. 1.2A and B).

Excitation causes a non-equilibrium state by altering the Boltzmann distribution from which the spins can return to their equilibrium value by exchanging energy with their surroundings (the lattice) via first-order process

[1] $2\Delta E$ is usually much smaller than kT at ordinary temperatures

of spin-lattice relaxation, characterised by the spin-lattice relaxation time, T_1 ($=1/R_1$, where R_1 refers to the relaxation rate).

In the vector model the spin-lattice relaxation process is depicted as the return to equilibrium of the longitudinal component of the magnetization; hence it is often referred to as longitudinal relaxation.

In contrast, another relaxation process which involves the exchange of energy between two opposite spin states with no loss of total energy of the system is referred to as spin-spin relaxation. In the vector model this can be visualized as a loss of phase coherence of the individual components of the transverse magnetization; hence it is referred to as transverse relaxation. Spin-spin relaxation time ($T_2 = 1/R_2$) determines the line widths of the resonances in an NMR spectrum whereas spin-lattice relaxation governs their intensities.[1]

So far the phenomena of excitation and relaxation were considered using two simplified models. Unlike most other forms of spectroscopy (in which resonance or absorption of energy is studied as a function of frequency), the observed NMR signal is a time evolution signal which for the current purposes is discussed in terms of the vector model.[2] A transverse magnetization component caused by excitation of the nuclei can be represented in the rotating frame as precessing at a frequency ν_o, which is the frequency difference (offset frequency) with respect to that of the transmitter or "carrier" (see sec. 2.1). The receiver coil of the spectrometer is designed to

[1]After excitation (by a 90° pulse), a sufficient relaxation delay (ca. $5T_1$) must be allowed for the system to return to thermal equilibrium, prior to repeating a pulse sequence.

[2]The quantum mechanical model using the density matrix approach will be given in Ch. V.

measure the induced voltage arising from this transverse magnetization. In single phase detection (SPD) spectrometers the y' component of the magnetization ($M_{y'}$) is detected following a pulse which is applied along the x' direction. It is also possible to detect $M_{x'}$ and $M_{y'}$ simultaneously by quadrature phase detection (QPD) which has several merits, including an improvement in sensitivity by a factor of ca. 1.4 over the SPD method.

The amplitudes of the signals detected along the x' and y' directions, $M_{y'}(t)$ and $M_{x'}(t)$, show characteristics of cosine and sine functions respectively.[1] The behaviour of the y' component, which is usually observed in "conventional" (SPD) NMR experiments, can be expressed as,[2]

$$M_{y'}(t) = M_o \sin(\alpha) \cos(2\pi\nu_o t) \exp(-tR_2) \qquad [1.8]$$

where, M_o represents a unit amplitude and the sin α term describes the effect of flip angle on the signal magnitude. The exponential term in the above equation indicates a "damping" of the NMR signal with time due to transverse relaxation.

In practice the detected signal is first digitized so that it can be stored, and subsequently processed in a computer. The conditions for data acquisition are determined by the sampling theorem which states that the highest frequency from the transmitter (in SPD) that can be correctly represented in a spectrum will be half the sampling rate, or Nyquist frequency. All frequency components outside the spectral width (SW) will be

[1]The FID signal in QPD can be regarded as a complex time signal. In this case it is possible to distinguish between positive and negative frequencies with respect to the transmitter.

[2]The signal that is measured in a spectrometer is compared (subtracted) with the reference frequency from the transmitter, hence the frequency term in equation 1.8 is represented by ν_o ($=\nu_t-\nu$), where ν_t = RF carrier frequency.

"folded back" into the spectrum. Since noise is also folded back, to the detriment of the overall signal to noise ratio, it is common practice to use suitable analog filters (to remove the unwanted frequencies) to improve the sensitivity.

The relationships between the various acquisition parameters are given by the following expressions

$$SW = \frac{1}{2(SR)} \qquad [1.9]$$

$$DR = \frac{1}{AT} = \frac{2(SW)}{BS} = \frac{1}{(BS)(DW)} \qquad [1.10]$$

where SR = sampling rate (points s^{-1}); AT = acquisition (sampling) time (s); SW = spectral width (Hz); BS = block size or number of sampling points; DW = dwell time (s); DR = digital resolution.

For a given spectrometer, the bandwidth of the power spectrum of the RF pulse will be inversely proportional to the pulse width (say, t_{90^o}). It is generally desirable to have the maximum excitation bandwidth and hence to use as short a sampling pulse as possible; commonly 90^o pulses of 5-50 μs are used. However selective pulses capable of exciting a single multiplet can be generated by using a lower transmitter power and longer pulse duration (ca. 10-100 ms). One of the advantages of using QPD is that the transmitter can be placed in the centre of the spectrum thus effectively halving the RF power requirements as compared to SPD in which the transmitter is placed at one end of the spectrum.

The digitized time domain signal is usually subjected to a mathematical treatment referred to as "digital filtering"; this is intended either to improve the resolution or the signal to noise ratio of the final spectrum, both of which are interdependent (14).

Fourier transformation of the time domain signal (eq. [1.8]) yields a complex, frequency domain spectrum (10),

$$S(\nu) = \frac{M_o' T_2 \sin\alpha}{1+(2\pi\Delta\nu T_2)^2} - \frac{iM_o' 2\pi\Delta\nu T_2^2 \sin\alpha}{1+(2\pi\Delta\nu T_2)^2} \qquad [1.11]$$

$$= a - d$$

where $\Delta\nu = \nu - \nu_o$. The real (a) and imaginary (d) parts correspond to the Lorentzian-absorption and -dispersion mode signals respectively.

In practice, however, instrumental factors such as receiver "dead time"[1] and analog filters introduce an additional phase term in the time-domain signal (eq. [1.8]), hence the resulting frequency-domain spectrum contains a mixture of absorption and dispersion terms. These are easily separated (phase corrected) by user-interactive data manipulation routines to yield the desired absorption mode peaks in the final spectrum.

The effect of pulse width or flip angle on the magnetization vectors was discussed earlier with the aid of equation [1.1] and Figure 1.2. It is also possible to change the phase (ϕ) of the RF pulses and thereby to change the sense of rotation of the magnetization; for example, a 90^o pulse applied along the -y' direction ($\phi = 90^o$) would flip the equilibrium magnetization about -y' onto the x direction. The possibility of using the variables α and ϕ, together with the durations (T) between a series of pulses to manipulate nuclear spins in a wide variety of ways has led to a new area of research, commonly referred to as "multipulse NMR spectroscopy". For many chemists some of the practically useful experiments of this class are high resolution solid state and 2D NMR spectroscopy. With the aid of (mini-)computers, pulse programmers and appropriate hardware devices it is now possible to "custom design" new NMR experiments by introducing these variables (ϕ, α and T) in a

[1] A delay ($\simeq$DW) prior to sampling, in order to minimize interference from the RF pulse.

multiple sequence. Such experiments can provide interesting molecular information, for example, regarding chemical structure and conformation, exchange phenomena and motional properties, etc. Recently the novel concept of double Fourier transformation has been introduced to NMR spectroscopy; as we shall see this results in an NMR spectrum which is displayed in two frequency dimensions and provides an elegant method for resolving and assigning complex spectra.

1.3 The concept of two-dimensional spectroscopy

The two-pulse inversion recovery sequence T1IR is one of the well known multipulse sequences used for the measurement of spin-lattice relaxation rates (R_1). This sequence may be represented as

$$\{180^\circ - T - 90^\circ - \text{Acquisition}\}$$

where T is a variable delay; 180° and 90° refer to the flip angle of the two pulses. The signals acquired for various delays T, may be presented, after Fourier transformation in a two-dimensional display as shown in Figure 1.3, which represents the exponential recovery back to thermal equilibrium of the magnetization vectors (or spins), which have been inverted by the 180° pulse, as a function of time T. These exponential rate constants are a direct measure of the respective R_1-values of the signals.

Let us now consider another two pulse sequence, the Carr-Purcell pulse sequence (T2CP; (15)), which is used for the measurement of spin-spin relaxation rates (R_2), represented by,

$$\{90^\circ - T - 180^\circ - T - \text{Acquisition}\}$$

As before, the observed magnetization (corresponding to a single trace in Fig. 1.3) is a function of two time variables (a "fixed" variable T and a running

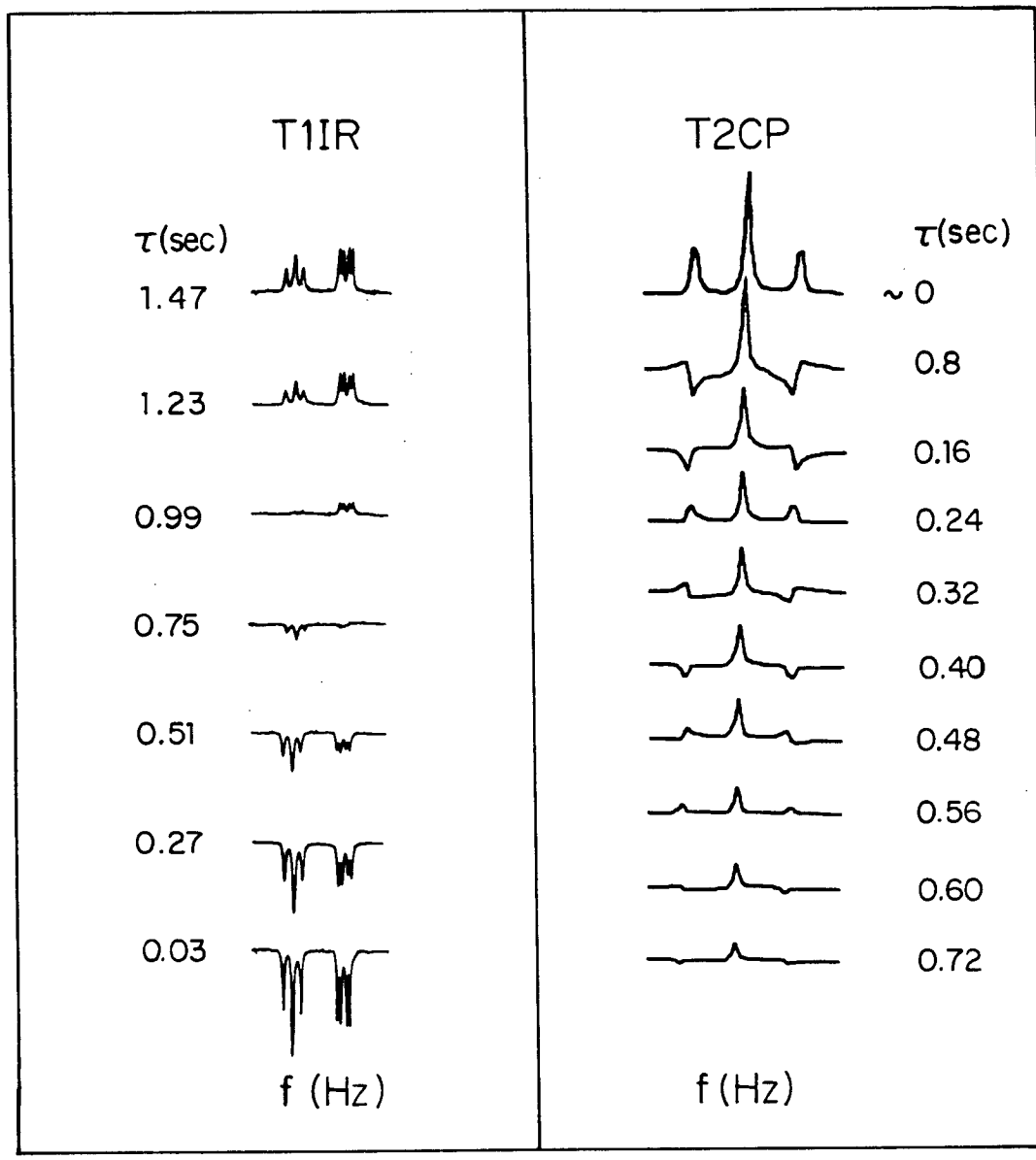

Figure 1.3: Spectra obtained from the spin-lattice, inversion recovery (T1IR) pulse sequence and the Carr-Purcell method for T_2 measurement (T2CP). The T1IR spectra show the negative (inverted) signals returning to their equilibrium values as a result of spin-lattice relaxation. The T2CP spectra represent the exponential decay of the signal amplitude (which is more clearly indicated by the unmodulated central peak) together with the phase modulation of the outer lines of the triplet as a function of τ.

variable from 0 to AT). However, in contrast to the T1IR experiment in which the signals show a simple exponential recovery from a negative to a positive signal, the spectra obtained from the T2CP experiment show, in addition to their exponential decay due to spin-spin relaxation, a phase modulation of the signals as a function of T. This modulation frequency is related to the spin-spin coupling constant and a detailed discussion follows in the next chapter.

It is also possible to design experiments such that the observed signals are amplitude and/or phase modulated with time (t_1), at some correlated frequencies. If these data arrays are subjected to a second Fourier transformation, with respect to t_1, this reveals the frequency components corresponding to the amplitude or phase modulations in a second dimension. The resulting signal matrix is referred to as a two-dimensional spectrum, and is equivalent to a conventional spectrum "resolved" in two frequency domains. More detailed discussions of the various aspects of these experiments will be presented in the following chapters.

1.4 Organisation of this thesis

The discussion in this thesis, for most part, are directed towards the application of proton NMR as an analytical tool in chemistry.[1] Chapter II of this thesis is concerned with the FT equivalent of the basic spin-echo experiment of Carr-Purcell (method A), and with a simple modification of the data processing routine (spin-echo absorption spectroscopy) which has several useful applications in chemistry and biology. The description of the effect

[1]The general discussions of the various multipulsed experiments apply only to weakly coupled systems.

of pulses on the spin system is also applicable to 2D J resolved NMR experiments which constitutes the principal emphasis of Chapters III and IV although other 2D techniques are also included.

Chapter V describes in detail the application of a zero quantum transition (ZQT), two-dimensional NMR experiment in chemistry; as will be seen, neither the vector model nor the simple quantum mechanical description introduced earlier are sufficient to explain all the features of the ZQT experiment, and the density matrix approach (16) is introduced in that chapter.

The reader will note that most of the chemical systems used in this thesis to illustrate the potential of the various experiments involve carbohydrates. The proton NMR spectra of these molecules are generally rather complicated mainly due to the presence of anomeric mixtures in aqueous solution and the extreme overlap of the resonances. Such spectra pose a serious challenge for chemists attempting to study these systems by conventional techniques. It is also worthwhile noting at this juncture that the first demonstration that NMR parameters exhibit chemically useful stereospecific dependencies was made on carbohydrates by Lemieux et al. (17,18) in 1958. In a more contemporary context, the numerous, important roles of carbohydrates in areas ranging from chemistry to biology and medicine, provide a compelling need for the exploration of new sources of structural information.

References (Chapter I)

1. Bloch, F., Hansen, W.W., Packard, M. Phys. Rev. (1946) 69, 127.

2. Bloch, F. Phys. Rev. (1946) 70, 460.

3. Bloch, F., Hansen, W.W., Packard, M. Phys. Rev. (1946) 70, 474.

4. Purcell, E.M., Torrey, H.C., Pound, R.V. Phys. Rev. (1946) 69, 37.

5. Shaw, D. "Fourier Transform NMR Spectroscopy", Elsevier: Amsterdam, 1976.

6. Martin, M.L., Martin, G.J., Delpuech, J.J. "Practical NMR Spectroscopy:, Heyden: London, 1980.

7. "Nuclear magnetic resonance of intact biological systems". Phil. Trans. R. Soc. Lond. B (1980) 289, 379, and references therein.

8. Gordon, R.E., Hanley, P.E., Shaw, D., Gadian, D.G., Radda, G.K., Styles, P., Chan, L. Nature (1980), to be published.

9. Aue, W.P., Bartholdi, E., Ernst, R.R. J. Chem. Phys. (1976) 64, 2229.

10. Freeman, R., Morris, G.A. Bul. Magn. Reson. (1980) 1, 5.

11. Hoffman, R.A., Forsen, S. "Progress in NMR Spectroscopy:, Emsley, J.W., Feeney, J., Sutcliff, L.H. Eds.; Pergamon Press: Oxford, 1966; Vol. 1, Chapter 2.

12. Cooley, J.W., Tukey, J.W. Math. Comput. (1965) 19, 297.

13. Ernst, R.R., Anderson, W.A. Rev. Sci. Instrum. (1966) 271, 93.

14. Ernst, R.R. "Advances in Magnetic Resonance", Waugh, J.S., Ed.; Academic Press: New York, 1966; Vol. 2, Chapter 2.

15. Carr, H.Y., Purcell, E.M. Phys. Rev. (1954) 94, 630.

16. Slichter, C.P. "Principles of Magnetic Resonance", 2nd ed., Springer-Verlag: Berlin, 1978.

17. Lemieux, R.U., Kullnig, R.K., Moir, R.Y. J. Am. Chem. Soc. (1958) 80, 223.

18. Lemieux, R.U., Kullnig, R.K., Bernstein, H.J., Schneider, W.G. J. Am. Chem. Soc. (1958) 80, 6098.

CHAPTER II

SPIN-ECHO FOURIER TRANSFORM SPECTROSCOPY

2.1 History

Hahn and Maxwell (1,2) in 1950 were the first to demonstrate that the decay of the NMR signal in the transverse plane, due to instrumental effects such as inhomogeneity of the magnetic field, can be reversed by the application two 90^{o} pulses to the spin system. The rejuvenation (refocussing) of the NMR signal after a time T (which was equal to the spacing between the two pulses) was refered to as spin-echo formation. Two practically useful pulse sequences were later published by Carr and Purcell (3) in 1954, which were initially used to measure spin-spin relaxation rates (R_2-values) and translational diffusion coefficients using the time domain NMR signals. The basic Carr-Purcell (C-P) pulse sequence differs from that of Hahn in that the second pulse is a 180^{o} pulse. The potential of the C-P experiment in chemical studies was not realized until the FT technique was introduced to NMR spectroscopy (4). In 1970, Allerhand and Cochran (5) published a Fourier transformed spectrum from a C-P pulse sequence, and the method was appropriately referred to as spin-echo Fourier transform (SEFT) spectroscopy. As a result it became possible to study the behaviour of the time domain signals in a spin-echo experiment in frequency space; obviously this makes the experiment suitable for the study of multi-line spectra.

It became apparent that for studies using multipulse sequences, imperfections in pulse flip angles could lead to cumulative errors and result in undesirable consequences particularly for quantitative experiments (6). The various phase-shifted pulse sequences suggested by Meiboom *et al.* (6) and by Freeman *et al.* (7) represent important examples of how some pulse imperfections can be corrected by including appropriate phase-shifts in a multipulse sequence.

One of the remaining limitations to the general application of the spin-echo pulse sequence in high resolution proton NMR spectroscopy to, for example, spin-spin relaxation time measurements or chemical exchange studies, is the phase modulation of the signals which arises as a result of homonuclear spin-spin coupling. Various methods have been suggested to overcome this problem and to obtain the desired high resolution absorption spectra, but these have generally been restricted in the range of molecules or spectra (7-11) to which they can be applied and as a result spin-echo techniques have not been widely applied to "chemical" systems. Its potential in biology was realized by Campbell et al. (12) who demonstrated that the sharp signals of a biomolecule associated with the slowly relaxing nuclei could be selectively studied by suppressing the broad (rapidly relaxing) peaks by SEFT spectroscopy. Later the same principle was used to study small molecules which are involved in the different metabolic pathways in live red blood cells (13). Even though the SEFT spectra obtained suffer the phase and intensity problem mentioned earlier, it provided a convenient method to "see" within the broad envelope which is characteristic of the NMR spectra of most macromolecules.

Bax et al. (11) have suggested a method, based on a Fourier transformation of the whole-echo signal, which eliminates the phase problem in spin-echo experiments. In its original form the above technique appears to be suitable only for molecules with long spin-spin relaxation rates and narrow spectral widths. However, a convenient procedure is described in this thesis whereby spin-echo absorption spectroscopy (SEAS) can be used for studying complex systems. The potential use of this method, is discussed in Sections 2.5 and 2.6.

2.2 The spin-echo pulse sequence

The basic Carr-Purcell (method A) pulse sequence includes a 90^{o} and a 180^{o} pulse separated by a delay T, followed by signal acquisition which usually commences after an equal delay T. The behaviour of the NMR signal (echo-formation) is illustrated in Figure 2.1. Fourier transformation of the (second) half-echo-signal will produce a frequency spectrum in which the phases of the peaks are modulated as a function of time T (due to spin-spin coupling when pulses are applied non-selectively). The decay of the magnitude of the peak with time (2T) will be due to the combined effects of spin-spin relaxation and diffusion of the spins in the sample during the delay 2T. The Carr-Purcell method B minimizes diffusion effects by using a series of 180^{o} pulses after an initial 90^{o} excitation pulse; this is represented by

$$\{90^{o} - (T - 180^{o} - T)_{n} - \text{Acquisition}\}$$

In this case study T is kept sufficiently short so that the molecules in the samples do not diffuse appreciably during that period.[1] However pulse imperfections (incorrect flip angles) in the above sequence will have cumulative effects, which may be compensated by using the Meiboom-Gill modification of the Carr-Purcell sequence, given by (6),

$$\{90^{o}_{y} - (T - 180^{o} - T - 180^{o} - T)_{n} - \text{Acquisition}\}$$

The 90^{o} pulse is phase shifted by $\phi = 90^{o}$, (i.e. the RF pulse is applied along the y' axis) as a result the imperfections in the refocussing pulse are

[1]The intensity of the transverse magnetization component along y' at time t is given by,

$$M_{y'}(t) = M_{o}\{\exp(-t/T_{2}) + (-\gamma^{2}G^{2}Dt^{3}/12n^{2})\}$$

G = field gradient along z (gauss cm^{-1}); D = diffusion coeficient. n will be equal to one in the C-P method A pulse sequence. The term on the right indicates the decay of magnetization due to diffusion of molecules in a magnetic field gradient. Note the t^{3} dependency.

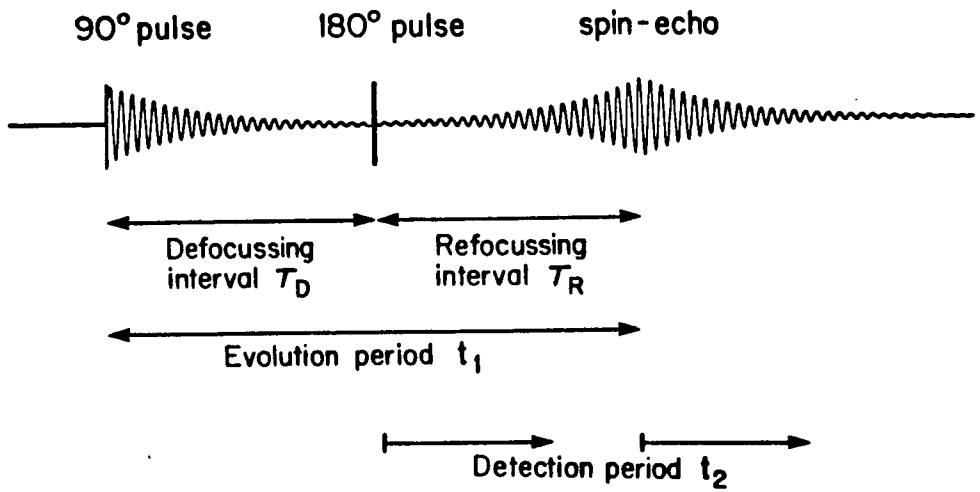

Figure 2.1: The Carr Purcell (method A) pulse sequence and the illustration of the spin-echo formation of the NMR signal. $T_D = T_R = \frac{1}{2}t_1$. The two detection periods represent the signal acquisition for whole-echo (SEAS) and half-echo Fourier transformation.

corrected on every even numbered echo. In another related procedure suggested by Freeman and Wittekoek (7), the phase of the refocussing pulse is alternated by 180° (i.e. the pulse is applied along the $\pm$x' directions). In most of those parts of this thesis involving SEAS and 2D J experiments, the Carr-Purcell method A with phase alternation procedure of Freeman *et al.* (7) was used. It will be noted later that use of such phase shifted pulse sequences is critical, particularly in SEAS.

The next section provides an introduction to the effects of RF pulses on a spin system. This can be easily visualized considering the magnetization vector model in a rotating reference frame to provide an understanding of the many features of spin-echo spectroscopy such as phase and amplitude modulation and refocussing effects. Since the same basic spin-echo pulse sequence is also used in 2D J and related experiments, this discussion also provides a basis for a qualitative understanding of the principles of those experiments which will be discussed in later chapters.

2.3 The effect of radio frequency pulses on a spin system

Using the nomenclature of the rotating reference frame model, the RF pulse of a conventional, single pulse NMR experiment creates a net magnetization in the x'-y' plane. This is illustrated in Figure 2.2 a-b where a 90° pulse applied in the x' direction, generates a transverse magnetization component by flipping the z' component onto the y' direction. When this excited system is allowed to "evolve" the magnetization vectors corresponding to each set of equivalent spins precess with their own characteristic frequencies which, in the rotating frame, is seen as precession of each vector at an offset frequency (ν_o) with respect to the transmitter.

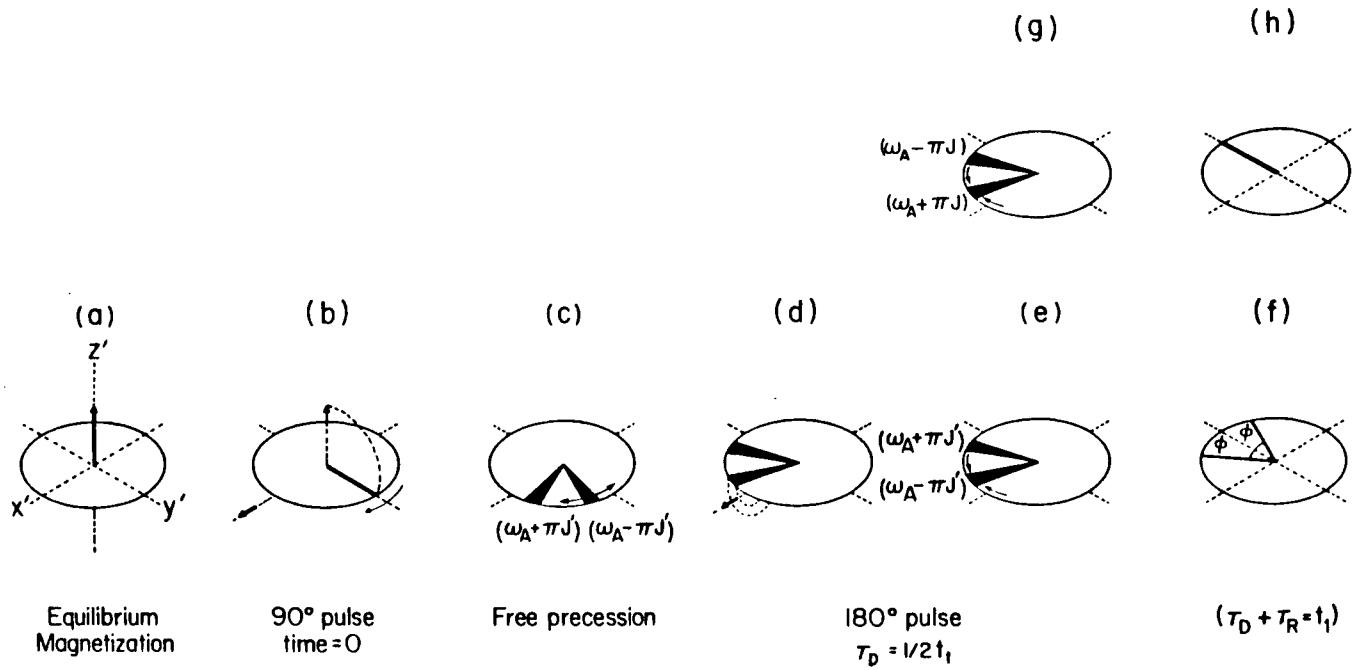

Figure 2.2: The behaviour of the A magnetization of an AX system in the rotating frame during the C-P pulse sequence. The sequence (a-f) represents the effect of a non-selective 180° pulse which results in an accumulation of a phase angle 2ϕ. Application of a selective 180° pulse to the A spins does not result in a phase modulation of the A components as a function of t_1 (a-d, g, h). The field inhomogeneity effects are represented by the "diffusion" of the magnetization vectors which are refocussed at t_1 (the relative velocities of the "isochromats" are indicated by the inner arrows). The chemical shift component will always lie along the $\pm y$ direction at t_1 (f and h) and are therefore "refocussed". ω_A and J' refer respectively to the angular velocity (ω_A=offset with respect to the transmitter) in the rotating frame, and the coupling constant in radians.

The magnitude of the transverse magnetization decays exponentially with time due to spin-spin interactions in the medium, which is characterised by its spin-spin relaxation rate ($R_2 = 1/T_2$). In practise, inhomogeneities in the static magnetic field B_o also contribute to the decrease of the transverse signal. This field inhomogeneity causes different regions of the sample to experience slightly differing local fields, thereby causing the nuclei in those different regions to precess at slightly different frequencies. This results in a loss of phase coherence (dephasing effect) of the magnetization "isochromats", which leads to a rapid damping of the transverse signal. For most practical purposes the composite decay rate is assumed to be exponential, with a time constant T_2^*, which is related to the resulting spectral line width at half-height given by,

$$\Delta\nu_{\frac{1}{2}} = \frac{1}{T_2^* \pi} = \frac{R_2^*}{\pi} \text{ (Hz)} \qquad [2.1]$$

The line widths observed in a conventional high resolution NMR experiment are usually governed by instrumental effects (R_2^i), and the relationship to the "natural" spin-spin relaxation rate can be represented by,

$$R_2 = R_2^* - R_2^i \qquad [2.2]$$

As a result line width measurements, do not therefore, provide a convenient method for spin-spin relaxation time measurements in most cases. However T_2 measurements can be made via the experiments based on C-P pulse sequence described earlier.

The consequences of the spin-echo pulse sequence on a spin system can be easily visualized in terms of classical magnetization vectors in the rotating reference frame (7). Figure 1.2 illustrates the effect of pulses on the A doublet of an AX spin system. At equilibrium, the total magnetization vector

corresponding to the A spins lies along the z' direction; the initial 90^{o} pulse transforms this magnetization onto the transverse plane, along y' as shown in Figure 2.2 a-b. During the delay T_D the magnetization of the A spins evolves and splits into two components, symmetrically disposed about the chemical shift component, and correspond to the two A transitions in a frequency spectrum. The phase angle between them will be proportional to the spin-spin coupling constant and the delay T. Inhomogeneities in the B_o-magnetic field, cause the magnetization "isochromats" to lose phase coherence; this is represented in Figure 2.2c as, each component "diffusing" or "fanning-out" in the transverse plane; the relative angular velocities are represented by the inner arrows indicating the "fast" and "slow" moving components.

In conventional pulsed NMR the resulting magnetization is detected over a period (usually $>3T_2^*$) equal to the sampling time, prior to Fourier transformation. The rapid decay of the magnetization due to the instrumental factors (static field inhomogeneity) or R_2^i effect can be reversed or "refocussed" by applying a 180^{o} pulse to the spin system. However, the ultimate result of this pulse on a spin system depends on the nature of the refocussing pulse; for example, the latter could be a non-selective pulse in a homonuclear system or a pulse applied selectively to only the A nuclei as in a heteronuclear case. A selective pulse applied along the x' direction to the A spins will have two effects on the R magnetization isochromats - a) it flips each vector into its mirror image position about the x' axis as shown in Figure 2.2d; this causes the relatively fast and slow components (which had developed as a result of both inhomogeneity effects and free precession) to be

placed in trailing and leading positions respectively in relation to the direction of precession (Fig. 2.2d,g). As a result, during the delay T_R, the magnetization isochromats of the two A vectors converge thus eliminating the effects due to magnetic field inhomogeneities at time $t_1 = T_R+T_D$ (Fig. 2.2h). At that same instant, the two components corresponding to the J_{AX}, scalar spin-spin coupling would have also refocussed and lie along the -y' direction. Hence in this experiment, the effects of magnetic field inhomogeneity, coupling constants and chemical shifts are all simultaneously refocussed or eliminated at the "echo-maxima".[1]

In contrast, if the 180° pulse is non-selective and is applied to both A and X spins, its effect in addition to that indicated in Figure 2.2d, will be to invert <u>all</u> spin states thereby "exchanging the identity" of the two A components as indicated in Figure 2.2e (<u>cf</u>. Fig. 2.2g). As a result these two components continue to diverge during time T_R and accumulate a total phase angle of 2ϕ between them at time T_D+T_R (Fig. 2.2f); note however that the effects of chemical shift and the magnetic field inhomogeneity are, as before, refocussed at this time.

For a general case of a multiplet, weakly coupled to X equivalent nuclei, the phase angle of each A component is given by,

$$\phi = \pm 4\pi M_X JT \text{ radians} \qquad [2.3]$$

where M_X is the total z spin component of the X spins and T the delay time between the pulses.

Fourier transformation of the half-echo signal will show the phase modulation of each frequency component according to equation [2.3] Its magnitude is given by the echo maxima which decays exponentially with a time

[1]This phenomenon can be used to distinguish homonuclear and heteronuclear spin-spin coupling in 2D J experiments (see Chapter IV).

constant T_2. These features are shown in Figure 2.3 for the triplet and quartet resonances (J = 7.1 Hz) of diethyl malonate, $((CH_3CH_2CO_2)_2CH_2)$ in $CDCl_3$ solution.[1] This cyclic variation of the phases of each component as a function of T is also referred to as J-modulation, and it has been one of the serious limitations to the application of the SEFT technique to chemical systems, eg. for T_2 measurements and related experiments in high resolution proton NMR spectroscopy. Although methods have been suggested to circumvent the problem of J-modulation in simple spin systems (8,9), for example, by choosing T values equal to an integer of 1/J,[2] by absolute value calculations or by selective excitation methods (7), these are however not generally applicable to typical (complex) organic molecules.

2.4 Spin-echo absorption spectroscopy

Recently Bax et al. (11) have shown using the Carr-Purcell-Meiboom-Gill sequence that proton spin-spin relaxation rates can be obtained by Fourier transformation of the whole-echo, rather than the half-echo signal generally used in SEFT applications[3]. The authors showed that a symmetric whole-echo

[1]Note that the individual components of a multiplet may have different spin-spin relaxation time.

[2]The acquired (half-echo) signal along the y direction is given by

$$S(t_2)_y \propto \cos(\omega+\phi)t \qquad [2.4]$$

$$S(t_2)_y \propto \cos(\omega t)\cos(\phi t) - \sin(\omega t)\sin(\phi t) \qquad [2.5]$$

Substituting n/J = T, (n=0,1,2,...) in equations [2.3] and [2.5] yields, after Fourier transformation, an absorption mode signal. In the case of a groups of protons coupled to many non-equivalent nuclei these equations become more complex.

[3]Although the original SEFT spectrum (5) was obtained by acquiring a symmetric whole-echo signal and folding it about the centre of the echo, the resulting spectrum (after cosine FT), would be expected to show an amplitude modulation as a function of T.

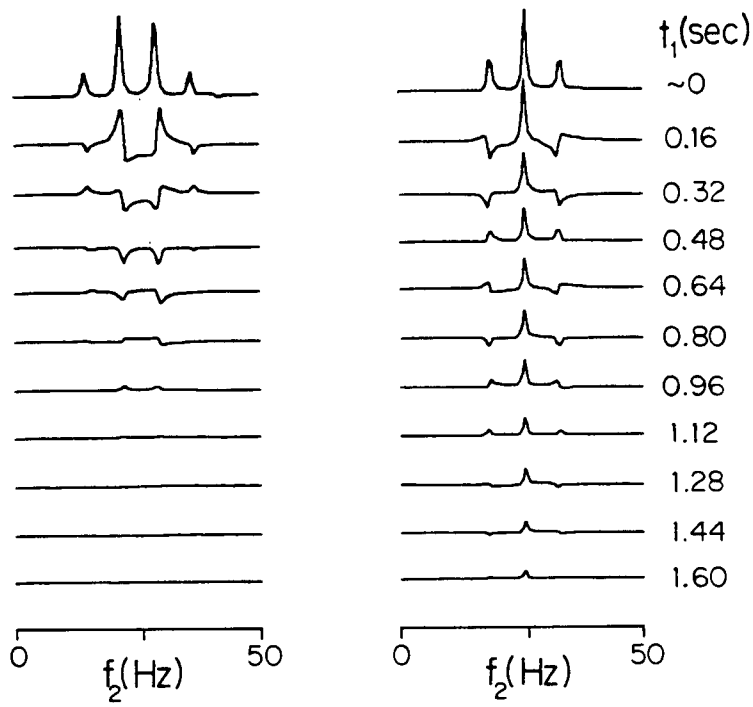

Figure 2.3: J modulation in (Carr-Purcell) SEFT spectroscopy. The traces corresponding to $t_1 \sim 0$ are equivalent to an A_2X_3 spectrum obtained in conventional FT spectroscopy, and show no phase or intensity anomalies. The individual peaks obtained by the half-echo FT show J modulation with an exponential decay due to spin-spin relaxation, as a function of time, t_1. Note that the central component of the triplet ($M_x=0$) shows no phase modulation.

signal when Fourier transformed and subjected to further data manipulation steps yielded for the sine and cosine transforms, pure absorption signals, whose amplitudes were respectively sine and cosine modulated as a function of T. In effect the dispersive components of a signal were eliminated from the resulting spectrum so that the magnitude spectrum in this case displays only pure absorption peaks. The major conditions for the Bax experiment are that:

a) the echo-signal should be symmetric with respect to the acquisition time t_2 (ie. $t_2 = 2T$),

b) relaxation (T_2) during the acquisition period should be negligible, and,

c) the signal at the beginning and the end of acquisition should be minimal (to avoid truncation effects).

It will be recalled that the digital resolution of the real part of the spectrum for example, is related to the acquisition time and spectral width, given by equation [1.10],

$$DR = \frac{1}{AT} = \frac{2.(SW)}{BS}$$

In order to obtain a suitable spectral resolution it may be necessary to acquire the NMR signal over a long period 2T, equal to the acquisition time. Although signals with long spin-spin relaxation times (T_2) can be acquired over a suitably long period, without significant loss of the echo-signal during acquisition, those with short T_2 value will lead to echo-signals which will be asymmetric.

It is apparent from the above discussion that the most suitable chemical systems for study by the above, spin-echo absorption mode spectroscopy are molecules with relatively small spectral widths and long spin-spin relaxation times (T_2), conditions which are generally found for only rather small,

simple molecules. Conversely, the above experiment appears to have serious limitations which prevents its use for studying larger molecules with wider spectral widths, and relatively short transverse relaxation times. Fortunately, as will be demonstrated these limitations can easily be overcome (in many cases) by using a very general pulse sequence and data processing routine (cf. Refs. 10 and 14); these can be easily performed with the standard software programs available with modern NMR spectrometers.

The pulse sequence for the SEAS experiment is given by,

$$\{90^{\circ} - T - 180^{\circ}_{\pm x} - \text{Acquisition}\}$$

where $\pm x$ refers to the phase alternation of the refocussing pulse by 180°. The signal is acquired on a suitable block size and zero-filled if necessary to provide the digital resolution needed in the final spectrum. In order to obtain a pure absorption mode frequency spectrum, the "echo-signal" should be completely symmetric.[1] Also, the echo-signal at the beginning and end of the acquisition should, ideally, be zero to minimize truncation effects in the Fourier transformed spectrum. The above condition is usually achieved in practice by applying the 180° refocussing pulse after the originally induced FID signal has decayed to a miminum; this is illustrated in Figure 2.1.

Spin-lattice relaxation during the delay T_D causes a longitudinal component of magnetization to develop, which also experiences the refocussing pulse; however, deviations in the flip angle from 180° will create a residual transverse magnetization, and give rise to a finite signal at the beginning of the data acquisition. The asymmetry caused by this residual signal may be eliminated by the use of suitable phase shifted pulse sequences.

[1]It should be noted that only the "echo-signal" needs to be symmetric for SEAS, and not the acquired whole-echo signal.

For example, alternation of the phase of the refocussing pulse by 180^{o} flips the longitudinal magnetization in opposite directions, which causes cancellation of the residual magnetization on alternate scans, while the desired transverse components contribute additive to the spin-echo signal. In the present work, particularly when dealing with systems having a wide dynamic range of signals, it was not possible to completely eliminate the residual signal by the above procedure. It is also possible to minimize the unwanted signal at the beginning of the acquisition by suitable digital filtration, or by "left-shifting" the acquired signal by a few data points.

It was assumed in the original paper by Bax et al. (11) that the echo-signal decays mainly due to instrumental effects (T_2*) and that spin-spin relaxation during acquisition can be neglected. Such assumptions are probably not valid for the type of molecules chosen in this study; the effect of this on the acquired signal would be to make it asymmetric as a result of exponential damping due to T_2 relaxation. It was found that this slight asymmetry can often be ignored, or else a symmetric echo may be generated by suitable digital filtration (11).

The above discussions dealt with the conditions for obtaining spin-echo absorption mode spectra, and how a whole-echo signal can be generated for a typical organic system. Fourier transformation of this signal, followed by magnitude calculation yields an absorption mode spectrum similar to that obtained in conventional high resolution spectra, and unlike half-SEFT spectra, these are independent of phase.

The importance of SEFT spectroscopy is due to the possibility of selectively observing the relatively slowly relaxing signals of a complex spin system. The principle involved can be easily explained with the aid of Figure

2.4; this represents the range of exponentially decaying signals in the transverse plane of, for example, a less "mobile" macromolecule (R_2 = 100-10s) and a smaller rapidly "tumbling" small molecule (R_2 = 2-1s). A SEAS spectrum from such a mixture obtained with an initial delay (T) of about 0.2s, will show "some" signals from both the slowly relaxing macromolecule and the rapidly relaxing small molecule; however, an initial delay of about 0.4s will contain, almost exclusively, the signals from the small molecule. A feature of practical importance is that in spite of the original dynamic range between the two systems, selective detection of one group of signals can be achieved. This feature could have a great potential in extending the scope of NMR spectroscopy to study biological systems (15,16) and the applications of SEAS for the study of such systems is discussed in the following sections in three contexts: the first, using a monomer and a polymer, the second using an enzyme, to distinguish the sharp components in the spectrum and finally to study low molecular weight metabolites in red blood cells.

2.5 Application of SEAS in chemistry

It is well known that studies of biochemical samples of high molecular weight by conventional proton NMR spectral analysis are frequently impossible due to extreme broadening of lines (ca. 10 Hz) resulting from the short spin-spin relaxation times (ca. 30 ms) of the signals (Fig. 2.5). Many macromolecules (ca. 5,000 MW) may be considered to give rise to two types of signals; one set of signals arising from nuclei attached to the relatively rigid backbone which contribute broad lines, and the second from those attached to relatively mobile parts of the molecule, which give rise to the sharper lines in the spectrum. Frequently the NMR spectra of biomolecules are

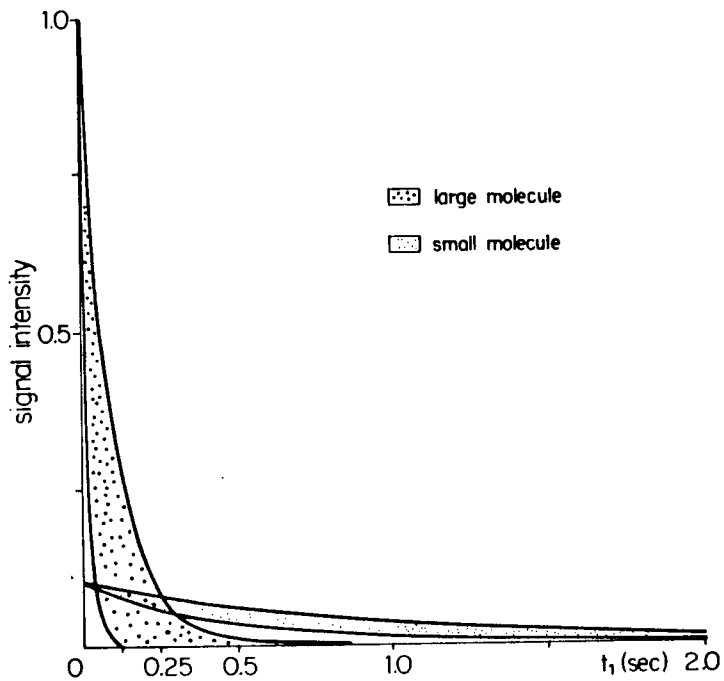

Figure 2.4: Comparison of the magnetization intensities of a "large" and small molecule in a SEFT experiment. The signals from the large molecule are assumed to be ten times more intense than the small molecule, with spin-spin relaxation rates ranging from R_2=100 to 10 s. For short delay times (t_1≈0.25 s) most of the magnetization detected is from the large molecule. However at longer delays t_1 (ca. 0.5 s), the small molecules in the mixture contribute significantly to the resulting spectra due to their relatively slower relaxation rates (R_2=2 to 1 s).

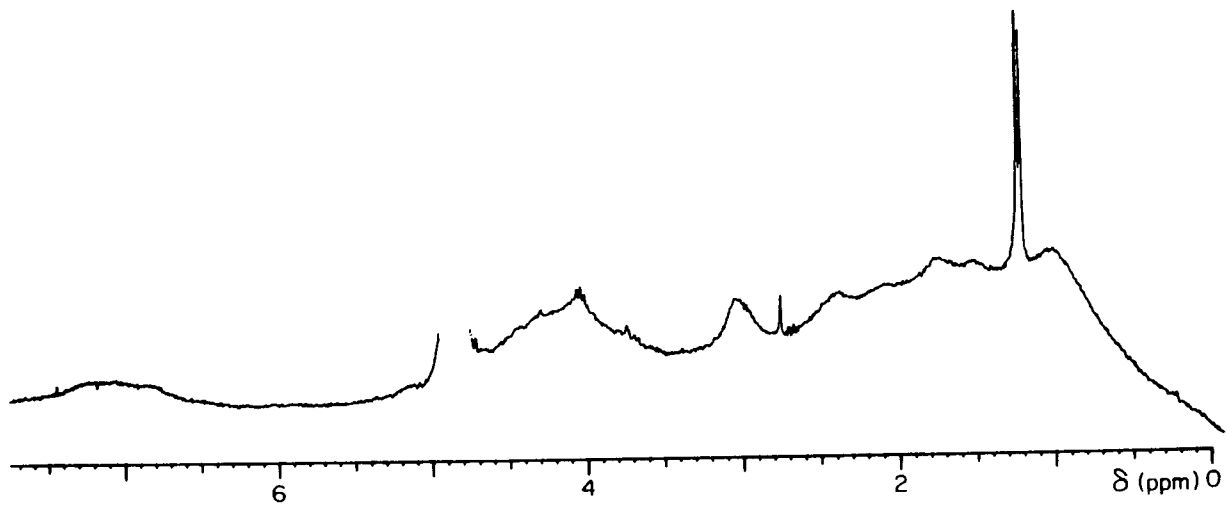

Figure 2.5: 270 MHz ^1H NMR spectrum of bovine serum albumin (BSA) in D_2O. Most of the sharper components are completely hidden within the broad signals which are from protons which have very fast spin-spin relaxation rates. The residual HOD peak at δ4.8 was (partially) presaturated; the signals at δ1.1 are due to impurities.

broadened to such an extent that the sharp components are hardly visible. Since the analysis of these sharp signals could provide interesting structural and motional information many methods have been suggested to detect these lines (15,16). Generally these methods are based on the differential relaxation times between the broad and narrow components and include a) delayed Fourier transform (DEFT; (17)), b) convolution difference (18), c) SEFT (12) and d) selective "spin-diffusion" or saturation transfer (19).

Convolution difference, and the related digital filtering techniques (20) are based on data manipulation of a conventional FID to eliminate the broad components. The method involving spin-diffusion is performed by irradiating a sample at an appropriate frequency for a given period (pre-saturation) prior to signal acquisition by the usual method. The broad lines can be selectively suppressed (saturated) by this method leaving the narrow lines in the resulting spectrum. It should be realized that the final result depends on the experimental conditions such as power, frequency and duration of the irradiating field. SEFT experiments are convenient and above all provide a method to study spectra as a function of a single variable t_1. This makes it more convenient to compare or standardize experimental data, for example, from the literature, and also to measure spin-spin relaxation rates either for the purpose of quantitative studies or for spectral analysis. The major limitation of the SEFT and DEFT techniques, however, are the phase and intensity anomalies due to J-modulation as discussed earlier. The SEAS experiment offers a convenient solution to this problem by eliminating the dispersive components from a Fourier transformed spectrum.

A practical application of SEAS technique is demonstrated here using a D_2O mixture containing respectively ca. 20, 10 and 5% by weight of

α,β-D-xylose (1, MW 150), α-cyclodextrin (2, MW 972) and dextran T-10 (MW ca. 10,000, a 1→6 linked polymer of D-glucopyranose, 3). The 400 MHz ^1H spectrum of the mixture is shown in Figure 2.6A (note the magnitudes of the signals in the mixture in relation to the xylose peaks); for reference purposes the spectrum of pure xylose is shown in Figure 2.6B. Fourier transformation of the whole-echo, followed by magnitude calculation yields, for different T values, the SEAS traces E, D and C in Figure 2.6D. It can be seen from these spectra that the signals from the polysaccharide and cyclic hexasaccharide may be selectively eliminated from the SEAS traces due to the relatively faster relaxation rates (R_2) of their constituent protons as compared to those of the monosaccharide; see, for example, the resolution in Figure 2.D of the H-2^{α} and H-5^{β}_{e} protons from within the broad peaks shown in Figure 2.6A. This illustrates the use of this technique for the selective detection of signals from the relatively more mobile units or molecules when they are normally hidden beneath broader lines; its effectiveness is essentially independent of the dynamic range between the signals (cf. Fig. 2.4). It can be noticed that the signals in Figure 2.6E are broader as compared to the other two SEAS traces; this broadening arises mainly from the dispersive contribution in the magnitude spectra due to the asymmetry of the echo-signal. Such lineshape distortions arise whenever a significant signal intensity is present at the beginning of the acquisition, whether it be due to pulse (flip angle) imperfections which generates a residual transverse magnetization, or to the application of the refocussing pulse before the initial signal has decayed (T_2* relaxation) to a minimum. The former signal contribution can be minimized in practice by suitable phase shifted pulse sequences, as discussed in the previous section.

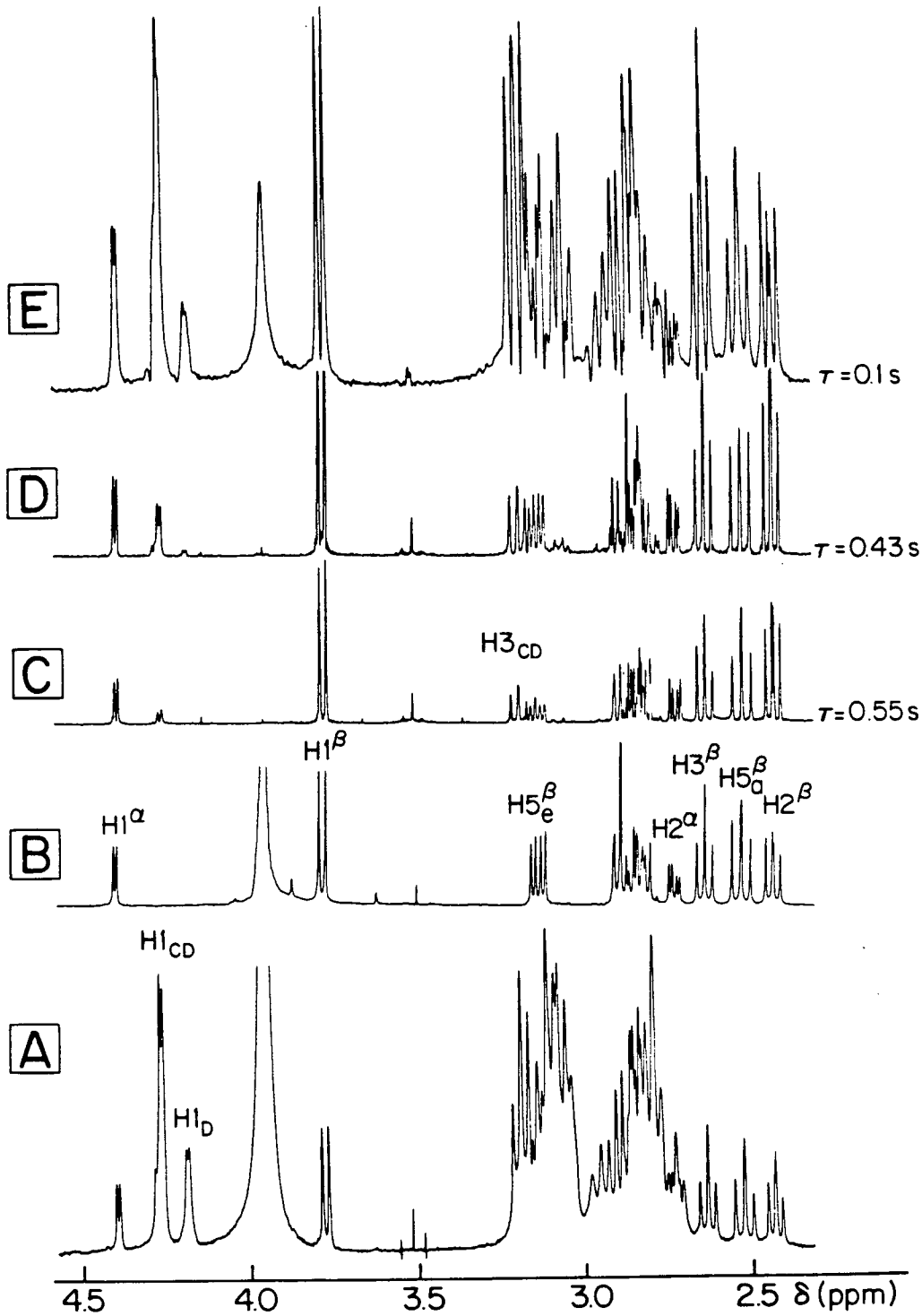

Figure 2.6: (A) the 400 MHz proton spectrum of a mixture of α,β-D-xylose (1), α-cyclodextrin (2) and dextran T-10 (3) in D_2O (ca. 20, 10 and 5% by weight respectively; NA=24, AT=5.45s; BS=16K)
(B) The equivalent spectrum of 1 in D_2O (C, D, E). Spectra (NA=64) obtained by Fourier transform of the whole-echo acquired on a 16K block size in the absolute value mode with the T values indicated. Note that in (C), all signals from the HOD and dextran T-10 have been suppressed, leaving some components from the α-cyclodextrin. Subscripts CD and D refer to the cyclodextrin and dextran units, respectively.

It was demonstrated by Bax et al. (13) that the whole-SEFT method can be used to measure transverse relaxation times of small molecules (1,1,2-trichloroethane). The SEAS method described here can also be used to measure spin-spin relaxation times of protons in larger molecules by studying the signal intensity as a function of t_1; this provides another NMR parameter for semi-quantitative spectral analysis. This application is illustrated using a model system containing a mixture of 0.01M Dextran T-10 and 0.1M β-methylxylopyranoside (4) in D_2O. The decay of the magnitude of the multiplets in the SEAS traces shown in Figure 2.7C, D and E represents the decay of each signal of the xyloside in the transverse plane due to spin-spin relaxation.[1]

Although the concept of "selective detection" based on transverse relaxation rates has been extended to the study of biochemical systems using the half-SEFT experiment, this has several intrinsic limitations. Figures 2.8B, C and D show the spectra obtained by Fourier transformation of the half-echo time domain signals from a mixture containing xylose, α-cyclodextrin and dextran T-10 (cf. Fig. 2.6). In common with the results given by other complex systems these spectra show the expected phase and intensity variations,

[1]In order that each SEAS trace in Figure 2.7 be directly comparable it is essential that the corresponding time domain signal be "similar" for the various delay times and be subjected to similar digital filter functions. This may be achieved by modifying the basic SEAS pulse sequence to

$$\{90^\circ - T_{VD} - 180^\circ - T_{FD} - 180^\circ - \text{Acquisition}\}$$

where T_{VD} and T_{FD} are respectively variable and fixed delays (T_{FD} would be the "minimum" delay before the refocussing pulse is applied prior to acquisition). This sequence ensures that the shape of the echo-signals are similar since the echo-maxima occur at T_{FD}. Corrections for pulse imperfections and diffusion effects can also be accommodated into the above pulse sequence by including, for example, the Carr-Purcell-Meiboom-Gill sequence, although these variations were not carried out in the present work.

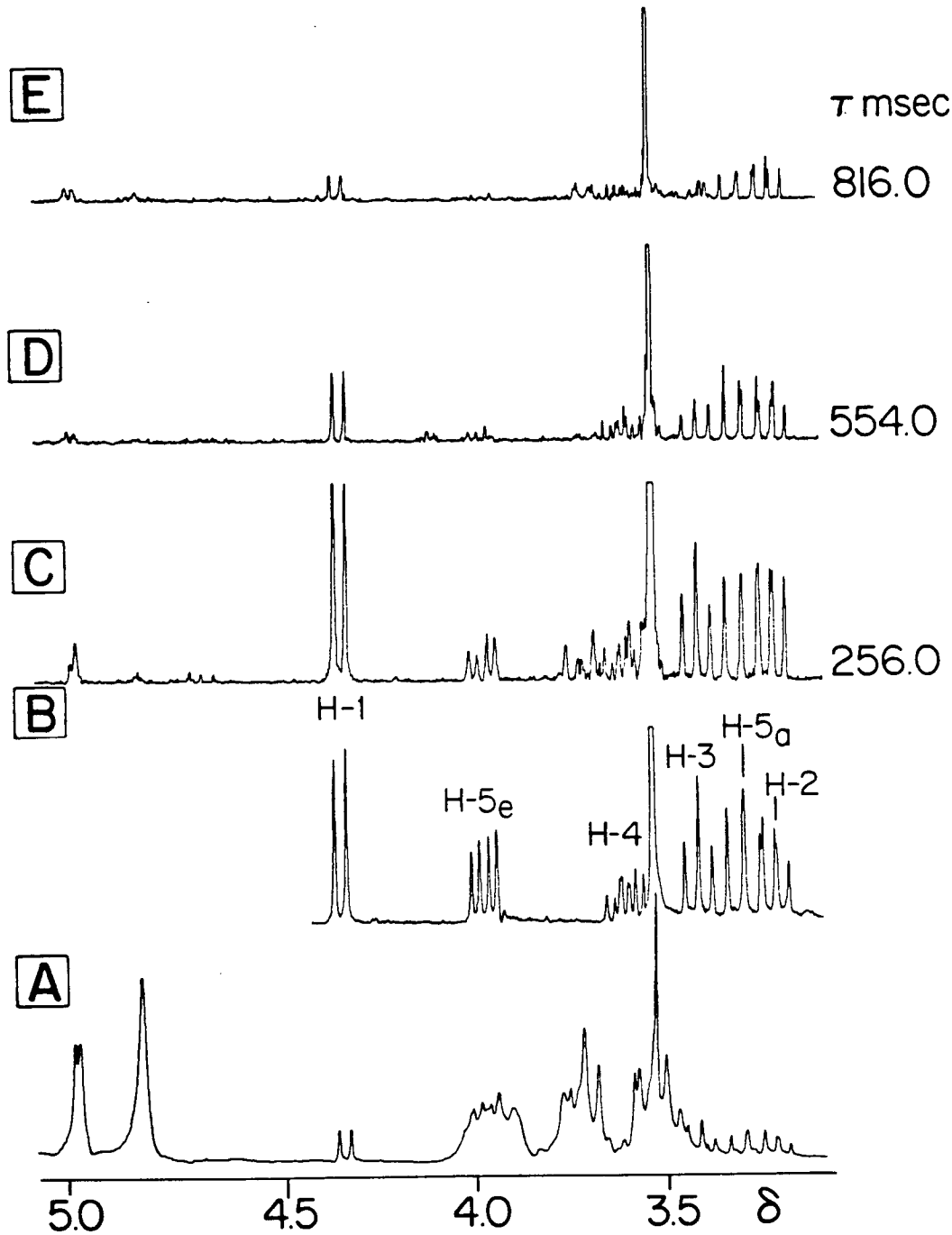

Figure 2.7: Conventional ^1H spectrum of a mixture of 0.01M dextran and 0.1M β-methylxylopyranoside (4) in D_2O (lyophilized three times in D_2O). (B) Spectrum of the pure xyloside (C, D, E) SEAS traces at different delay times plotted in the absolute value mode (NA=48). (C) shows mostly the signals from the xyloside, but some residual signals from the dextran still remain; (D) and (E) show the gradual disappearance of those signals depending on their spin-spin relaxation rates.

and the resulting distortions. It should be cautioned that interpretation of the multiplet patterns of spectra which contain such J modulations (as suggested in Ref. 11) can be misleading; for example, the rather small differences between the spin-spin coupling constants ($J_{5a,5e}$ = 11.7; $J_{5a,4}$ = 10.6; $J_{4,3}$ = 9.4; $J_{3,2}$ = 9.4 Hz) of the "triplets" H-3^{β}, H-5^{α}_{a}, and H-2^{β} are nevertheless sufficient for them to give completely differing responses as a function of the T values.

The selective detection of the narrower components in the NMR spectrum of a biomolecule is demonstrated using lysozyme (MW = ca. 14,500, 15% w/v in D_2O, pD 4.0). The line widths (and also chemical shifts) of the signals corresponding to their individual amino acid constituents of enzymes (proteins) are largely dependent on the relative position of a unit in the macromolecule. Thus protons of the units on the more mobile side chains of the protein tend to show somewhat narrower line widths when compared to those which are part of the rigid "backbone", or those which are sufficiently embedded in the core of the molecule as to be subjected to rapid relaxation by their neighbouring protons (dipolar interactions, (21)).

Since the acquisition of the whole-echo in SEAS is limited by the choice of an initial, minimum delay, for the reasons discussed earlier, this experiment is generally best suited for studying the relatively slowly relaxing signals. A comparison of SEAS and the half-SEFT method is given in Figure 2.9; the conventional FTNMR spectrum shows the presence of broad and narrow components in the biomolecule. Even short delay time (T=10 ms) such as that used to measure Figure 2.8B (by the half-SEFT), allows most of the rapidly relaxing components to relax in the transverse plane thereby decreasing the intensity due to the broader components in the resulting

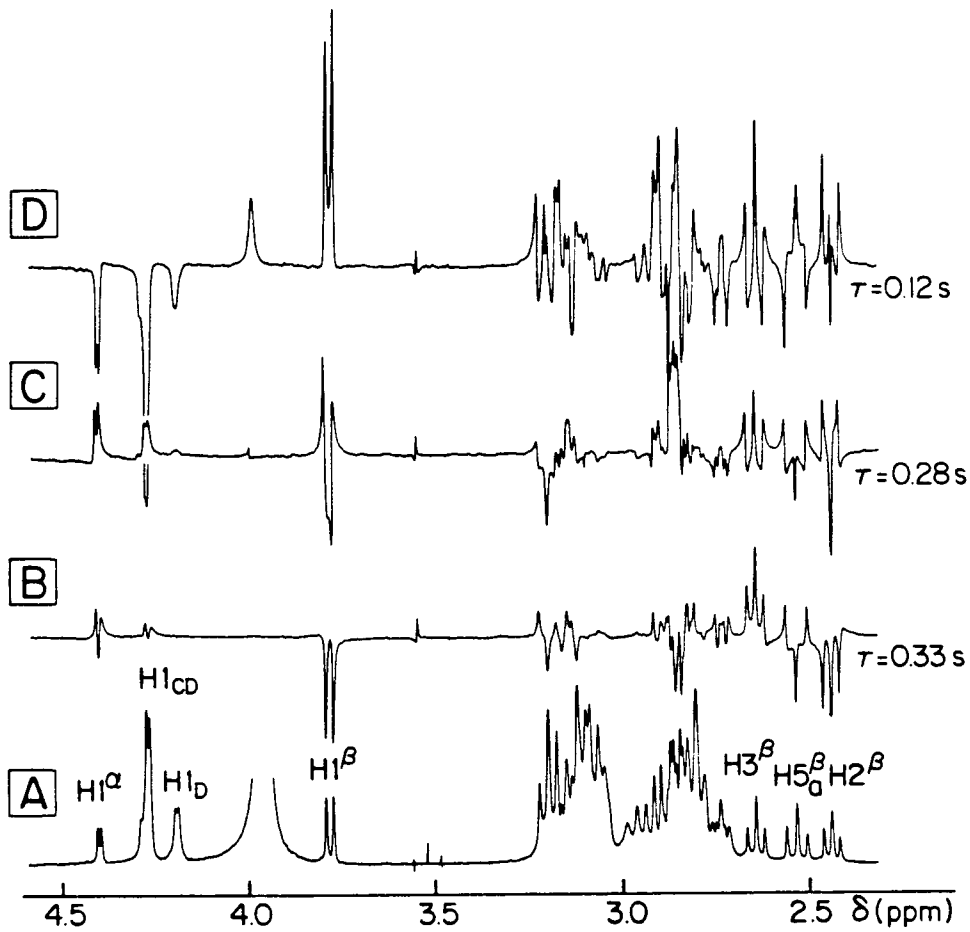

Figure 2.8: (A) As for Fig. 2.6A. Traces (B), (C) and (D) were obtained by Fourier transformation of the half-echo from a C-P pulse sequence with the values indicated.

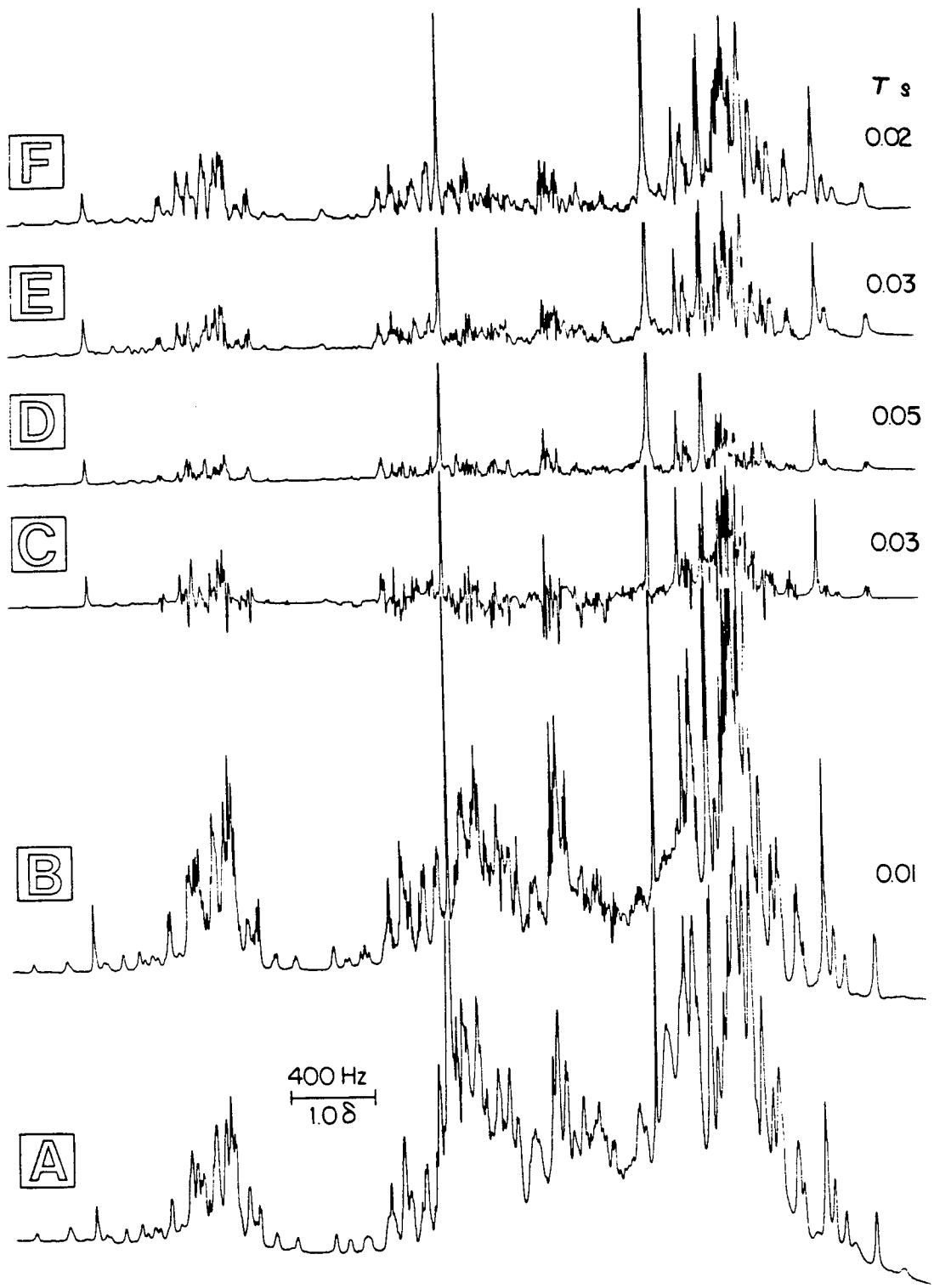

Figure 2.9: (A) The normal 400 MHz proton spectrum (NA=64) of a 15% D_2O solution of lysozyme (from Worthington Biochemicals Co.; lyophilized three times in D_2O) at pD 4.0. (B, C) Spectra obtained by Fourier transformation of the half-echoes and (D-F) those obtained by the whole-echo Fourier transform of signals from the C-P pulse sequence, with phase alternation of the 180° pulse (NA=200; temperature=50°C; SW=400 Hz; BS=16K).

spectrum. As a result many of the (well dispersed) peaks that appear as broad singlets in a conventional spectrum, show definite spin-spin coupling patterns (cf. Fig. 2.8A and 2.8B). Inevitably though, increasing the delay T, in addition to eliminating the broad components also introduces phase anomalies due to J-modulation, which can be seen in Figure 2.9C. These anomalies are suppressed in the absorption-mode spin-echo spectra which are shown in Figure 2.9D, E and F.

A further advantage of SEAS is that, because the whole-echo is subjected to Fourier transformation the resultant spectrum is expected to show an improvement in sensitivity by a factor of about 1.4 over the half-echo method.

2.6 Applications of SEAS in biology

The previous studies illustrate some of the problems facing the application of conventional NMR to biochemical samples and some possible applications of SEAS. In order to probe the possible extension of this work to "living" systems, some SEAS experiments involving red blood cells (RBC) were undertaken. Although the proton NMR spectrum of the RBC sample were not expected to provide useful information (Fig. 4.10A), it was anticipated that it should be possible to monitor the spectra of small molecules associated with them.

In this work, SEAS was used to study the behaviour of glucose (5) in RBC; the initial aim of this work was to compare SEAS with the half-SEFT (12) technique. However, due to some differences between this study and previous data in the literature, it was necessary to perform additional control experiments. The results summarised here allow us to make some conclusive statements on the system studied and also raises some questions on the assumptions and conclusions reached by the previous workers (22,23).

RBC are one of the simplest cells, with the cytoplasm comprising of mainly haemoglobin (an iron containing protein) and the remaining protein being mainly enzyme systems for the various metabolic pathways that take place within the cell.[1] The cell itself is highly active, and is involved with various dynamic processes such as the vital metabolic pathways, and controlled diffusion of molecules or ions across the cell membrane. The studies of biochemical pathways have always been of interest to biochemists from a clinical point of view since they provide information on physiological processes at the molecular level. For example, studies have been made to establish correlations between the relative concentration of molecules (or metabolites) in cells and different ailments using fresh RBC samples from patients (26). That spin-echo NMR techniques offer a convenient, non-destructive method for studying such systems has already been claimed in the literature (12,13) and this point is further demonstrated here using SEAS for RBC-glucose systems.[2]

One of the vital metabolic pathways in living animal cells is the Embden-Meyerhoff or glycolytic pathway (25). One of the functions of this process is the utilization of glucose (via the pentose phosphate pathway) to provide the energy needed in chemical form as adenosinetriphosphate (ATP);[3] one of the end products is lactic acid ($CH_3.CH(OH).CO_2H$).

[1]For detailed structure and function of RBC the reader is referred to references 24 and 25.

[2]Sample preparations were carried out by Rob Snoek in the Pathology Department at UBC.

[3]The energy is released in cells with the linkage of one of the phosphate bonds to form adenosinediphosphate and inorganic phosphate.

Small molecules within the cell such as glucose, lactic acid, pyruvic acid, glycine and oxidized glutathione can diffuse across the cell membrane, and are controlled by processers called "facillitated diffusion pumps".

The RBC were prepared[1] from freshly drawn venous blood and washed in phosphate buffered saline solution. They were then washed in Krebs-Ringer solution (pH 7.2) with (Procedure B) or without (Procedure A) 10 mM glucose. The sample that was exposed to glucose was incubated in glucose for two hours at room temperature. The samples were centrifuged and either the supernatant or the "pellet" was used in the NMR studies. The haematocrit of the pellet samples were usually 85-95%.

The NMR spectrum of a sample of RBC (pellet) shows, as expected, a broad envelope arising from the various high molecular weight substances (Fig. 2.10A). Perhaps the only signals that could be assigned are in the aromatic region, and arise from the histidine residues of the haemoglobin. SEAS can be used to reveal the signals that are normally hidden under this broad background as shown by the corresponding traces in Figures 2.10 and 2.11.

Figure 2.11A shows a SEAS spectrum of a RBC (pellet) sample, which was obtained after washing with an isotonic saline (Krebs-Ringer) solution containing 10 mM glucose (Procedure B). As expected, the trace in Figure 2.11A shows in addition to the normal peaks (Fig. 2.10B) the peaks corresponding to glucose (Fig. 2.11D) and the lactate peak at 1.28δ. Because most of the ring protons of glucose appear as overlapping multiplets in the region 3 to 4δ, it is more convenient to use the signals of the anomeric protons to monitor the concentration of glucose in the sample.

Figure 2.11B shows a SEAS spectrum obtained from a RBC sample which was washed with Krebs-Ringer solution (without glucose) and then made up to about

[1]See Experimental Section (Ch. VII).

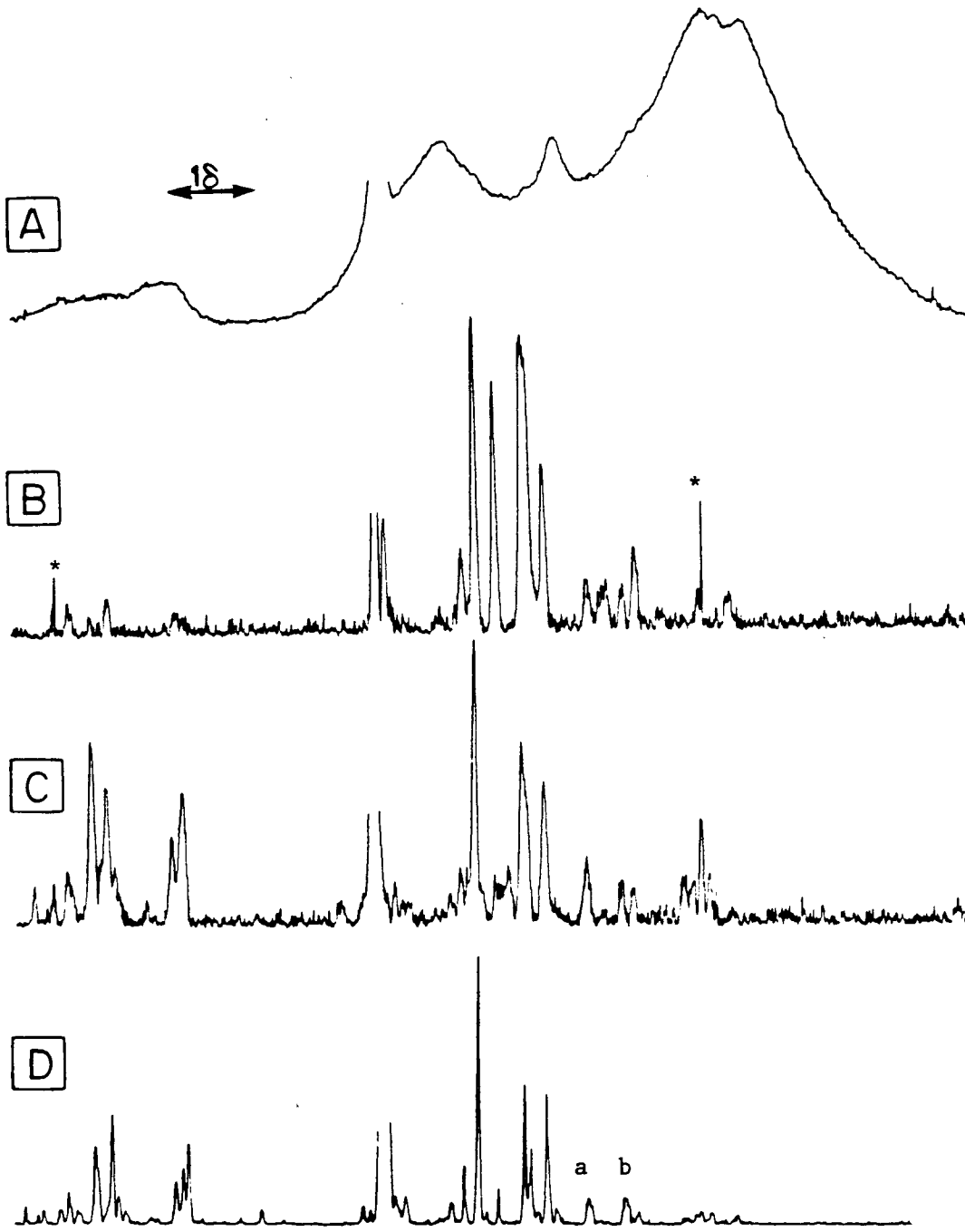

Figure 2.10: (A) The normal 270 MHz spectrum of RBC pellet (NA=32) with the solvent nulled by an inversion recovery sequence (T1IR). (B) The spectrum from SEAS, T=60 ms of a glucose depleted sample measured about 30 hours after preparation. Note the signals corresponding to the haemoglobin residues due to partial lysis. (C) The SEAS spectrum (T=60 ms) of an RBC pellet, which was incubated in glucose and partially lysed. (D) The SEAS spectrum of the supernatant of a lysed RBC sample (T=80 ms). The solvent peak in B, C and D were presaturated. The time domain signal was multiplied by a linear function to eliminate the residual transverse magnetization and then by an exponential function. *indicate spikes caused by the decoupler. (see experimental section).

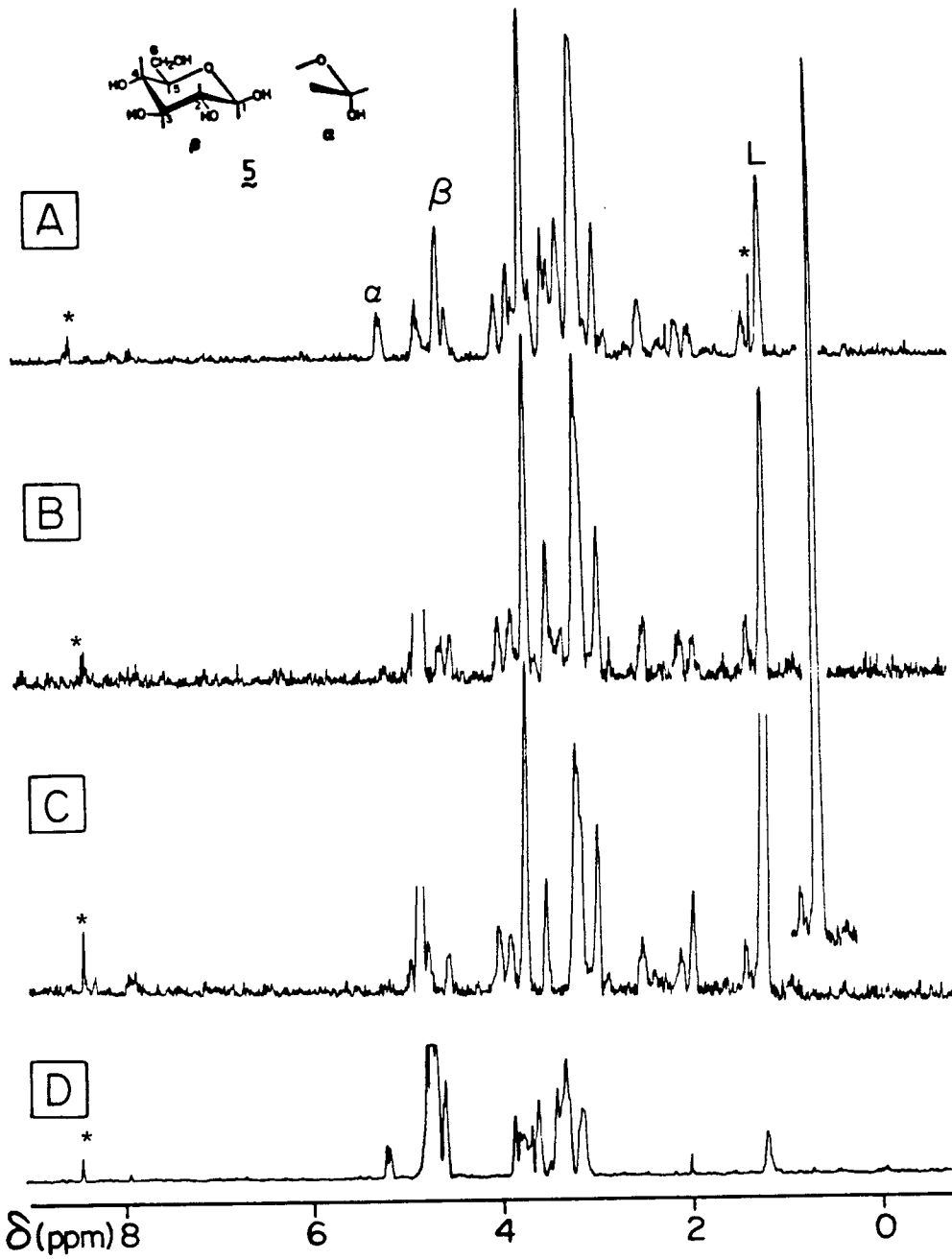

Figure 2.11: Spectra from SEAS with T=70 ms. (A) RBC (haematocrit 90%) incubated for 2 hours in 10 mM glucose, (B) RBC depleted in glucose but with equal volume of 10 mM glucose added (haematocrit 50-60%). (C) Same as for (B) but the experiment was carried out about 10 hours later. (D) Supernatant of the RBC and glucose mixture (NA=200) showing mostly the glucose spectrum and some lactate signals. Experimental times were approximately 1½ to 2 hours using 1400 acquisitions for A, B and C. α and β refer to the anomeric protons and L to the methyl signal from lactic acid (see experimental section)

60% haematocrit solution by adding 10 mM glucose in D_2O containing the Krebs-Ringer buffer solution. The appearance of the lactate peak indicates that within the time course of the experiment ($\simeq$ 2 h), glucose has diffused into the cell and has been metabolized. With time, this lactate peak increases in size due to the glucose metabolism by the glycolytic pathway, and this effect is accompanied by a decrease in the intensity of the glucose peaks in the SEAS trace (Fig. 2.11C). The initial increase in the lactate resonance is subsequently followed by a decrease in intensity which is due to the exchange of the protons in the methyl group with the solvent deuterons (figure is not shown). These observations are as expected and have been reported by earlier workers using the half-SEFT technique (13). However, a striking feature of the traces shown in Fig. 2.11A, B and C is the absence of the signals corresponding to haemoglobin, which were a dominant characteristic in all the half-SEFT spectra reported in the literature. With time, however, we did see signals corresponding to haemoglobin; the example shown in Figure 2.10B is from a RBC sample (prepared via Procedure A) after about thirty hours. It was also noted that the intensity of the haemoglobin signals in the samples containing glucose (Procedure B) was smaller than in those that were depleted in glucose, indicating the relative stabilisation of RBC in an aqueous glucose medium.

Figure 2.10C shows a SEAS trace that was obtained from a solution prepared by lysing the RBC pellet (via Procedure B) by the addition of a few drops of D_2O.[1] Now the characteristic peaks, mostly due to the histidine residues

[1]RBC are sensitive to slight changes in the osmotic pressure ("tonicity") of the medium. A few drops of D_2O decreases the tonicity, causing lysis (release of haemoglobin, etc.). This is seen as a bright red coloration of the supernatant. For obvious reasons this is not noticeable in the pellet.

of haemoglobin, are clearly seen. In order to resolve the peaks in the SEAS traces more clearly, the supernatant from a lysed RBC sample (depleted in glucose) was subjected to SEAS with a delay, T = 80 ms, and with sample spinning (cf. Figs. 2.10C and D); note the resolution of peaks "a" and "b" which are clearly visible as a triplet and quartet respectively.

As expected SEAS can be used to obtain high resolution spectra of small molecules from within the broad peaks of the RBC, without the complications of phase- and intensity-anomalies which are implicit in the half-SEFT experiment. Based on our albeit limited experience so far, it would seem that SEAS leads to the following information about RBC:

a) The decrease in intensity of the signal of the anomeric proton of the glucose is an indication of the consumption of glucose by the glycolytic pathway in the RBC.

b) The appearance of the lactate peak, both in the sample containing the pellet (Fig. 2.11B) and in the supernatant liquid (Fig. 2.11D) are indicative of the diffusion of glucose into, and of lactate out of the cells.

Studies of the supernatant liquid, rather than of the cell suspension (pellet) itself, offer number of advantages. In terms of the NMR experiment, the supernatant liquid is a homogeneous solution and provides spectra which can be studied by most of the conventional NMR techniques to provide high resolution NMR spectra (eg. Figs. 2.10C and 2.11D).[1] In terms of the biochemistry of the system, this provides a suitable method for following the kinetics of the system. However, since the RBC are undergoing dynamic changes

[1]The relaxation times of solutes in the supernatant are much longer than those in the pellet; this favours the conditions for an "ideal" SEAS experiment (see Sec. 2.4) and also improves the sensitivity of the technique (it shall be recalled that the intensity of signals in a spin-echo experiment is related to their spin-spin relaxation times as explained in Section 2.2).

both "chemically" and "physically" (eg. diffusion of molecules across the membrane) such studies will be limited if the total data acquisition time for an experiment is too long.

The absence of haemoglobin peaks in those RBC samples (eg. Fig. 2.11A) which had been freshly prepared, and the appearance of these signals in partially lysed samples, suggests strongly that it is not possible to detect resonances from haemoglobin within the RBC. This observation and conclusion contradicts that suggested by earlier workers who have assumed that the signals detected in (half-)SEFT experiments are from molecules within the RBC. It also seems apparent from all the half-SEFT spectra previously published that partial lysis of cells had occurred during the course of the experiment. Unfortunately, it is not possible to conclude from the SEAS experiments performed so far whether the signals corresponding to the smaller molecules (eg. glucose and lactate) represent molecules which are internal and/or external. Such small molecules can diffuse across the membranes and hence may either be present in the internal cytoplasm or in the aqueous extracellular space. Brindle et al. (22) have assumed that the internal medium is magnetically homogeneous whereas the extracellular space is magnetically inhomogeneous, and on that basis have concluded that the signals from molecules outside the cells relax more rapidly than those within the cell.[1] This conclusion was based on their observation of a constant rate of increase of externally added (0.01 ml of 0.3M) alanine peak in their SEFT experiment, both with and without the addition of a paramagnetic reagent (0.001 ml 0.025 M Dy-DTPA[2]). It was assumed that Dy-DPTA, which is a large

[1]The signals were considered to decay as a function of T^3 (see the footnote on p. 19), due to the larger field gradients outside the cells.

[2]Diethylenetriamine penta-acetic acid.

paramagnetic complex, does not diffuse across the membrane, and would affect only the external molecules by creating large field gradients in the extracellular region. The increase in the alanine (or lactate) peaks were then regarded as due to diffusion of these molecules into the cells. However, there seems to be a number of inconsistencies in those studies; the addition of very small volumes of (relatively concentrated) material and its subsequent diffusion or mixing in the "heterogeneous" and viscous RBC medium should have been evaluated. In addition, the effect of lysis should have also been taken into consideration in their study. These factors may well be the reason for some of the rather substantial inconsistencies in their experimental results as quoted; for example (22), "it was also found that variations in transport rate for alanine up to $\pm$ 50% were observed in erythrocyte from different people. This was much greater than the experimental error and larger than the differences observed between samples prepared in $^{1}H_2O$ and $^{2}H_2O$. At present the origin of these variations is not clear."

It has been reported by many workers that glucose binds chemically and physically with haemoglobin and other proteins (27); although the extent of binding is not yet clear, some have suggested up to 80% of glucose may be in bound form in RBC. If this were so, it would not seem unreasonable to suggest that most of the glucose may be in bound form inside the cell and hence be undetectable by SEFT techniques. Certainly the mobility of the bound glucose units would be reduced significantly over that of the free molecules and as a result the spin-spin relaxation rates of the corresponding protons would be increased and hence the corresponding NMR signals would decay so rapidly during the (T) delay period as to be undetected.[1]

[1]In a different series of experiments it was observed that the signal corresponding to a carbohydrate unit which was linked to bovine serum albumin was virtually undetectable (at T~60 ms) and decayed almost at a similar rate (R_2) as the BSA signals.

In order to reach a positive conclusion as to whether the detected signals of small molecules in the SEFT experiment were from inside or outside the cells it would be necessary to study molecules but with all diffusion processes across the membrane frozen by the use of a specific "paralysing" agent. A preliminary attempt was made in this study using $HgCl_2$ to inhibit the "glucose diffusion pump"; unfortunately, however, the $HgCl_2$ changed the physical nature of the sample which was not satisfactory for a comparative NMR study involving T_2 experiments. At the time of submission of this thesis we were investigating suitable agents for use with RBC systems, but the substances required were not available.

It is apparent from this study, as from the other, that biological samples can, under well controlled conditions, be studied by NMR techniques. However as with most other biochemical studies proper control experiments are needed to understand the effect of a foreign environment to living systems and the associated chemical and physical changes of the sample on the NMR (SEFT) experiment.

References (Chapter II)

1. Hahn, E.L. Phys. Rev. (1950) 80, 580.
2. Hahn, E.L., Maxwel, D.E. Phys. Rev. (1952) 88, 1070.
3. Carr, H.Y., Purcell, E.M. Phys. Rev. (1954) 94, 630.
4. Ernst, R.R., Anderson, W.A. Rev. Sci. Instrum. (1966) 27, 93.
5. Allerhand, A., Cochran, D.W. J. Amer. Chem. Soc. (1970) 92, 4482.
6. Meiboom, S., Gill, D. Rev. Sci. Instrum. (1958) 29, 688.
7. Freeman, R., Hill, H.D.W. "Dynamic Nuclear Magnetic Resonance Spectroscopy", Jackman, L.M., Cotton, F.A. Eds.; Academic Press: New York, 1975; Chapter 5.
8. Shaw, D. "Fourier Transform NMR Spectroscopy", Elsevier: Amsterdam, 1976.
9. Martin, M.L., Martin, G.J., Delpuech, J.J. "Practical NMR Spectroscopy", Heyden: London, 1980.
10. McLaughlin, A.C., McDonald, G.G., Leigh, J.S. J. Magn. Reson. (1973) 11, 107.
11. Bax, A., Mehlkopf, A.F., Smidt, J. J. Magn. Reson. (1979) 35, 373.
12. Campbell, I.D., Dobson, C.M., Williams, R.J.P., Wright, P.E. FEBS Lett. (1975) 57, 96.
13. Brown, F.F., Campbell, I.D., Kuchel, P.W., Rabenstein, D.C. FEBS Lett. (1977) 82, 12.
14. Hall, L.D., Sukumar, S. J. Magn. Reson. (1979) 38, 559.
15. Dwek, R.A. "Nuclear Magnetic Resonance in Biochemistry", 2nd ed., Clarendon Press: Oxford, 1975.
16. James, T.L. "Nuclear Magnetic Resonance in Biochemistry", Academic Press: New York, 1975.

17. Seiter, C.H.A., Feigenson, G.W., Chan, S.I., Hsu, M. J. Amer. Chem. Soc. (1972) 94, 2535.

18. Campbell, I.D., Dobson, C.M., Williams, R.J.P., Xavier, A.V. J. Magn. Reson. (1973) 11, 172.

19. Akasaka, K., Konrad, M., Goody, R.S. FEBS Lett. (1978) 96, 287.

20. De Marco, A., Wuthrich, K. J. Magn. Reson. (1976) 24, 201.

21. Richarz, R., Wuthrich, K. J. Magn. Reson. (1978) 30, 147.

22. Brindle, K.M., Brown, F.F., Campbell, I.D., Grathwohl, C., Kuchel, P.W. Biochem. J. (1979) 180, 37.

23. Brown, F.F., Campbell, I.D. Phil. Trans. R. Soc. Lond. B. (1980) 289, 395.

24. Rose, I.A., Rose, Z.B. (1969) Compr. Biochem. 17, 96.

25. Sturgenor, D.M. (ed.) "The red blood cell", 2nd ed., Academic Press: New York, 1974.

26. Jones, A.J., Kuchel, P.W. Clinica Chemica Acta (1980) 104, 77.

27. Nathan, S. Scientific American (1980) 243, 90.

CHAPTER III

TWO-DIMENSIONAL FOURIER TRANSFORM SPECTROSCOPY

3.1.1 Introduction

The concept of a two-dimensional Fourier transform NMR experiment was first proposed by Jeener in 1971 (1), but the importance of his idea was not realized until several years later. The first experiments related to high resolution NMR were published in 1975 (2,3) by Ernst's group in Switzerland, to be followed later by a detailed theoretical analysis of 2D NMR spectroscopy (4) which has formed the basis for most subsequent developments in this area. This concept has also been applied in solid state NMR (5,6), zeugmatography (7), and in detection of forbidden (zero and multiple quantum) transitions (4). The work of this thesis deals mainly with proton 2D J spectroscopy, but also includes heteronuclear chemical shift correlation (2D) spectroscopy and preliminary results from zero quantum transition (2D) spectroscopy (8,9).

2D Fourier transform NMR experiments involve the generation of a data matrix, $S(t_1,t_2)$, which represents the responses of the nuclear spins as a function of two time variables t_1 and t_2. Double Fourier transformation of this data array with respect to these two time domains generates a two-dimensional spectrum, $S(f_1,f_2)$, in which the magnetization response of the system is displayed over the orthogonal frequency axes, f_1 and f_2 respectively. The f_2 domain generally represents the conventional (or the observable) spectrum and the f_1 domain represents some "correlated" frequencies; the choice of the two frequency domains depends on the nature of the pulse sequence used. For example, in the ^{13}C ^{1}H 2D chemical shift correlation experiments (10,11,12) the two dimensions represent proton and carbon resonant frequencies respectively, and in 2D J spectroscopy (13,14) the two domains correspond to chemical shifts and coupling constants respectively. Thus this technique can be used to either separate or correlate NMR frequency

components in a variety of rather unique ways. Such information may be obtained by multiple resonance methods (15) in one-dimensional (1D) NMR spectroscopy, however, the versatility of the 2D technique substantially extends the potential of NMR spectroscopy for the solution of chemical and biological problems.

Most of the discussions in the following sections pertain to proton 2D J spectroscopy, giving the advantages and limitations of the technique and including various modifications developed during the present study which make it suitable for general chemical applications. Initially the basic pulse sequence and the data processing procedures are explained, followed by a more practical approach of the features of 2D J spectroscopy. The latter part of the chapter contains more detailed discussion of a few topics related to 2D J spectroscopy which are of practical significance. This approach was adopted for the convenience of the reader who may not be familiar with the concepts and nomenclature in 2D NMR spectroscopy. It should be noted that the general discussions are strictly applicable only to weakly coupled systems.

3.1.2 The pulse sequence and data acquisition

The basic pulse sequence used in homonuclear (proton) 2D J spectroscopy is that of Carr and Purcell (C-P, method A; (18)) represented by,

$$\{90^{o} - n.T - 180^{o} - n.T - \text{Acquisition}\}$$

and is diagramatically represented in Figure 3.1;[1] the basic pulse sequence and its effect on the magnetization vectors was previously discussed in Chapter II in relation to the spin-echo FT experiments. In a 2D J experiment

[1]The "heteronuclear" analogue of this experiment, for example ^{13}C 2D J spectroscopy is performed by either simultaneously applying an 180° pulse to both nuclei ("proton-flip" (14)) or by gating the ^{1}H decoupler during one of the delay periods (13,14).

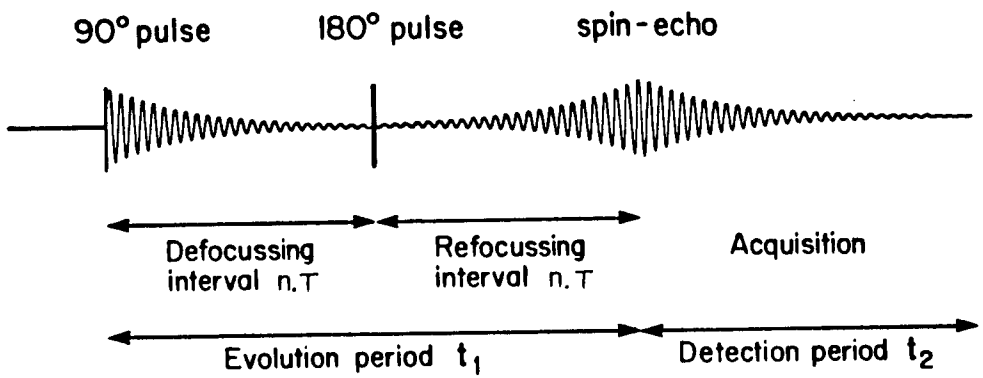

Figure 3.1: The 2D J pulse sequence N half-echo signals are acquired for different evolution periods (t_1, which are incremented by a constant value of 2T. n=0, 1, 2 ... N-1).

a series of C-P pulse sequences are performed in which t_1 is incremented by a constant time T so that $t_1 = 2nT$, where n = 0, 1, 2, ... N-1. The sampling rate in the t_1 domain is equal to 1/2T corresponding to an f_1 spectral width of $\pm SW_1 = 1/4T$. The number of experiments N will correspond to the number of points in f_1, resulting in a digital resolution of 1/2NT Hz[1]. The signals that are acquired, $S(t_1,t_2)$, for each t_1 increment are saved for subsequent data processing routines.

3.1.3 Data processing

The various data processing steps involved in 2D J spectroscopy are summarised in Scheme 1. The acquired signal $S(t_1,t_2)$ encodes all the characteristics of a conventional free induction decay signal containing chemical shift and coupling constant information, with each component decaying at its characteristic decay rate (R_2*). The phases of these components are, however, dependent on the effect of the 180° pulse on the magnetization vectors during the evolution period, t_1. The "pre-acquisition" information of each component are coded into the detected signal, $S(t_1,t_2)$ and are reflected in the spectra $S(t_1,f_2)$ shown in Figure 3.2, which were obtained after the first Fourier transformation with respect to t_2. The phase and intensity variations observed, as a function of time t_1 are predictable as discussed in Chapter II, and has been reviewed in the past (19,20). The homogeneity- and chemical shift-refocussing effects of the 180° refocussing pulse are not obvious from Figure 3.2, nor is the fact that the behaviour of the signals as a function of t_1 is only related to the spin-spin coupling

[1]In practice it is preferable to set the ratio of the digital resolution in f_2 to f_1, to an integer value to minimise distortions arising from 2D interpolation procedures in subsequent data processing routines.

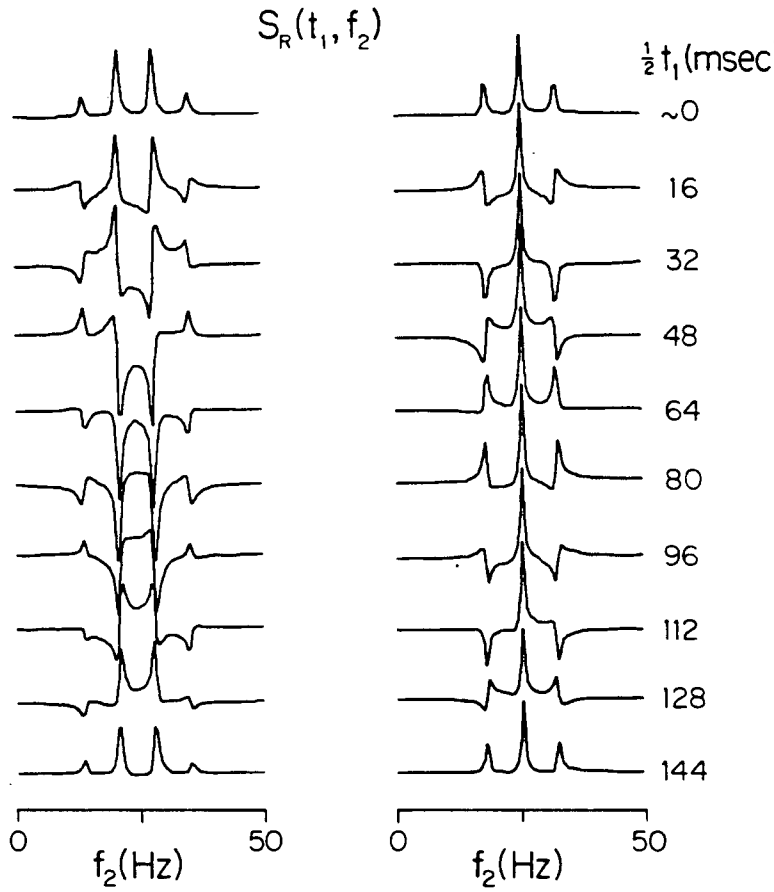

Figure 3.2: Phase modulation of spin-echo spectra. The quartet and triplet resonances of diethyl malonate showing the J modulation after the first FT. The phase of the outer lines of the quartet is "cycled" three times (3x360°), while the phase of the inner ones changes through one cycle in the same period. For the triplet the outer lines are cycled twice; however the central component is unmodulated (see text).

SCHEME 1

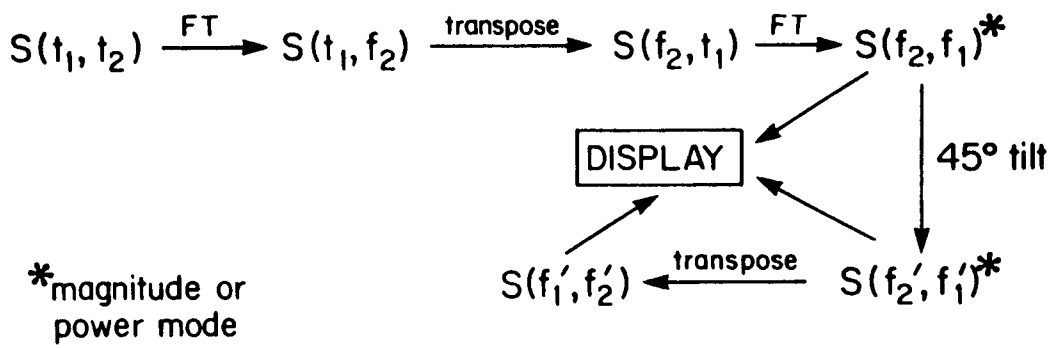
S(t1, t2)
FT
S(t1, f2)
transpose
S(f2, t1)
FT
S(f2, f1)*
DISPLAY
45° tilt
S(f1′, f2′)
transpose
S(f2′, f1′)*
*magnitude or power mode

constant. However, these features can be visualized by transposing the data matrix $S(t_1,f_2)$ to $S(f_2,t_1)$, since this makes it possible to trace the behaviour of both the real and imaginary points corresponding to any chosen resonance frequency in f_2, as is shown in Figures 3.3 and 3.4.[1]

In weakly coupled systems these t_1 time domain signals contain the following characteristic features:

a) since chemical shift effects are "refocussed" at the echo maxima (Fig. 2.2) the "echo-interferograms" (21), $S(f_2,t_1)$, do not contain chemical shift frequency information,

b) according to equation [2.2] the phase of each signal of an A_nX_m spin system is given by

$$= \pm 2\pi M_x J t_1 \text{ radians;} \qquad [3.1]$$

this reflects the opposite phases of the high and low frequency components of a multiplet (cf. Figs. 2.2 a-f, 3.3 and 3.4). Note that singlets and central component of a multiplet (for which $M_x = 0$) are unmodulated.

c) the time dependent (t_1) phase modulation of each component which is also referred to as J-modulation, occurs at a frequency proportional to the magnitude of the spin-spin coupling constant,

d) because the static magnetic field inhomogeneity effects are refocussed at the echo maxima, it follows that each "echo-interferogram" will show an exponential damping with a rate constant equal to the "natural" spin-spin relaxation rate (R_2) (diffusion effects and experimental imperfections being neglected).

[1]The time domain signal, $S(f_2,t_1)$ is analogous to the complex time signal observed by quadrature phase detection in conventional NMR. The major difference being that the latter is obtained as a result of resonance (or coherence) phenomenon whereas the former is due to either phase or amplitude modulation (eg. "gated decoupler" method) of signals.

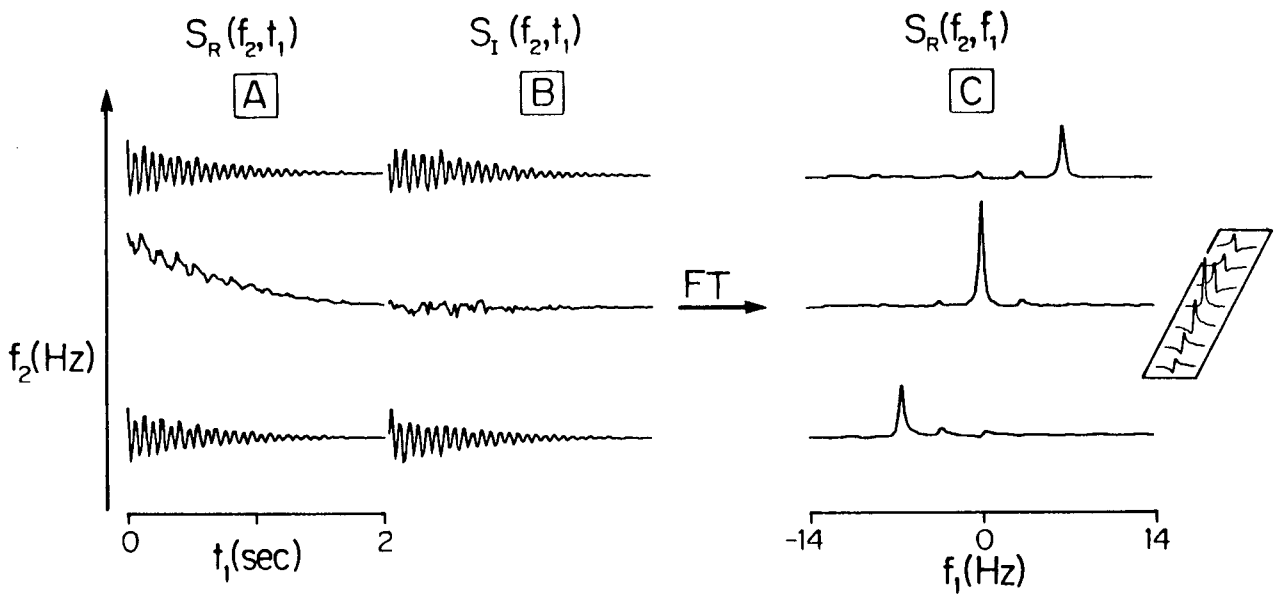

Figure 3.3: A and B represent selected real and imaginary time domain signals in t_1 of the triplet components of diethyl malonate obtained by transposing the $S(t_1,f_2)$ data matrix. A second Fourier transformation yields the corresponding traces $S(f_2,f_1)$, of the 2D J spectrum (C). The outer lines of the triplet correspond to positive and negative frequencies, as a result of the sense of phase modulation, which can be seen in the upper and lower traces of B (cf. Figs. 3.2 and 2.2). The ripples on the unmodulated time domain signal are due to noise and artifacts which are visible in the Fourier transformed spectrum. The adjacent traces from a 2D plot are shown in the inset to illustrate the "phase-twist" effect of 2D peaks.

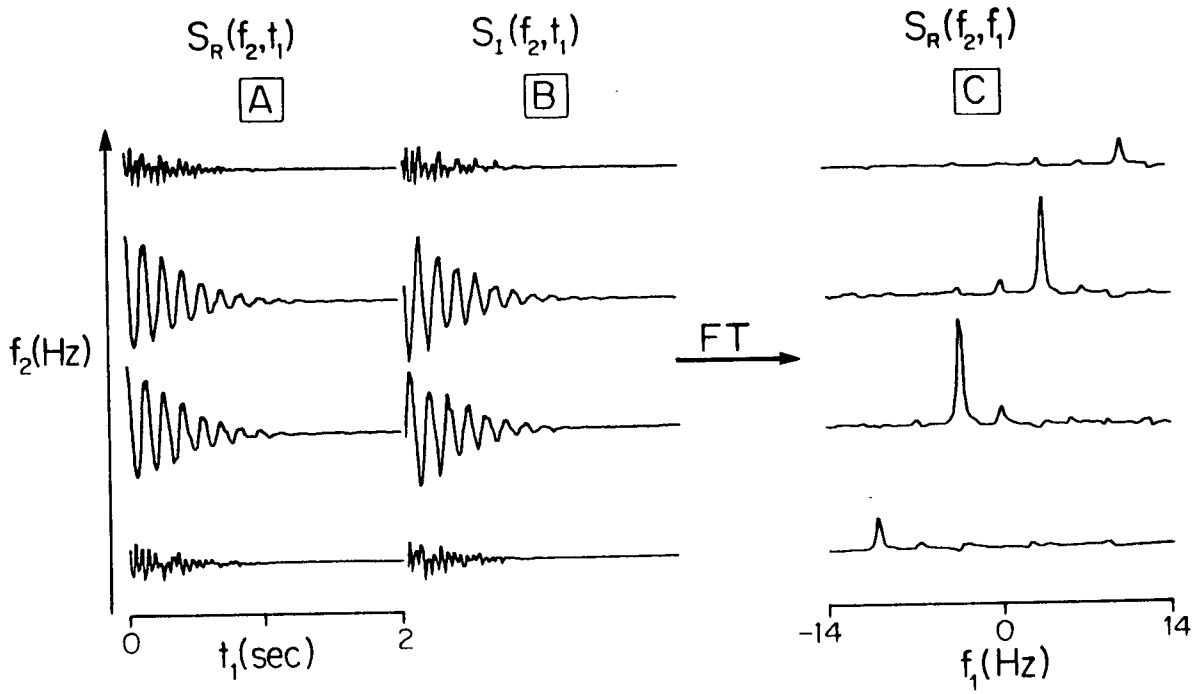

Figure 3.4: As for Figure 3.3, but showing the components of the quartet of diethyl malonate.

The implications of these features becomes more obvious in the frequency space display, $S(f_2,f_1)$, which is obtained by a second Fourier transformation of $S(f_2,t_1)$ with respect to t_1; Figure 3.3C and 3.4C show the relevant traces of the triplet and quartet respectively. These traces correspond to the peaks seen in the partial J spectra (22) which are obtained from the final 2D J spectrum; all multiplets in the f_1 domain are symmetric with respect to zero frequency, and the linewidth of each peak is determined by its characteristic spin-spin relaxation rate, R_2.

Although the traces in Figures 3.3C and 3.4C correspond to resonance frequency in f_2, reflecting a pure absorption signal (after applying the same phase correction), the complete 2D J spectrum will show a complex two-dimensional lineshape which consists of a mixture of two absorption and dispersion signals; this is referred to as the "phase-twist" and is illustrated by the inset in Figure 3.3 (4,21). These complications are often conveniently avoided by presenting the absolute-value mode display.

There are many ways of displaying a 2D J spectrum in order to extract the necessary information from it. One method is to plot all the traces in the form of a "stacked plot"; although aesthetically pleasing, this display suffers from the principle disadvantages that it is rather time consuming and it is inconvenient to obtain from it by direct measurements the NMR parameters of interest. A more rapid display routine for complex 2D spectra may be the isometric (contour) plot; this provides a convenient means of representing frequencies and intensities as illustrated by the plot of the 2D spectrum of a quartet in Figure 3.5.

Perhaps the most useful and convenient displays for measuring frequencies and intensities are obtained by taking projections of selected regions of a 2D

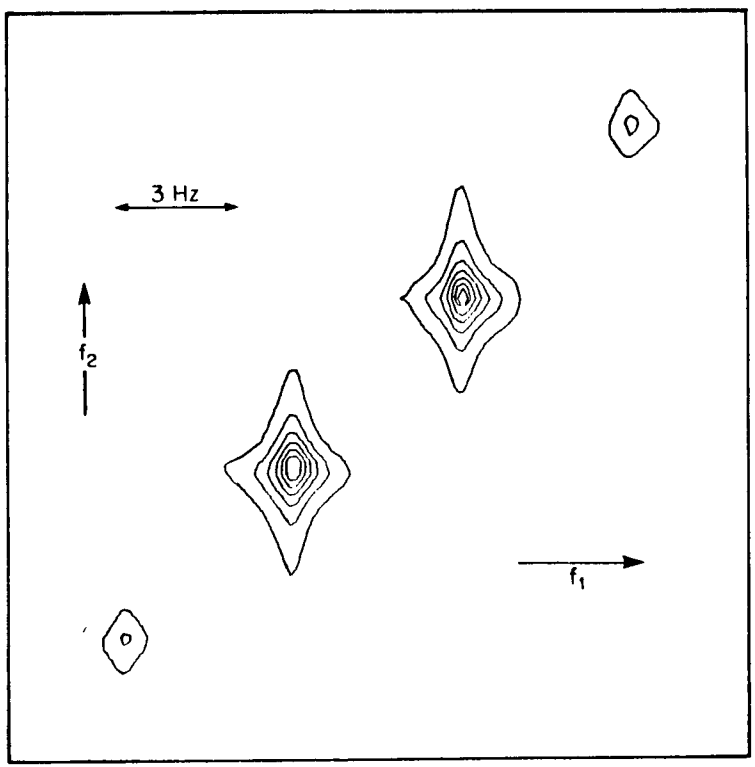

Figure 3.5: Contour diagram of the quartet resonance of diethyl malonate from a 2D J spectrum plotted in the absolute value mode. The two axes have identical scales hence the multiplet lies along the diagonal or at 45°. As expected the "tails" along f_2 appear broader than those along f_1.

spectrum onto various axes (23). The "summed" or "integral" projection is obtained by summing each point of a 2D spectrum taken along a specified direction onto an axis perpendicular to it. A "maximal" projection (24) corresponds to a trace representing the highest point along a particular direction.

A diagrammatic representation of the various display modes are shown in Figure 3.6; the "model" 2D J spectrum in Figure 3.6A is shown as a contour (isometric) plot.

It is worthwhile noting at this juncture that each component of a weakly coupled multiplet in a 2D J spectrum lies on an axis such that, $\delta f_2/\delta f_1 = 1$; if both f_1 and f_2 are plotted on the same scale, as in Figure 3.5, this axis would be set along the diagonal or at 45^{o} to the reference axis. Projection (integral) of the 2D spectrum onto the f_2 axis gives the equivalent of the conventional, one-dimensional spectrum (Fig. 3.6a) and shows a well resolved quartet and, although it is not unambiguous, two overlapping triplets. A projection of the 2D J spectrum onto an axis such that $\delta f_2/\delta f_1 = -1$, gives three "singlets" each corresponding in f_2 value to the chemical shift frequency of the resonance; this arises, as explained earlier, because each multiplet in a 2D J spectrum lies at "45^{o}" (25). This trace is often referred to as 45^{o} or "skew" projection, and corresponds to a "broad-band proton-decoupled" proton spectrum. Projection onto the f_1 axis of the section (slice) corresponding to each multiplet from the 2D J spectrum yields a "partial J spectrum". This is illustrated by Figure 3.6C for the quartet and Figure 3.6C for the triplets; the latter inevitably result in the overlap of both the triplets, centred about zero-frequency in f_1. Although in a limited number of cases this projection may help to resolve overlapping

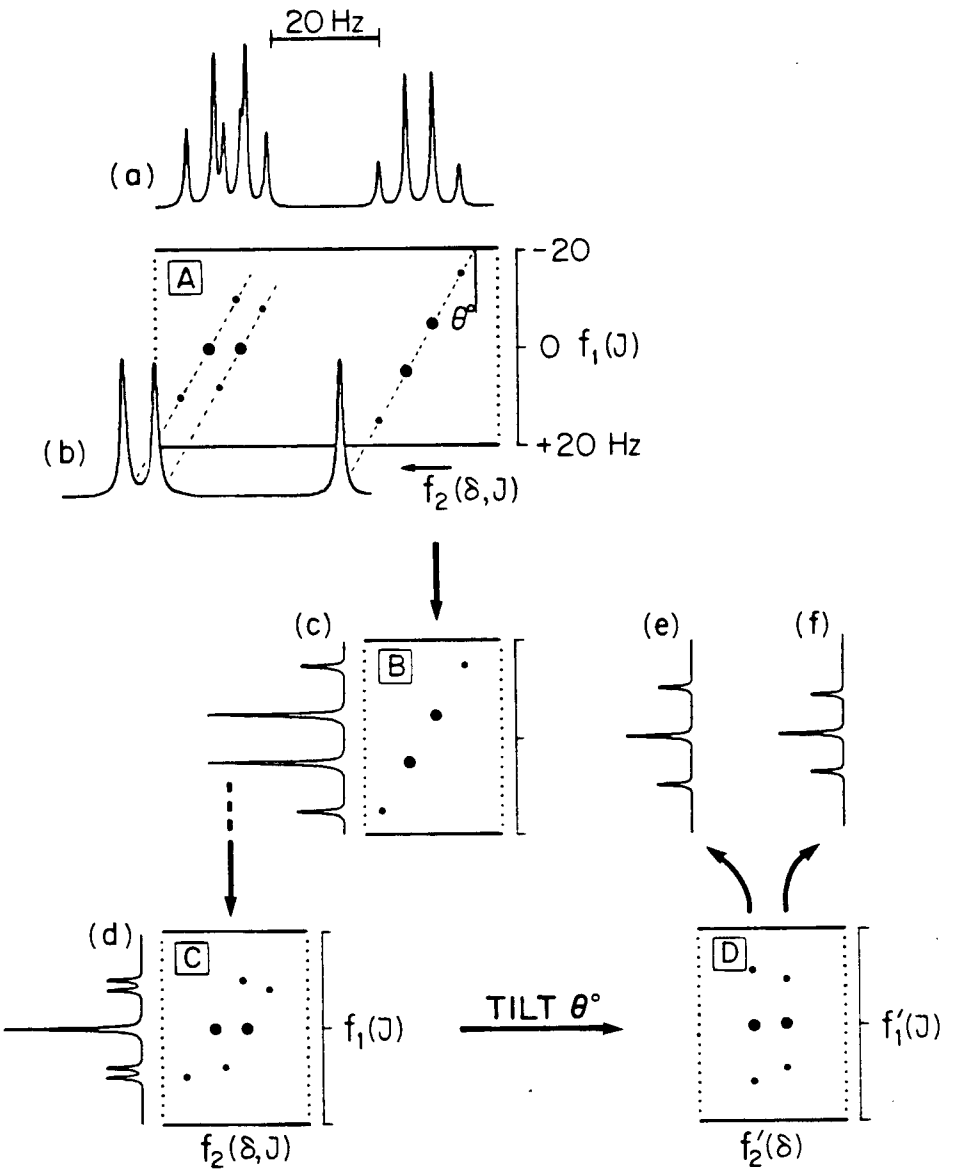

Figure 3.6: Diagrammatic representation of the various display modes used in proton 2D J spectroscopy including the tilt routine. The (untilted) 2D J spectrum (A) when projected onto the f_2 axis yields the conventional spectrum, (a). A 45° projection gives a "proton-decoupled" proton spectrum, (b). Projection of a slice of the 2D J spectrum (B) gives the partial J spectrum (c) of the quartet. Similar projection of C, yields a trace with the triplets superimposed (d). Tilting the 2D J spectrum by (45°) yields a $S(\delta,J)$ matrix (D); cross-sections at the respective chemical shifts give the partial J spectra of the triplets.

multiplets (26), this is generally not the case in practice, particularly when dealing with complex molecules. Fortunately a more elegant method has been described by Nagayama et al. (23) - the whole 2D data-array is "tilted" by an angle θ (equivalent to 45^{o}) about $f_1 = 0$ using an interpolation procedure, to yield a "tilted 2D J spectrum", $S(f'_1, f'_2)$ or $S(J, \delta)$. As represented by Figures 3.6C-3.6D, this procedure allows complete separation of chemical shift and coupling constants onto perpendicular axes; it is now possible to "pick out" from the 2D spectrum the particular f_2 trace corresponding to each multiplet as shown in Figure 3.6e and 3.6f. In effect this amounts to taking "cross-sections" of a 2D J spectrum, $S(f_1, f_2)$ along the dotted lines as indicated in Figure 3.6A. This data manipulation procedure converts the 2D J experiment into an extremely powerful technique for resolving overlapping multiplets.

At the time this thesis work was started there were two excellent papers in the literature, one based on a theoretical (4) description and the other giving a more practical (21) approach to 2D NMR spectroscopy. Also, two preliminary communications, one using a mixture of amino acids (27) and a second, a biomolecule (28) had been published to illustrate the potential importance of proton 2D J spectroscopy in biochemistry. However there was little insight or practical details which would enable a practicing chemist to know in advance, or with certainty, the types of practical difficulties which might accompany any attempt to apply proton 2D J spectroscopy to typical organic molecules; development of that insight was chosen as the principal objective of the studies described here. As will be seen in the following discussion, this led to recognition of several limitations of the method and

solutions to them. Overall, the general strategy and objective of the study was development of convenient, efficient and versatile procedures for analysis of NMR spectra of complex molecules.

3.2 Applications of proton 2D J spectroscopy in chemistry

3.2.1 General analysis

Some of the general features of proton 2D J spectroscopy will now be illustrated using as a "model" trideuteriomethyl 2,3,4,6-tetra-O-trideuterioacetyl-α-D-glucopyranoside (6) (26). The 2D J spectrum, $S(f_2,f_1)$, of a 0.1M solution of 6 in benzene-d_6 is displayed in the power mode in Figure (3.7). Although such multiple-trace or "stacked plot" displays often reveal interesting new information (for example, in this case that both H-3 and H-4 are doublets-of-doublets rather than triplets), considering the time required for the complete plot (ca. two hours in this case for plotting the 128 traces of the 2D J spectrum), the useful NMR information is best, certainly most rapidly, obtained from the various projections of the 2D J spectrum. Thus the 45^{o} projection yields the proton-decoupled proton spectrum shown in Figure 3.7B (and hence the proton chemical shifts) and a projection onto the f_2 axis corresponds to the conventional one dimensional spectrum (Fig. 3.7A). Projection of different "slices" of the 2D J spectrum onto the f_1 axis yield the partial J spectra for each multiplet as shown in Figure 3.8. Comparison of these traces with the spectra obtained by conventional Fourier transform NMR (Fig. 3.7A) shows the enhancement of resolution due to static field inhomogeneity refocussing effect of the spin-echo pulse sequence; therefore this approach leads to a

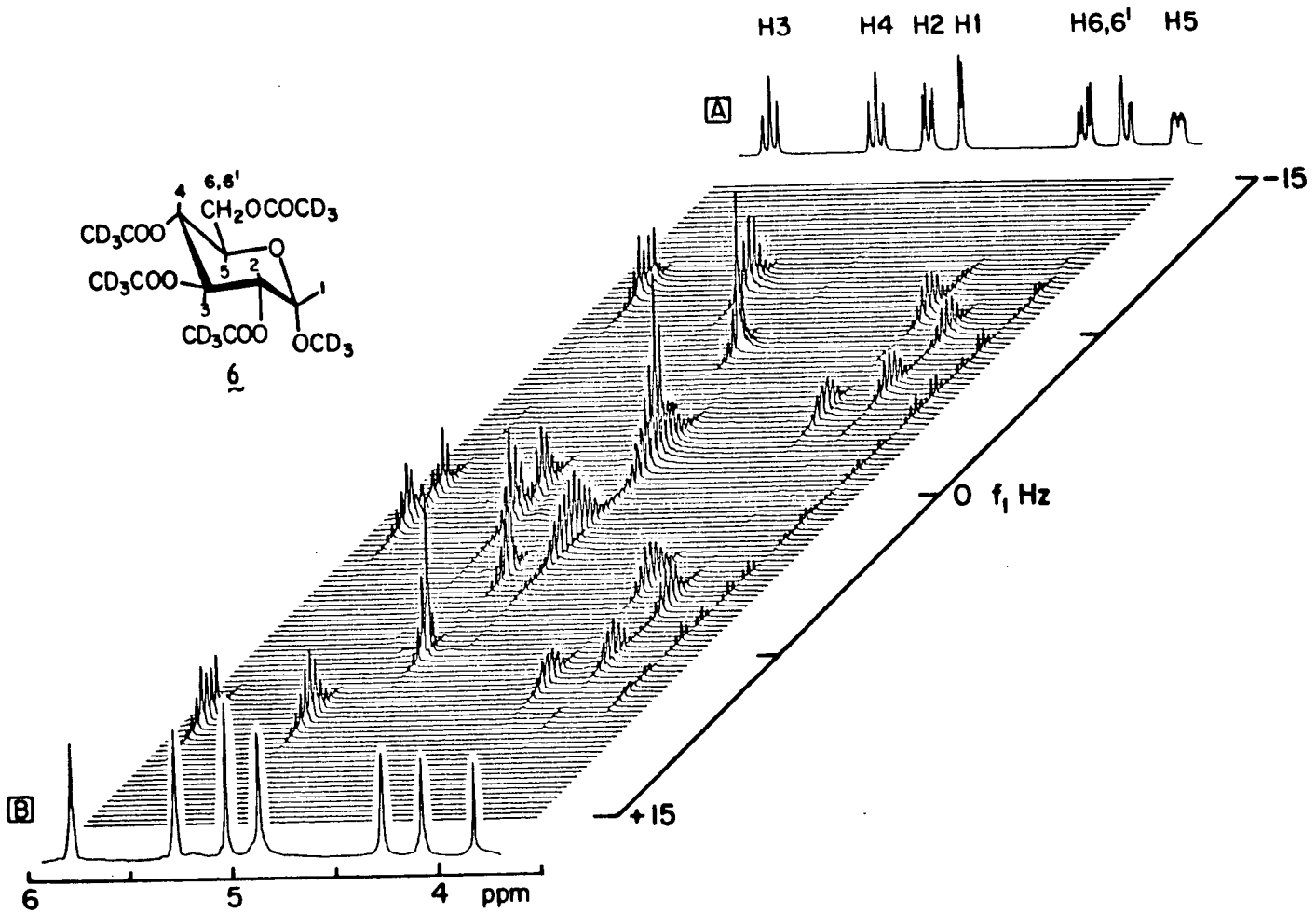

Figure 3.7: 2D J spectrum of the α-methyl glucoside (6) plotted in the power mode. A and B are the normal and proton-decoupled proton spectra respectively. Note the resolution enhancement effect of the multiplets in the f_1 dimension (cf. Fig. 3.8). Experimental parameters: NA=4; SW=1250; AT=0.82 s; N=128; M=4096; T=17.86 ms; SF=270 MHz.

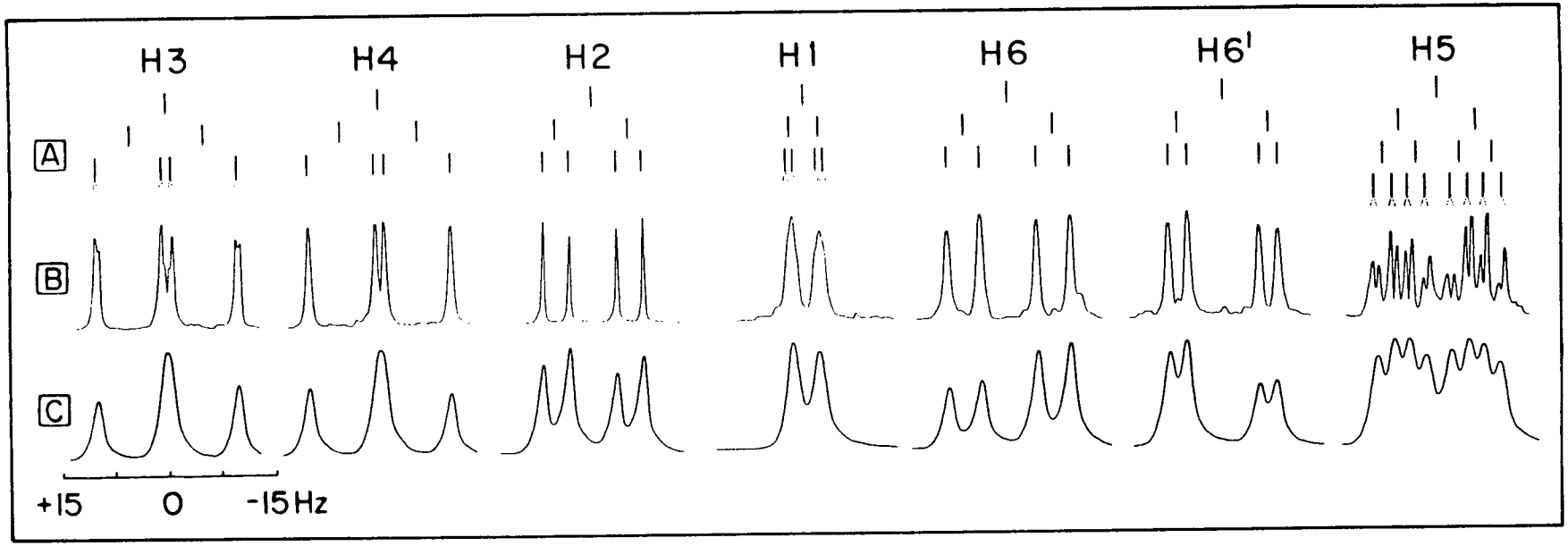

Figure 3.8: Comparison between the normal (C) and partial J spectra (B) obtained from the 2D J spectrum shown in Figure 3.7. The improved resolution is clearly noticeable, especially in the H-3 and H-5 multiplets which show a long-range coupling of ca. 0.9 Hz. The apparent broadening of the H-1 signals in the partial J spectra is due to the presence of unresolved long-range couplings to H-3 and H-5.

more accurate determination of J values.[1] For example, the multiplet due to H-5, which appears as eight lines in the normal spectrum now appears as sixteen lines, showing the long-range coupling (J~0.9 Hz) across four bonds to H-1 which was originally obscured by the field inhomogeneity broadening (29); a small long range coupling in H-3 is only partly resolved because of inadequate digital resolution.

In normal practice, however, NMR spectra are often complicated by either strong coupling or overlap of resonances, or sometimes both; Figure 3.9 illustrates the analysis by 2D J spectroscopy of a typical example, 2,3,4-tri-O-acetyl-6-deoxy-α-D-glucopyranosyl- 3,4-di-O-acetyl-1,6-dideoxy-β-D-fructofuranoside (7). Figure 3.9A shows a region of the normal 1D spectrum below which is the corresponding 45° skew projection (Fig. 3.9B). Although the normal spectrum is complicated by some overlap, most of the individual proton chemical shifts can be easily measured from proton-decoupled proton spectrum (Fig. 3.9B). The exceptions involve strongly coupled multiplets from the 3-F and 4-F resonances (F and P refer to the furanose and pyranose rings respectively), which give more complicated patterns because of the strong coupling within each geminal pair; this illustrates one of the serious limitations of both 2D and conventional NMR spectroscopy and is one of the several reasons why it is preferable to work at the highest magnetic field strength available. A more detailed discussion of strong coupling effects in 2D J spectroscopy is given in Section 3.2.6.

Returning now to the disaccharide (7), the normal and partial J spectra of the 2-P and 4-P region are shown in Figures 3.9C and 3.9D respectively. Assignment of the spectral pattern of the 1D spectrum is not immediately

[1]The NMR parameters are tabulated in Chapter V along with the ZQT spectroscopy data on compound 6.

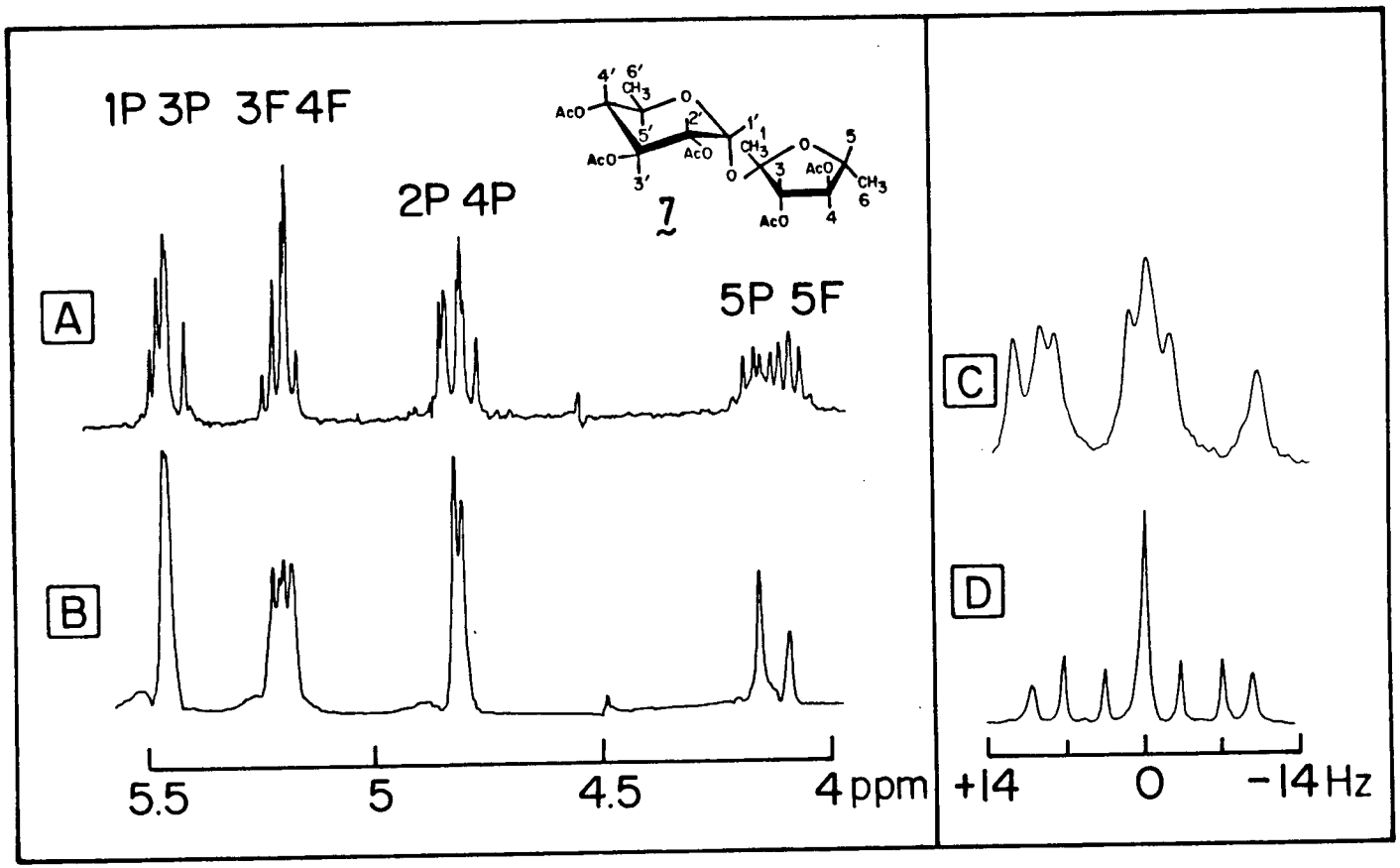

Figure 3.9: Partial 2D and 1D proton spectra of 7 in $CDCl_3$ (0.1M). A, the normal and B, the proton-decoupled proton spectra; in the latter spectrum the weakly coupled protons appear as singlets, but the strongly coupled regions of the 3F and 4F protons give more complex patterns.C, is an expansion of the 2P and 4P region from a 1D spectrum and D, the corresponding partial J spectrum obtained by projecting the 2D J spectrum onto f_1. The P and F suffixes refer to the pyranose and furanose units respectively.

obvious; however, the partial J spectrum shows the two multiplets symmetrically disposed with respect to zero-frequency, which can be assigned on the basis of their differing line widths. The three broader components constitute the H-4' multiplet and the narrower, doubleted doublet are due to the H-2' resonances. In conventional high resolution NMR the line widths are usually determined by the instrumental line broadening effects rather than the "natural" spin-spin relaxation time, which makes assignments based on line widths difficult, or more often impossible; it will be recalled that the partial J spectra represent line widths that reflect the respective "natural" spin-spin relaxation times.

In both the above two examples the spectra were displayed in the power mode[1] and as a result the triplet intensities in Figure 3.9D appear in the ratio of 1:4:1 rather than the familiar 1:2:1 pattern. Although these examples illustrate two potential advantages of 2D J spectroscopy in chemistry, namely the simplification of a complex spectrum in the form of a proton-decoupled proton spectrum and the resolution of overlapping signals using partial J spectra, these advantages are also associated with a number of practical limitations. Accordingly, an attempt is made in the next section to analyse these aspects of 2D J spectroscopy from a practical standpoint and this is followed by more detailed discussions of some specific topics of interest.

3.2.2 The phase twist effect in two-dimensional spectroscopy

Previous workers have shown (4,21) that double Fourier transformation of the $S(t_1,t_2)$ data matrix obtained from a 2D experiment leads to a complex two-dimensional lineshape given by,

[1]Power spectrum = $\{(\text{real})^2 + (\text{imaginary})^2\}$; Magnitude spectrum = $\{(\text{real})^2 + (\text{imaginary})^2\}^{\frac{1}{2}}$

$$S_R(f_1,f_2) = A(a_1a_2 - d_1d_2) \qquad [3.2]$$

$$S_I(f_1,f_2) = A(a_1d_2 + a_2d_1) \qquad [3.3]$$

which represent the real and imaginary components of the 2D spectrum respectively (a and d refer to the Lorentzian absorption and dispersion lineshapes (eq. [1.11]) and the subscripts refer to the two domains). The two-dimensional lineshape was shown in Figure 3.3 in the form of a stacked plot, corresponding to equation [3.2]; the lineshape at "exact" resonance frequency in either dimension is represented by an absorption signal, but the profile tends towards a dispersion signal away from the resonance frequency. In the corresponding imaginary part of the 2D spectrum the lines are 90^o out of phase with respect to the former showing a dispersion lineshape at resonance frequency and the "tails" approaching absorption lineshape characteristics.[1]

Largely as a result of these characteristics, the major limitations of phase-sensitive 2D J spectra are,

a) the 45^o integral projection leads to net cancellation of the signals,

b) the dispersive components are characterized by wide "tails" away from exact resonance frequency which can lead to undesirable interference effects between neighbouring signals, and

c) it is inconvenient to display such spectra in suitable form to extract the spectral information.

A convenient method of avoiding this phase twist problem is to calculate the magnitude or power spectrum. Unfortunately both these display modes introduce an additional array of problems of their own, a discussion of which is given in the next section.

[1]Such complex lineshapes arise as a result of double Fourier transformation; a more detailed account of lineshape characteristics in 2D J spectroscopy is given in Section 3.3.3.

These considerations prompted us to consider methods to obtain absorption mode 2D J spectra for protons. For heteronuclear (eg. ^{13}C- ^{1}H) systems, experiments using "alternate" pulse sequences to create "reverse precession"[1] of the spins to eliminate the dispersive components, have been suggested by Ernst's (30) and Freeman's (31) groups. Unfortunately these methods are not generally applicable to proton, or homonuclear, systems since the pulses in these cases are usually applied non-selectively to all the spins. Bax et al. (33) have described a whole-echo Fourier transform method to obtain a pure absorption 2D J spectrum, which is analogous to the SEAS experiment, described in Section 2.4, for eliminating the dispersive components. Although this procedure appears to be suitable for simple spin systems which have slow spin-spin relaxation rates and narrow spectral widths, these conditions do not often pertain to complex molecules, so this approach appears to lack generality.

A more practical and general approach appears to be manual phase correction of the relevant phase-sensitive cross-sections or "sub-spectra". In the ^{13}C- ^{1}H case, for example, the relevant multiplets can be directly obtained from the 2D J spectrum since the protons can be decoupled during the detection period; the f_1 trace at the chemical shift of each resonance yields a partial J spectrum, containing both the real and imaginary parts. Recently an interactive, two-dimensional phase correction routine has been demonstrated by Levitt et al. (32), however this has not yet been widely applied. Phase correction in proton 2D J spectra is usually more complicated

[1]For example, this condition can be achieved in ^{13}C- ^{1}H systems by applying a 180° pulse to the carbon-13 spins at the end of the evolution period (30) or by alternating the decoupling period between T_R and T_D (31) in the "gated decoupler" method.

because of the overlap of resonances particularly when dealing with typical organic molecules and, also, the multiplets lie at 45^{o} with respect to each axis. Separation of the multiplets can be achieved in this case by taking phase-sensitive cross-sections of sub-spectra (34), and Sections 3.3.2 and 3.3.3 deal with more detailed analysis of this procedure.

3.2.3 Problems associated with the magnitude- or power-mode displays of 2D J spectra

The major disadvantage in displaying a 2D J spectrum in the magnitude mode is the associated line broadening effect. This arises because of the resulting lineshape function which can be represented by,

$$S_M(f) = (a^2 + d^2)^{\frac{1}{2}} \qquad [3.4]$$

Using equation [1.11] this can be shown to be of the form

$$S_M(f) = \frac{M_o''}{(1+(2\pi\Delta f T_2)^2)^{\frac{1}{2}}} \qquad [3.5]$$

The lineshape function of the above signal shows broad "tails" characteristic of absolute value mode spectra; these often lead to interference from neighbouring peaks, especially from the tails associated with intense resonances. (The practical implications of this is discussed in the next section).

The two-dimensional, magnitude value, line shape may be easily derived from equations [3.2] and [3.3] to be,

$$S_M(f_1,f_2) = \{S_R(f_1,f_2)^2 + S_I(f_1,f_2)^2\}^{\frac{1}{2}} \qquad [3.6a]$$

$$= A\,[a_1 a_2]^{\frac{1}{2}} \qquad [3.6b]$$

which on a contour plot has a shape of a four pointed star (Fig. 3.5). Note however, for the condition $T_2^{(1)} = T_2^{(2)}$ a diagonal cross-section through a peak gives a pure Lorentzian lineshape (23).

The power spectrum derived from equation [3.2] and [3.3] has the form,

$$S_p(f_1,f_2) = A^2[a_1a_2] \qquad [3.7]$$

which corresponds to signals with Lorentzian absorption lineshapes along both dimensions; however the intensities will be the square of their normal values. When the signals of interest are of similar magnitude, the above procedure yields desirable 2D J spectra with predictable intensities (26). Since all the signals intensities are squared, the 2D spectrum will show an apparent improvement in sensitivity (signal to noise ratio). However, both the magnitude- and power-mode spectra will cause distortions and non-linear intensity effects in regions of overlap, which can have serious consequences, particularly in high resolution 2D J spectroscopy.

When dealing with complex spectra, with many overlapping resonances, particularly in the absolute-value mode, it is generally desirable to multiply the time-domain signal with suitable (digital) filter functions. This type of digital filtering can help to enhance the effective resolution of peaks and also minimize the interferences from neighbouring peaks by its line-narrowing effect. It is also important to be aware that use of filter functions, such as sine-bell (35), double-exponential (36), etc., invariably introduces some noise thereby causing a loss of effective signal-to-noise, and also leads to intensity distortions within closely spaced or overlapping multiplets. Therefore the use of these functions generally requires that the original time-domain signals have sufficiently high signal to noise ratio, particularly if the resolution enhancement is to be applied in both t_1 and t_2 time domains; it is also necessary to select the optimum weighting functions.

As will be discussed in Section 3.3.2 and 3.3.3, the phase-sensitive tilt routine offers a convenient solution to most of the above problems since it

makes use of phase-sensitive spectra and provides the option of conventional 1D spectrum manipulations on each individual multiplet sub-spectrum.

3.2.4 The dynamic range problem in 2D NMR spectroscopy

The relative intensities (dynamic range) of the various signals of a spectrum has to be given serious consideration in 2D J spectroscopy, especially when "conventional" 2D data acquisition and processing methods are employed. Such dynamic range problems are commonly associated with intense solvent residual peaks(37), methyl singlets from methylated derivatives (eg. compound 7) or intensity differences between a major and minor component in a mixture (38), etc. The major causes for this limitation are associated with the line-broadening effect of magnitude spectra, and the amplitude deviations in the power spectra; both these effects are amplified when dealing with large intensity differences. In the integral projection mode of display, the broad tails of intense resonances are summed over the region of interest and lead to undesirable effects for example in partial J spectra of nearby resonances, often causing weak multiplets to be completely obscured (Ref. 37; Sec. 3.3.1). In the power mode display, each trace in a 2D spectrum may have to be heavily "under-scaled"[1] in order to normalize the intensities which can lead to the loss of low intense signals from a spectrum.

[1]The digitized NMR signal is usually represented by words in a computer. A twenty bit word can be correctly represented by signals whose intensities vary from zero to $2^{20}-1$ integer numbers. If a signal is higher than this limit, it is usually scaled down by a suitable normalization factor in order to be represented by the twenty bit word. This "down-scaling" process can reduce low intense signal to less than unity, and thus result in loss of these signals. However the dynamic range of signal intensity can be increased by representing the data by two words (eg. double-precision integer or floating point representation).

Often, these limitations can be avoided by:

a) making use of phase-sensitive display modes instead of absolute or power mode display (which was referred to in Section 3.2.2),

b) using suitable digital filter functions to narrow the line widths of (intense) signals,

c) the use of analog filtering - it should be possible to sample frequencies covering a selected band-width with respect to the transmitter by using suitable filters, thus minimising the intensity of unwanted signals from outside this frequency range,

d) nulling any intense resonance which has a long spin lattice relaxation time by use of an inversion recovery sequence prior to a 2D J pulse sequence (Sec. 3.3.1; Ref. 37),

e) nulling those signals which have a short spin-spin relaxation rate by delayed 2D J spectroscopy (Sec. 3.3.1; Ref. 39),

f) selective excitation techniques for either pre-saturating the solvent or observing the signals of interest.

It should be noted however that the optimum solution depends on the system under consideration, as should become clear with discussion of the various examples that are considered in this study.

3.2.5 The "overlap" or "hidden resonance" problem in NMR - the use of tilted 2D J spectra

Unravelling the overlapping components from many, closely spaced, multiplets is one of the more serious problems encountered by chemists attempting to obtain structural information from proton NMR spectra. Although the wide dispersion obtained with modern spectrometers (superconducting

magnets operating at 11.7T, ie. 500 MHz for ^1H are commercially available) have considerably eased this problem, some of the examples considered in this present work (38) show that straightforward analysis by inspection would still be difficult even at higher magnetic fields far beyond the capabilities of present day technology. In the past this problem has been conventionally solved by rather demanding (and time consuming) INDOR (Inter Nuclear DOuble Resonance) studies (40,41) and related double resonance studies such as NOE-difference (42) and spin-decoupling difference methods (43). 2D J spectroscopy offers a useful solution to the above problem, and will be discussed now.

Consider, for example, the partial 2D J spectrum of the H-1' and H-5 resonances of uridine (8) shown in Figure 3.10 (cf. Fig. 3.11). The projection of this "untilted" spectrum onto the f_2 axis gives the normal spectrum, and shows the overlap of the two doublets (Figs. 3.10a; 3.11A). Because of their close proximity, a projection of the 2D J spectrum onto the f_1 axis yields a partial J spectrum in which the two multiplets appear superimposed (Figs. 3.10b; 3.11C). Although in this case the two doublet components can be easily assigned by inspection, it is obvious that for more complex multiplets such unequivocal assignment is rather improbable. Now consider the projections of the tilted 2D J spectrum of Figure 3.10D which was obtained by subjecting the original data-matrix, $S(f_1,f_2)$, to a 45^o-tilt in frequency space (23). Although the projection onto the f'_1 axis is identical to that in Figure 3.10A the projection onto the f_2' (δ) axis now produces a singlet for each proton at the f_2' value corresponding to its chemical shift; this is because components of each multiplet now lie parallel to the f_1' axis (Fig. 3.10c; 3.11B). Traces taken from the 2D J spectrum at

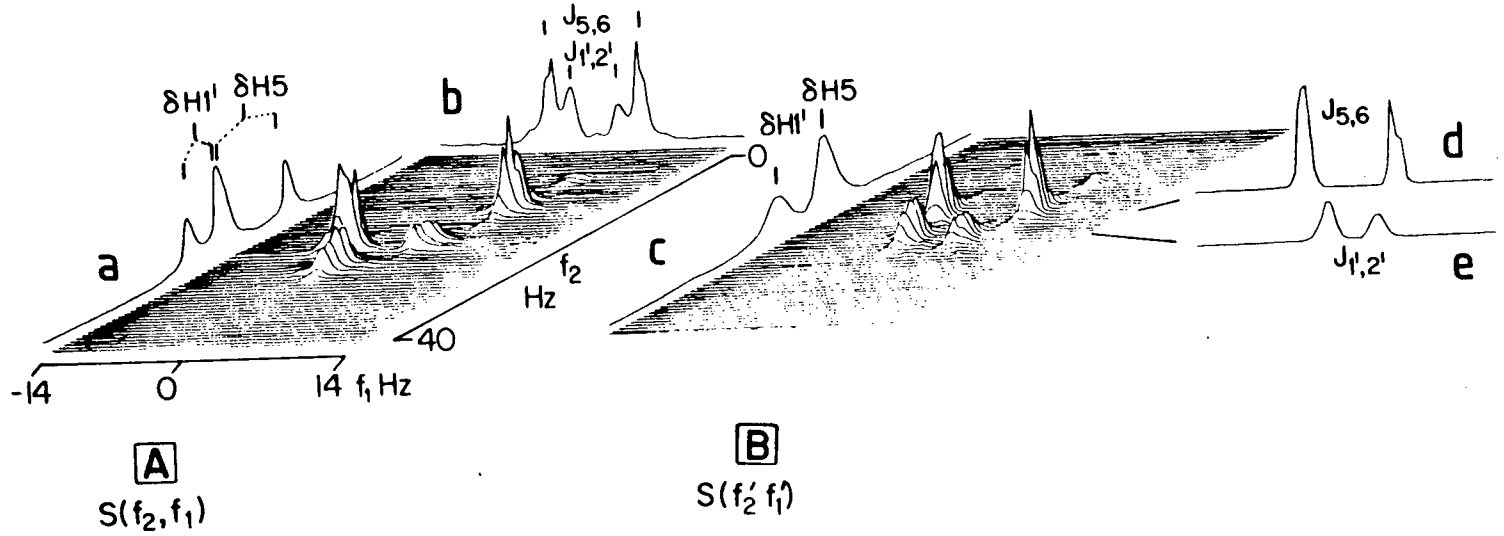

Figure 3.10: The tilt operation to illustrate its advantages in 2D J spectroscopy. A, the 270 MHz proton 2D J spectrum of the H-1' and H-5 resonances of uridine (8) 0.3M in D_2O. The f_2 projection of A is equivalent to a conventional spectrum (a) and the projection onto f_1 gives the superimposed J spectrum (c). The tilted data matrix, B, when projected onto f'_2 yields proton-decoupled proton spectrum (c); cross-sections (d, e) at the respective chemical shift frequencies give the partial J spectra of the two protons, thus resolving the overlapping multiplets (cf. Fig. 3.11).

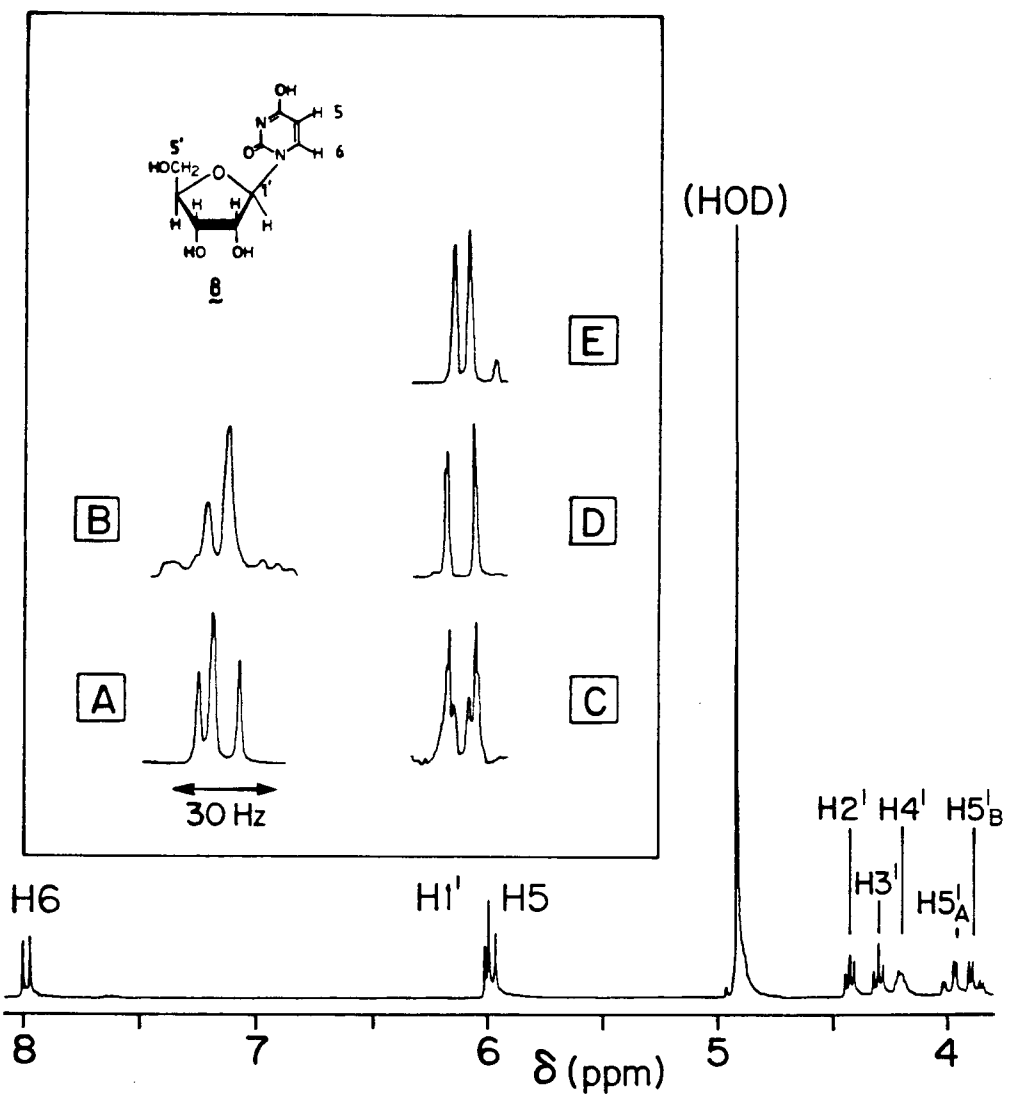

Figure 3.11: The lower trace shows the 1D spectrum of 8 in D_2O. The inset shows the conventional spectrum (A), proton-decoupled proton spectrum (B), J spectrum (C), and the cross-sections (D and E) of the H-5 and H-1' resonances, derived from the 2D J spectra in Figure 3.10.

the two chemical shifts (in f_2), now give individual partial J spectra (cross-sections) as shown in Figures 3.10d,e and 3.11D,E.

The advantages of using tilted 2D J spectrum become increasingly important for more complex (overlapping) regions of a spectrum; this point is illustrated in Figure 3.12 for α,β-D-xylose (1) in D_2O. Most of the conventional spectrum can be assigned by inspection, leaving only the region between δ3.3-3.5 which contains the overlapping resonances of five, potentially inequivalent protons. The proton decoupled spectrum (obtained by projecting the titled 2D J spectrum onto f_2') shows the expected sharp singlets corresponding to the chemical shift of each weakly coupled proton. The region of interest contains one such singlet at δ3.35 (the other four resonances give broad responses which is usually characteristic of strongly coupled systems); a cross-section at this chemical shift gives the partial J spectrum (inset) for this proton; all of the vicinal couplings can be easily measured and the resonance assigned as that of the H-4 proton of the β-anomer.

The importance and usefulness of the above method can be seen in an even more complicated example, namely an anomeric mixture (α:β=1:3) of cellobiose (9) in D_2O. The multiplets corresponding to the eighteen (non-anomeric) protons appear within a region of ~200 Hz (Fig. 3.13B), as a result complete analysis of the spectrum using techniques such as double resonance or spectrum simulations are essentially impossible. Remembering that in a proton spectrum, weakly coupled spins give sharp singlets (whereas ill defined, broad peaks are usually produced by strongly coupled signals), projection onto f_2' of the 2D J spectrum of this sample at 270 MHz provides a convenient spectral simplification. Cross-sections taken at these frequencies (corresponding to sharp singlets) give the partial J spectra of a total of eleven protons as

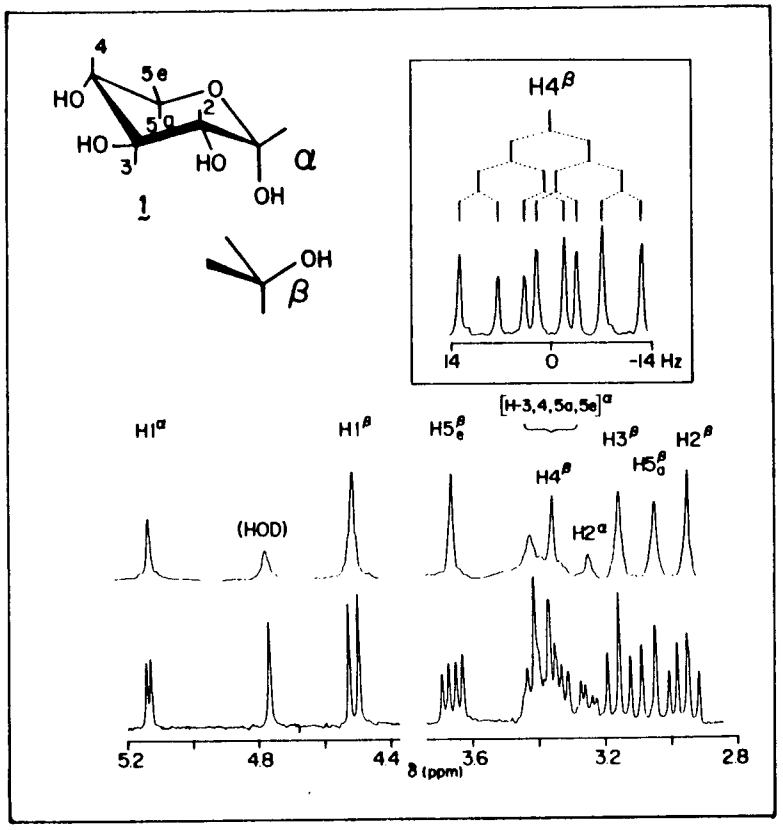

Figure 3.12: The lower trace shows the 270 MHz proton spectrum of α,β-D-xylopyranose (1; 0.3M in D_2O) and the upper trace the corresponding proton-decoupled proton spectrum obtained by projecting the tilted 2D J spectrum onto f'_2. The inset is the partial J spectrum of H-4$^\beta$ obtained by taking a cross-section af f'_2=3.35δ.

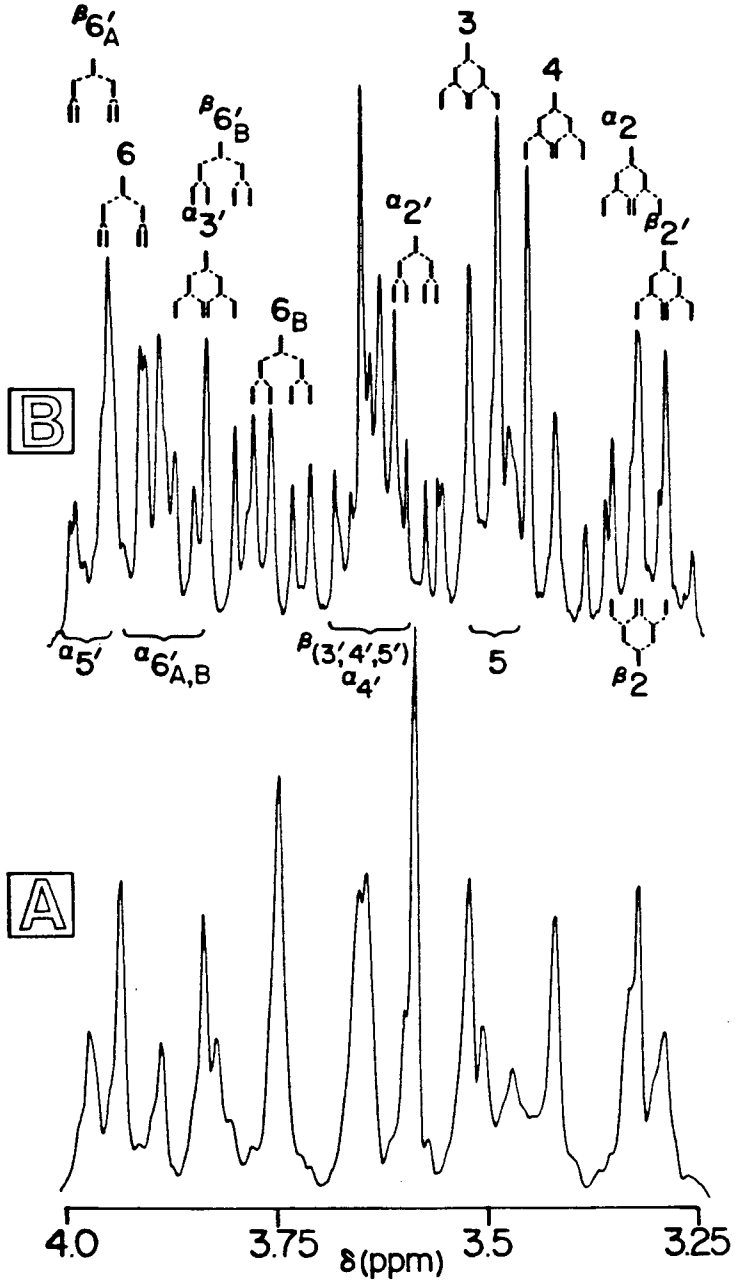

Figure 3.13: Partial 270 MHz proton spectrum (B) and the proton-decoupled proton spectrum (A) of α,β cellobiose (9), 0.3M in D_2O. The multiplet structures shown as "stick" diagrams and the trace A were obtained from the 2D J spectrum shown in Figure 3.10. The multiplet structures corresponding to strongly coupled spin systems and from those with low intensity were difficult to resolve and assign (see text).

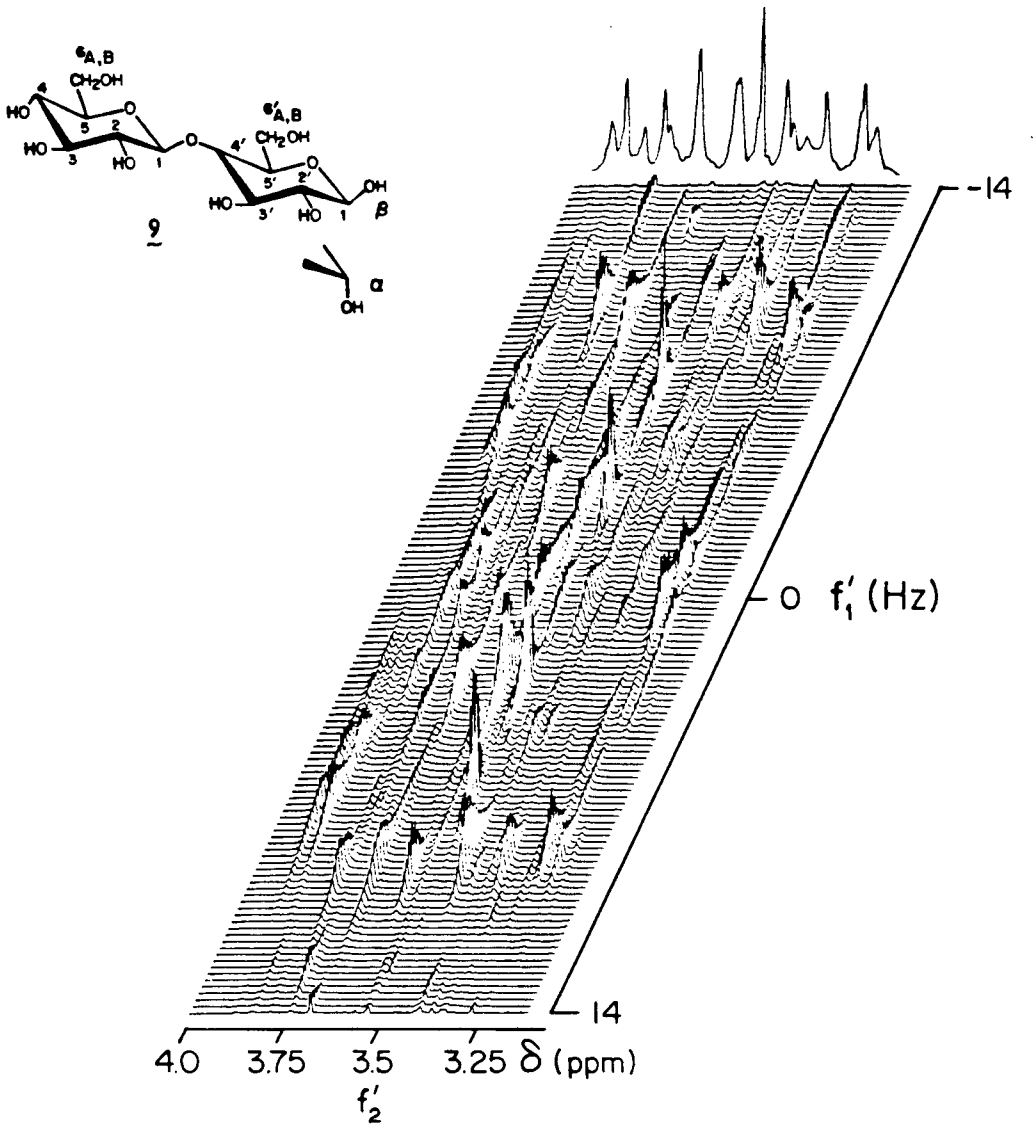

Figure 3.14: Tilted 2D J spectrum of the non-anomeric protons in α,β cellobiose (9) in D_2O (0.3M). The top trace is the projection onto f'_2; cross-sections parallel to f'_1 yielded the multiplet patterns shown diagrammatically in Figure 3.13. Sine-bell resolution enhancement was used in the f_2 domain to minimise the line broadening effect of the absolute value display.

indicated in Figure 3.13B. (It was not possible to obtain meaningful partial J spectra for the strongly coupled resonances.)

Providing the chemical shift separation between two multiplets can be resolved in f_2 (eg. by increasing the digitization or resolution enhancement), it should be possible to resolve those individual multiplets by the above procedure. In the above case, for example, the chemical shift difference between $^{\beta}H\text{-}2$ and $^{\beta}H\text{-}2'$ is less than 3 Hz. It has been possible in another study to resolve multiplets which were about 0.5 Hz apart (45).

Although it is possible to "resolve" the NMR spectrum of cellobiose in this manner, assignments of the individual multiplets based either on matching of coupling constants, or on chemical shift arguments are impossible because each of the (six) geminal protons and similarly the eight methine protons are all expected to have almost identical multiplet structures (Table 4.1). Given this difficulty and the fact that one-dimensional double resonance methods are not suitable for the analysis of such crowded spectra, it is fortunate that two-dimensional correlated spectroscopy exists. As will be discussed later in Chapter IV $^{13}\underset{\sim}{C}$- ^{1}H chemical shift correlated spectroscopy was used in the above case to assign all the proton chemical shifts and thereby complete the spectral assignment (38).

3.2.6 Strong coupling effects in 2D J spectra

Strong coupling represents a serious limitation in 1D proton NMR spectral analysis and the same is equally true for 2D spectroscopy (4,46-48). Second order multiplets can be asymmetric about the chemical shift in a 1D spectrum; however a homonuclear 2D J (or the analogous heteronuclear "proton-flip" experiment) yields a symmetric 2D spectrum with additional lines, some with

negative intensities. Since strong coupling often results in the components of a multiplet being spread over a wider frequency range than when the same nuclei are studied under weak coupling conditions (eg. at high magnetic fields), this often leads to fold-over of peaks in the f_1 dimension. Unlike weakly coupled multiplets, all the components of a strongly coupled system may not lie precisely along a 45° axis with respect to the principal axes; this results in more complex patterns in proton-decoupled proton spectrum (45° projection), which are often broadened due to overlap of many closely spaced lines. These effects are demonstrated using 1',4,6,6'-tetrachloro-1',4,6,6'-tetradeoxy-galacto-sucrose tetramesylate (10) as an example. The weakly coupled methine ring protons in 10 appear in Figure 3.15 as singlets in the proton-decoupled proton spectrum, whereas the three pairs of strongly coupled methylene protons show more than nine major lines. Clearly this behaviour could lead to confusion in attempting to analyze a complex 2D J spectrum. Although such spectra can be analysed by computer simulation (48) this is invariably a tedious and inefficient process even by the standards of conventional 1D second-order spectrum simulations and analysis. As an example, the 2D J spectrum of the 6-P and 6'-P protons (AB part of an ABX system) in 10 was simulated using the values, $J_{6,6'} = 11.5$, $J_{5,6} = 7.1$, $J_{5,6} = 6.2$ and $\Delta_{6,6'} = 14$ HZ.[1] The contour diagram along with the experimental plot in the absolute value mode, is illustrated in Figure 3.16;[2] the folded-back (•) and negative peaks (⊖) are also indicated in the figure (cf. Fig. 3.17). The different projection and the calculated "stick" diagrams are indicated in Figure 3.17.

[1] $\Delta_{6,6'}$ refers to the chemical shift difference between 6-P and 6'-P

[2] The computer simulation program was kindly provided by Dr. G.A. Morris.

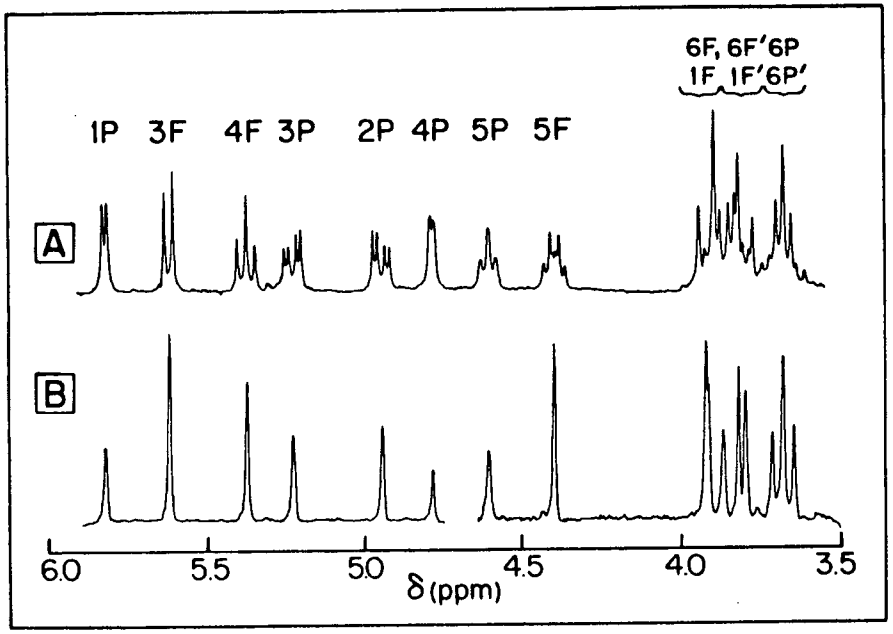

Figure 3.15: The normal 270 MHz proton spectrum (A) and the proton-decoupled proton spectrum (B) of 0.1M solution of 10 in $CDCl_3$. Sine-bell resolution enhancement was used in the f_2 domain. Each weakly coupled proton gives a singlet in B, whereas the strongly coupled protons (3.5 to 4.0δ) give more complex patterns.

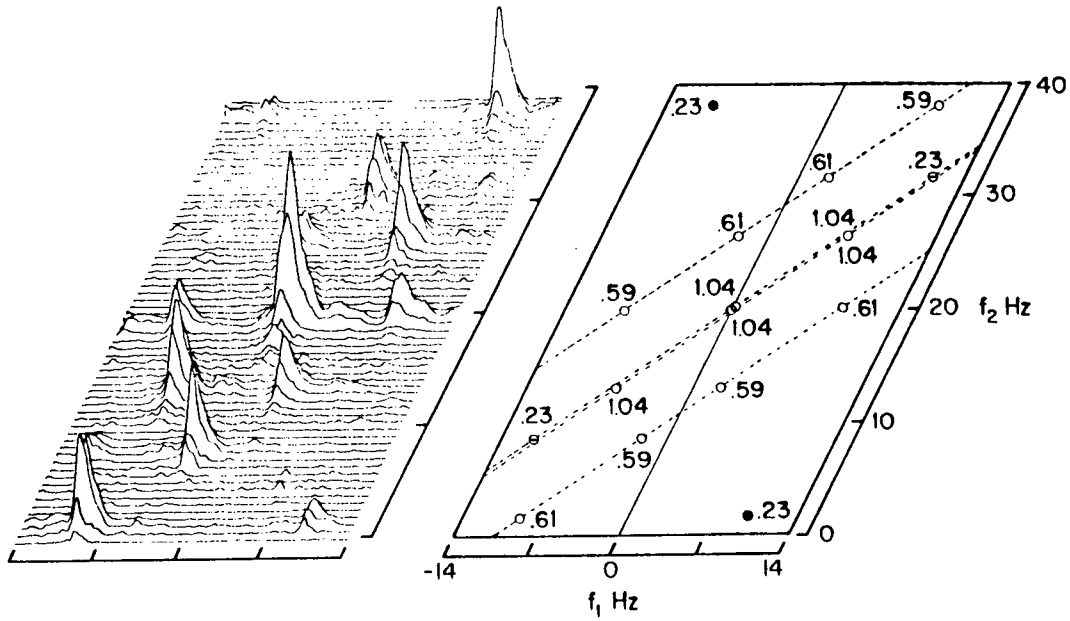

Figure 3.16: The plot on the left is an experimental 2D J spectrum of the 6P and 6P' protons of 10, plotted in the absolute value mode. The diagram on the right was constructed by computer simulation of this strongly coupled region using the parameters $J_{6,6'}$=11.5, $J_{6,5}$=6.2, $J_{6',5}$=7.1 and $\Delta_{6,6'}$=14 Hz. The numbers represent the absolute intensities. The dark circle represents fold-over in f_1. (The signals associated with an intensity of 0.23 correspond to negative peaks).

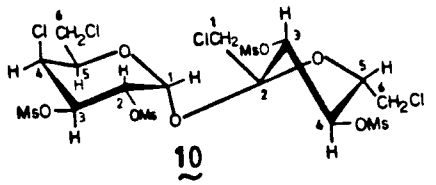

10

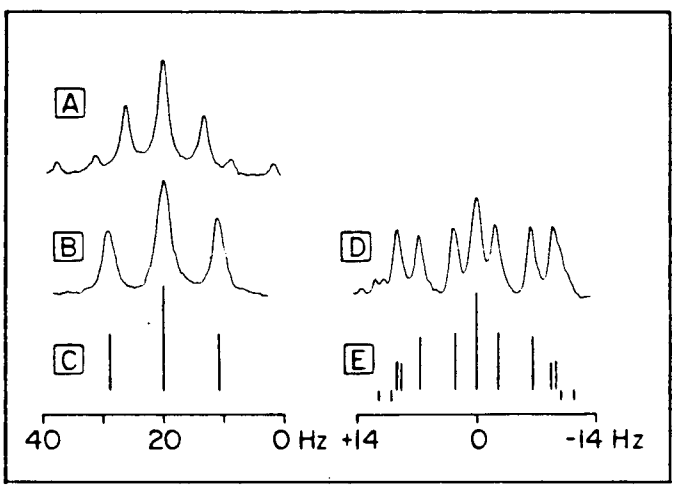

Figure 3.17: A, B and D are the projections of the 2D spectrum shown in Figure 3.16 onto different axes, and correspond to the normal, proton-decoupled and J spectra respectively. C and E were constructed from computer simulation data.

Since strong coupling usually leads to rather unpredictable cross-sections, it is advantageous when analysing complex spectra to have some prior knowledge of the regions of a spectrum containing strongly coupled systems. This may be achieved either by viewing the 45^{o} projection (remembering that strongly coupled peaks often give broad responses) or by directly viewing the cross-sections (weakly coupled systems give simpler and symmetric responses in f_1' at their respective chemical shift frequencies in f_2').

Various alternative methods exist for minimising the ambiguities associated with strongly coupled systems. These include:

a) obtaining measurements at the highest possible magnetic field for larger chemical shift dispersion,

b) inducing chemical shift dispersion with the help of paramagnetic shift reagents (49) or solvents; it should be mentioned that in a) and b), it is only necessary to cause a small change in the relative chemical shifts within a strongly coupled system so as to convert it to a pseudo first-order level,

c) using a $^{13}\underset{\sim}{C}$- ^{1}H 2D shift correlation experiment to determine the approximate chemical shift of each strongly coupled proton prior to analysing a 2D J spectrum (38),

d) analysis of the 2D J spectrum by computer simulation as discussed earlier, and

e) simulation of the strongly coupled NMR spectrum in 1D rather than 2D; since the chemical shifts and coupling constants of weakly coupled protons can be easily derived by 2D J spectroscopy, it may now be more convenient to analyse (by simulation) the conventional NMR spectrum. For example, if the - and J-values of a weakly coupled multiplet from an overlapping strongly coupled region (eg. H-4^{β} in Fig. 3.12) can be obtained, then it should be

possible to subtract its partial (simulated) spectrum from the normal spectrum and thereby obtain the spectrum corresponding to the second-order peaks which would thereby be simplified for 1D analysis.

In the current study attempts were always made to identify any strongly coupled protons, but further analysis was not pursued.

3.3 Miscellaneous topics related to 2D J spectroscopy

3.3.1 Elimination of dynamic range effects in 2D J spectroscopy

a) Solvent nulled 2D J spectroscopy

The problems arising from a large dynamic range of signals were discussed previously in Section 3.2.4; in extreme cases, such as when the spectrum has a strong residual solvent peak, a commonly encountered problem with biochemical samples, this can completely jeopardise the usefulness of the 2D J technique by distorting substantial regions of the 2D spectrum. Fortunately these problems can often be conveniently avoided by modifying the 2D J pulse sequence, using approaches similar to those used in 1D NMR spectroscopy for solvent suppression (50,51). One example of the problem and its solution will suffice here to make the point.

The protons of uridine ($\underset{\sim}{8}$, 0.3M in D_2O) have much faster spin-lattice relaxation rates ($\simeq$ 0.4 s^{-1}) than the residual proton in the solvent (0.11 s^{-1}). This difference can be advantageously used to selectively null the solvent resonance prior to the 2D J pulse sequence by application of a non-selective inversion-recovery pulse sequence during the preparation period; this is represented by,

$$\{180^{\circ} - T_{null} - 90^{\circ} - n.T - 180^{\circ} - n.T - \text{Acquisition}\}$$

where T_{null} is set equal to the time required for the HOD signal to reach

its "null-point" (52). Phase alternation of both the 180° pulses by 180° is generally recommended to minimize artifacts in the final spectrum (53,19). The rapidly relaxing uridine protons regain their equilibrium magnetization condition during the time T_{null} and are ready to experience the 2D J pulse sequence. The effectiveness of this approach is clearly discernible by comparison between the 2D J spectra in Figure 3.18. It can be seen in the latter that the distortion arising from the HOD signal has been completely eliminated from the 2D J spectrum.

The impact of this procedure on the corresponding partial J spectra is demonstrated in Figure 3.19. The various traces were obtained by projecting sections of the 2D J spectra onto the f_1 axis; those in Figure 3.19A show a significant signal at zero-frequency due to the tails of the residual solvent resonance, even though it is about 270 Hz to low-field of the H-5_B' resonance (see Fig. 3.11). For weak signals such as the H4' multiplet which also shows signals near the zero frequency in the f_1 dimension, the tail of the HOD signal completely distorts the partial J spectrum, so that it cannot be interpreted (Fig. 3.19A); in contrast the equivalent trace obtained by the solvent-nulling 2D J procedure is free from this defect (Fig. 3.18B).

Another useful technique for solvent nulling in aqueous (D_2O) samples, often used in the course of these studies was selective irradiation or pre-saturation (54). This procedure can be used when the signal to be irradiated has a relaxation time similar to the resonances that are to be studied.

b) Delayed 2D J spectroscopy

In the previous section elimination of the intense signals was achieved by taking advantage of the large differences in spin-lattice relaxation rates

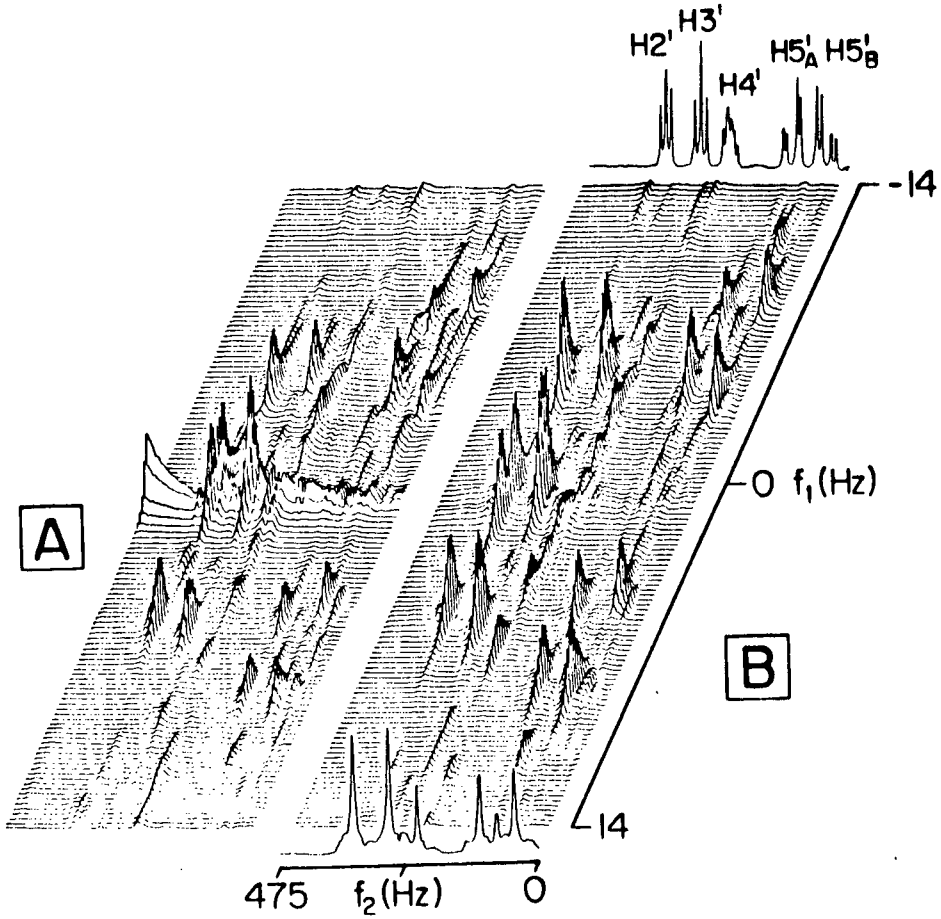

Figure 3.18: (A) Proton 2D J spectrum of the high field region of uridine(8) in D_2O (cf. Fig. 3.11), showing the distortion at zero frequency in f_1 due to the "wing" of the HOD peak. (B) The same region, from an experiment in which the solvent resonance was eliminated by an inversion recovery sequence prior to the 2D J pulse sequence. The top and bottom traces show the normal and proton-decoupled proton spectrum respectively. Both spectra are plotted in the power mode with exponential multiplication in both time domains.

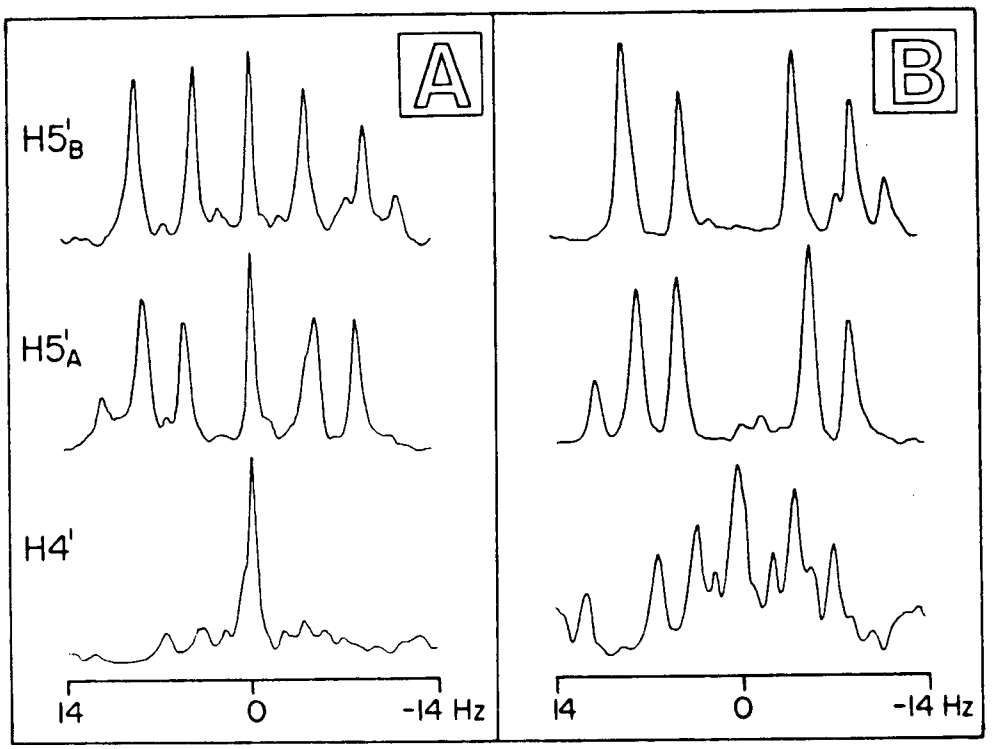

Figure 3.19: (A) Partial J spectra of the H-4', H-5'$_A$ and H-5'$_B$ resonances of β obtained by projecting sections of the 2D J spectrum (Fig. 3.18A) onto the f_1 axis, each showing, at zero frequency, the signal from the "wing" of the HOD signal; note the effect of the solvent peak on H-4' signals. (B) The corresponding regions obtained from Figure 3.18B; each of these partial J spectra agree with spectra simulated to include effects of strong coupling.

between the solvent and the protons in the molecule. In this section another approach, "delayed" 2D J spectroscopy, will be discussed which can be used when the intense signal has a much shorter spin-spin relaxation rate than the resonances of principal interest (cf. SEAS).

Figure 2.7A shows the 1D spectrum of a D_2O solution containing 10% (0.01M) dextran T-10 (MW ca. 10,000, a 1→6 α linked polymer of D-glucopyranose; 3) and methyl β-D-xylopyranoside (0.1M; 4). Comparison with the spectrum of 4 shows the extent of overlap and dynamic range of signals between the polymer and monomer. Use of "conventional" 2D data processing to resolve the xyloside spectrum would result in a predictably distorted 2D J spectrum for the various reasons discussed earlier (cf. Sec. 3.2.4), particularly for the H-5_e and H-4 resonances due to extreme overlap. This problem may be avoided by acquiring the initial 2D J data after a suitable delay time (T_i), during which the transverse magnetization component of the rapidly relaxing polymer signals would have decayed due to spin-spin relaxation. (The corresponding spectra from the SEAS experiment (Fig. 2.7) indicate the extent to which the polymer signals can be eliminated from a spectrum, for a suitable delay time T_i.) From the resulting partially relaxed 2D J spectrum it is possible to obtain partial J spectra of, for example, the H-5_e and H-4 protons as seen in Figure 3.20A and C which are displayed in the phase-sensitive mode; the corresponding regions from SEAS are also shown in the figure for comparison. These cross-sections may be difficult to phase correct[1] but may be conveniently displayed after suitable spectrum manipulations (Sec. 3.3.2). Note the resolution enhancement associated with

[1]The phase of each component of the multiplet will be modulated as a function of T_i as discussed in Chapter II; a suitable phase independent display mode may be preferable in many instances.

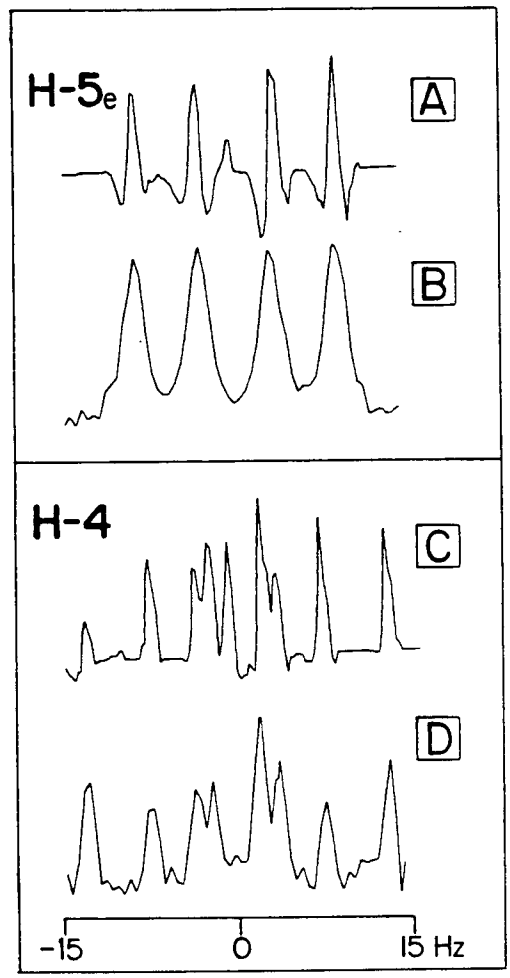

Figure 3.20: (B, D) The H-5_e and H-4 multiplets of β -methyl xylopyranoside (4) obtained from SEAS data for values of 192 and 544 ms respectively. (A, C) The corresponding partial J spectra obtained from phase-sensitive, tilted, partially relaxed 2D J spectrum. Note the line narrowing effect and the lineshapes. The signal near zero frequency in C is the dispersive tail from the methyl resonance. The digital resolution is 0.49 Hz/point.

the partial J spectra of the H-5_e proton - this is due to the line narrowing effect implicitly associated with the phase-sensitive tilt routine.

3.3.2 Phase-sensitive tilt routine

The importance of the "45°-tilt" routine was clearly demonstrated in the previous sections with the help of a diagrammatic sequence of the data processing steps (Fig. 3.6), and a few examples using typical organic molecules in Section 3.2.5. It will be recalled from previous discussions that the necessary spectral information regarding a weakly coupled multiplet is contained in the relevant 45° cross-sections of a 2D J spectrum. The f_2' and f_1' frequencies of this single trace will provide the chemical shift and coupling constants respectively, and the area represents the intensity;[1] these are generally the most useful parameters for NMR spectral and structural analysis of molecules. It follows from this that any display mode which optimises the information content of cross-sections is of substantial relevance to practical applications of 2D J spectroscopy.

The above feature makes it necessary to consider only the cross-sections of equivalent groups of protons at their respective chemical shifts to obtain phase-sensitive information from a 2D J spectrum. In general the phase-sensitive display mode would be preferred over the absolute value mode, mainly to retain the Lorentzian characteristics of the former, but also to determine the signs of signal intensities which have significance when dealing with 2D J spectra of strongly coupled systems (and in chemical shift correlated

[1]Because the line widths of individual multiplets are often different (particularly if digital filtering is used) and interference of neighbouring lines causes non-linear intensity relationships, cross-sections cannot be used to provide accurate intensity measurements. In the case of isolated multiplets, however, integral projections can be used to provide information on the relative number of protons giving rise to each multiplet.

spectroscopy). Unfortunately the methods to obtain phase-sensitive 2D J spectra mentioned in Section 3.2.2 are not generally applicable to complex proton 2D J spectra obtained from typical organic molecules. However, the phase-sensitive tilt routine (Scheme 2), which will be discussed in detail here, offers a convenient method for analyzing complex 2D J spectra. The calculation of the tilt routine (TILT I) mentioned in the previous sections was performed on the $S(f_2,f_1)$* data matrix by first reading into the computer memory the necessary number of traces from the original data matrix, followed by a linear interpolation procedure to construct the tilted trace of cross-sections. The overall efficiency of this procedure is determined by the core memory size of the computer, which is a major limitation when dealing with large data arrays. For that reason, another related procedure (TILT II) was developed which is more suitable for minicomputers; this involves tilting the $S(f_1,f_2)$ data matrix by "shifting" each trace in the f_2 dimension, followed by a (parabolic) interpolation procedure. In this case the f_2 size can be almost as large as the core memory size since each f_2 trace is shifted independent of the other traces.[1] This operation $S(f_2,f_1)$ $S(f_2',f_1')$, is illustrated in Figure 3.21 which is plotted in the absolute value mode for convenience.

Each multiplet in a 2D J spectrum will be set at a particular angle ($\theta = 45^o$), with respect to the f_1 axis. The offset by which each f_2 trace is to be shifted is given by,

$$\Delta = \text{Tan}\,\theta \,.n_1 h_1$$

where n_1 is equal to the f_1 trace number and h_1 the digitization in the f_1 dimension. Since the data is digitized the shift is followed by a

[1]Although each operation involves a "shift" of an f_2 trace, its ultimate effect on the 2D J spectrum is equivalent to "tilting" it by 45^o.

SCHEME 2

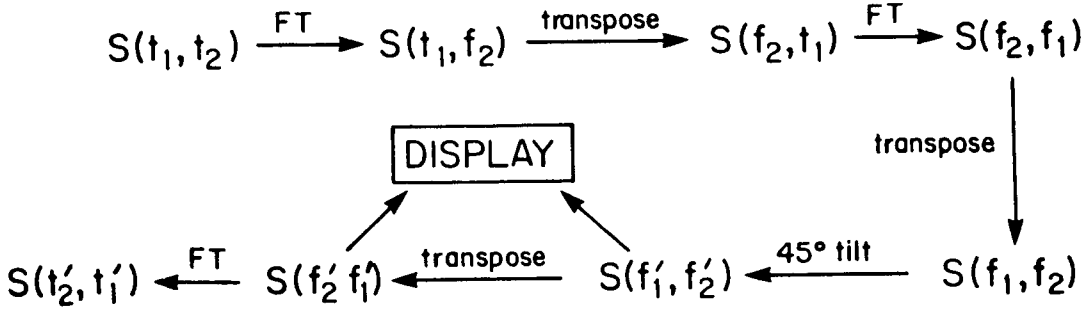
$S(t_1, t_2)$
FT
$S(t_1, f_2)$
transpose
$S(f_2, t_1)$
FT
$S(f_2, f_1)$
transpose
DISPLAY
$S(t_2', t_1')$
FT
$S(f_2' f_1')$
transpose
$S(f_1', f_2')$
45° tilt
$S(f_1, f_2)$

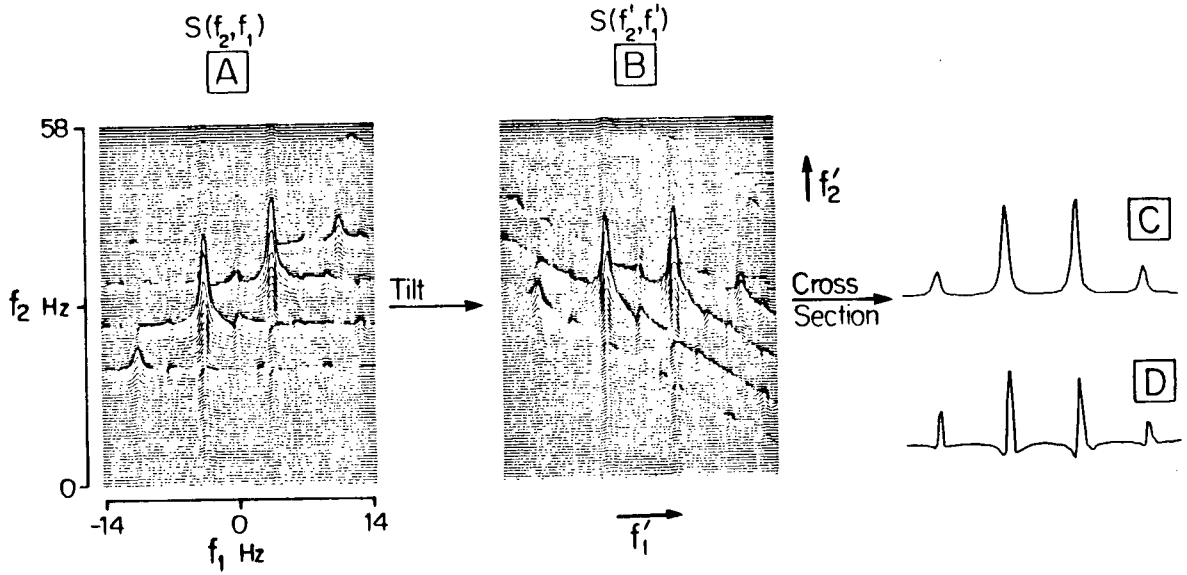

Figure 3.21: (A) The 2D J spectrum of the quartet in diethylmalonate in $CDCl_3$. The tilt operation transforms the $S(f_1,f_2)$ matrix into $S(f'_1,f'_2)$, B. A cross-section of B at the chemical shift yields C, the partial J spectrum shown in the absolute value mode. A similar trace from the corresponding phase-sensitive 2D J spectrum yields a sub-spectrum representing the real (D) and imaginary (not shown) parts. Note that the f_1 tails (including the noise and artifacts) are tilted at "135°" to the f'_1 axis.

parabolic interpolation procedure which may be of critical importance, particularly when dealing with limited digitization of signals or when attempting to resolve closely spaced lines. However for many practical cases in the current work, the interpolation procedure was omitted in order to minimize the total data processing time.[1] The original computer programme written in Nicolet 1180 BASIC is given in Appendix A.

It can be seen from Appendix A that both the real and imaginary parts of the 2D J spectrum are processed independently. As a result, the final tilted cross-section of a multiplet contains the real and the corresponding imaginary parts; in effect, this is equivalent to a spectrum obtained by selective excitation of that proton. This "sub-spectrum" can be inverse Fourier transformed to yield the corresponding time domain signal $S(t_2', t_1')$. This data processing method has a number of advantages over "conventional" 2D J data processing routines, particularly because now each sub-spectrum can be individually subjected to the various data manipulation procedures in the time domain (t_1'), such as zero-filling, digital filtering, etc. For example Figure 3.22D shows a sub-spectrum of a doublet (J = 2.65 Hz) obtained by zero-filling and "sine-bell" resolution enhancement; the corresponding region from a normal spectrum is shown in Figure 3.22A.

In practice, the NMR time domain signals are often zero-filled to improve the digitization (and hence the lineshapes) of the resulting Fourier transformed spectrum. In 2D spectroscopy this invariably leads a larger data matrix, and hence will increase the total data processing time, which can be

[1]As written by the author, the tilt routine was the most inefficient step of all the 2D J data processing steps because of the limited capabilities of the Nicolet 1180 BASIC programme; recently D. Dalrymple (Nicolet) provided us with a more efficient assembly language version of TILT II incorporated into the standard NTCFT programme.

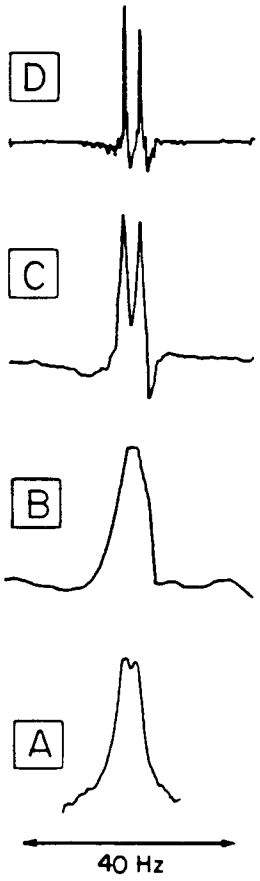

Figure 3.22: (A) The normal spectrum of a doublet (J=2.65 Hz) having a digital resolution (DR) of 0.34 Hz/point. (B) The same region with DR=1.37 Hz; this was the f_2 resolution that was used in the 2D J experiment which yielded the partial J spectra C and D. C is the (phase-sensitive) sub-spectrum with DR_1=0.34 Hz. Trace D was derived from C, by inverse Fourier transforming the spectrum digital filtering for enhancing the resolution zero-filling and another (forward) Fourier transformation. (The negative peak in trace C is an artifact from a neighbouring signal).

significant when dealing with, for example, natural products such as steroids (43,55) which have wide spectral- and multiplet widths.[1] The procedure described earlier, in which only the relevant sub-spectra are zero-filled, is a practically useful feature.

Some of the features regarding phase-sensitive cross-sections are summarised below:

a) the need for either magnitude-or power-mode spectra are eliminated and so, thereby, are the limitations arising from those display modes,

b) phase-sensitive information, such as (positive and negative) peak intensities, can be obtained,

c) the sub-spectra show a resolution enhancement (line-narrowing) effect which is implicitly associated with the tilt routine,

d) data manipulations (digital filtering, convolution, etc.) can be performed on each individual sub-spectrum at the final stage (after double Fourier transformation) rather than on the original data matrix; as a result the weighting function for each multiplet can be individually optimised,

e) since it is unnecessary to zero-fill the time domain signals of the original matrix, this can minimize both data processing time and limitations in handling large data arrays.

The phase-sensitive tilt routine in homonuclear 2D J spectroscopy results in non-Lorentzian lineshapes and this is discussed in the next section.[2]

[1]The f_1 spectral width in this case may be over 50 Hz, therefore the t_1 signals may have to be zero-filled to give an f_1 spectrum with 256 or 512 points in order to improve the lineshapes and resolve small, long range couplings.

[2]It should also be mentioned that Lorentzian absorption mode partial J spectra can be directly obtained from ^{13}C-^{1}H (heteronuclear) 2D J spectrum since the signals are generally acquired under proton decoupled conditions and yield a $S(\delta,J)$ matrix.

3.3.3 Lineshape characteristics in phase-sensitive, tilted 2D J spectra

Fourier transformation of time-domain NMR signal (FID) generates both an absorption and a dispersion signal, which are 90^{o} out of phase with respect to each other; if the original FID is exponential then the resulting frequency domain signal will be Lorentzian in shape. In contrast, each 2D signal in a spectrum resulting from double Fourier transformation contains a mixture of absorption and dispersion components which together give rise to the so called "phase-twist" effect as illustrated in Figure 3.23. As we have already noted this problem due to the phase-twist can be conveniently eliminated by displaying absolute value spectra; however, this results in the characteristic, and undesirable line broadening effect. The above feature often leads to interference from neighbouring signals which can be a major limitation in the application of 2D J spectroscopy in high resolution studies, particularly in proton NMR spectroscopy.

The nature of this phase twist is illustrated in Figure 3.23; for the real part of the 2D Fourier transform, given by (4),

$$S_R(f_1,f_2) = M_o\{ a_1(f_1).a_2(f_2) - d_1(f_1).d_2(f_2)\} \qquad [3.8]$$

where a and d refer to the Lorentzian absorption and dispersion terms respectively in their corresponding frequency domains

$$a(f) = \frac{T_2'}{1+\{2\pi\ \Delta f\ T_2'\}^2} \qquad [3.9]$$

and

$$d(f) = \frac{2\pi\ \Delta f\ T_2'^{\,2}}{1+\{2\pi\ \Delta f\ T_2'\}^2} \qquad [3.10]$$

T_2 and T_2^* are the decay constants in t_1 and t_2 respectively and $\Delta f = (f-f^o)$, where f^o is the offset frequency from the carrier (cf. eq. [1.11]).

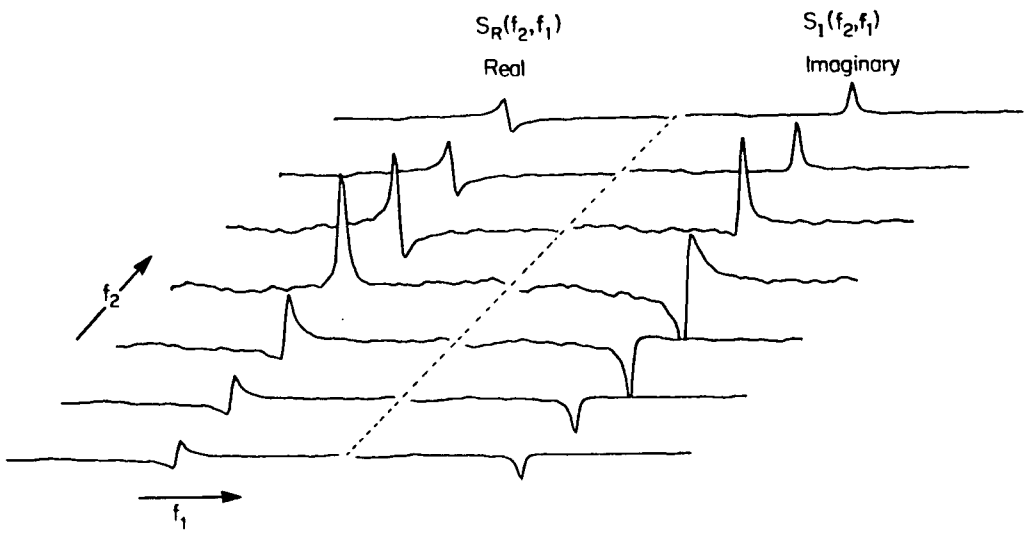

Figure 3.23: Experimental traces showing the lineshape characteristics in 2D J spectroscopy - the "phase twist" effect. (The subscripts R and I refer to the real and imaginary spectra).

Each trace in Figure 3.23 refers to a fixed f_2 in equation [3.8]. When Δf_2 is large (ie. away from "exact" resonance in f_2) the absorption terms become negligible, which result in the dispersive signals as shown by the $S_R(f_2,f_1)$ traces in Figure 3.23; note the change in sign (or the sense of rotation) of the dispersion line shape. At exact resonance[1] however $\Delta f_2 = 0$, and hence the trace will correspond to a Lorentzian absorption signal, with a half-height width of $\pi^{-1}R_2$ Hz, which corresponds to the "natural" line width (neglecting diffusion and instrumental effects).

Similarly the corresponding imaginary spectrum in Figure 3.23 is given by,

$$S_I(f_1,f_2) = M_o\{a_1(f_1)d_2(f_2) + d_1(f_1)a_2(f_2)\} \qquad [3.11]$$

which will be 90^o out of phase with respect to $S_R(f_1,f_2)$, showing a dispersive signal at the f_2 resonance frequency and absorptive signals with opposite intensities away from "exact" resonance. Similar explanations can be offered for the lineshape behaviour when viewed perpendicular to the f_2 axis; the line widths will now be characterized by R_2^*, which includes the magnetic field inhomogeneity effects.

The absolute value 2D J spectrum can be shown to be (4,21,23),

$$S\ (f_1,f_2) = M_o\{a_1(f_1)T_2.a_2(f_2)T_2^*\}^{\frac{1}{2}} \qquad [3.12]$$

and is characterised by the broad "tails" at "exact" resonance in both dimensions, which are clearly seen in a contour plot as in Figure 3.5.

The expression for a cross-section taken at angle θ at a fixed f_2' from the above spectrum can be represented by (23),

$$S\ (f_1') = M_o\{a_1(f_1'\cos\theta - f_2'\sin\theta)T_2.a_2(f_1'\sin\theta + f_2'\sin\theta)T_2^*\}^{\frac{1}{2}} \qquad [3.13]$$

Note that for the condition $T_2 = T_2^*$, a slope at 45^o ($\sin\theta = \cos\theta$), both lineshape functions become similar yielding a partial J spectrum with a

[1]It should be recalled that the f_1 frequency is not due to a resonance phenomenon, but rather a modulation.

Lorentzian absorption lineshape. These features may be visualized from a contour plot the 2D peak (Fig. 3.5) in which those sections through the peak that are parallel to either f_1 or f_2 axes are broad (according to eq. [3.12]), whereas the sections taken through the diagonal appear narrow. In practice, however, the cross-sections may also contain the (dispersive) tails from neighbouring resonances.

In some previous examples it was noted that partial J spectra, or sub-spectra, from tilted, phase-sensitive 2D J spectra showed a resolution enhancement effect with lineshapes similar to those obtained by 1D resolution enhancement procedures such as using "sine-bell" functions (35). This effect can be easily visualized from the 2D lineshape shown in Figure 3.23. A sub-spectrum will be represented by a diagonal sections through both the real an imaginary parts of the 2D peak; thus, for example, a section at 45^{o} with respect to the f_1 axis, through the $S_R(f_2,f_1)$ peak will show a Lorentzian absorption characteristic at "exact" resonance, tending towards "negative" dispersion signal away from resonance. In effect the lineshape may be considered as an absorption peak narrowed by two negative halves of a dispersion signal. The real part of these sub-spectra for a fixed f_2' can be given by (eqs. [3.5] and [3.10]),

$$S_R(f_1')) = M_o\left[a_1\left(\frac{f_1'-f_2'}{\sqrt{2}}\right).a_2\left(\frac{f_1'+f_2'}{\sqrt{2}}\right)-d_1\left(\frac{f_1'-f_2'}{\sqrt{2}}\right).d_2\left(\frac{f_1'+f_2'}{\sqrt{2}}\right)\right] \qquad [3.14]$$

The above equation represents the phase-sensitive f_1' traces derived from the $S(f_2',f_1')$ 2D spectrum.

Figure 3.24 shows phase-sensitive traces which were obtained using equation [3.14]; the 2D plot was simulated using a programme written in Nicolet 1180 BASIC language (Appendix B). The trace at the f_2' resonance

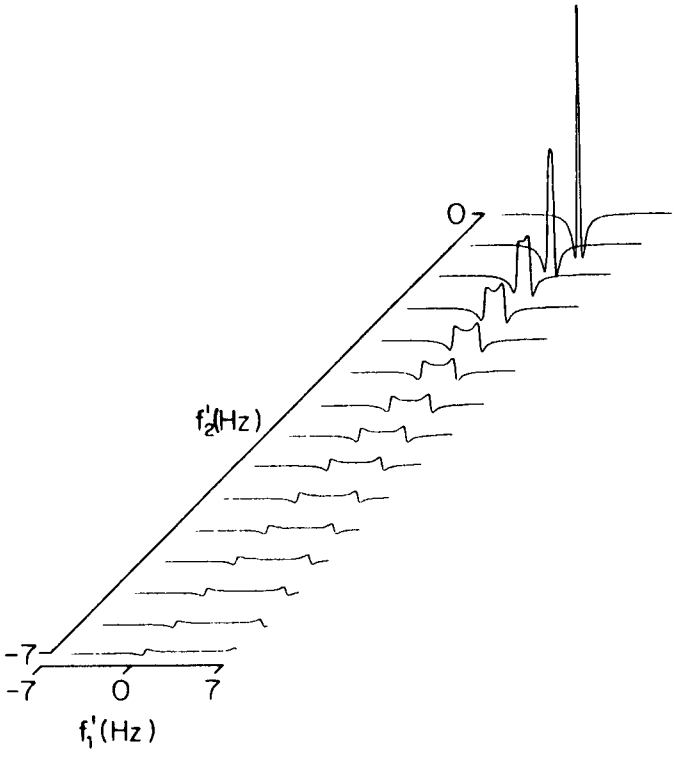

Figure 3.24: A phase-sensitive, tilted, 2D J spectrum, simulated using the LINSIM programme given in Appendix B, for values of T^*_2=1.2 s; T_2=1.0 s; DR_2=0.5 Hz; DR_1=0.05 Hz. Note the f_1 tails set at 135° to the f_1 axis.

frequency shows the characteristic lineshape behaviour observed in earlier examples. The tilt routine has the effect of tilting the tails of the signals in the f_1 domain ("f_1 tail") by 45°, as was already seen in Figure 3.21. This feature can also be seen in the simulated 2D J spectrum in Figure 3.24.

In order to make direct comparison between the simulated and experimental plots, selected phase-sensitive cross-sections from a 2D J spectrum of a singlet are shown in Figure 3.25. A noticeable feature in the above traces is the band of noise that appears along the "f_1 tail". This noise results from experimental imperfections and appears along the f_1 domain at the resonance frequency, and is referred to as "t_1 noise" (21); because this noise is random, it can be minimized by signal averaging.

For practical purposes, the resolution enhancement effect which is implicitly associated with the phase-sensitive tilt routine often helps with the measurement of high resolution information which might otherwise be obscured in an absolute value display. However, one should be aware of the lineshape characteristics and also its effect on neighbouring lines. Figure 3.26 shows a comparison of simulated peaks, before and after the tilt operation, for different line widths. The line narrowing effect for the broadest peak ($\Delta\nu_{\frac{1}{2}}$ = 0.64 Hz) is particularly noteworthy. This feature has already been in this laboratory used to advantage in the study of resonances which have been broadened by paramagnetic reagents (56);[1] conventional, absolute mode displays of the above multiplets are so broad that individual couplings cannot be detected, whereas those subjected to the phase-sensitive tilt are clearly resolved.

[1]The simulated sub-spectrum also showed a loss in signal intensity. It should be possible to resolve the multiplet patterns in the above example by applying resolution enhancement in both f_1 and f_2 domains.

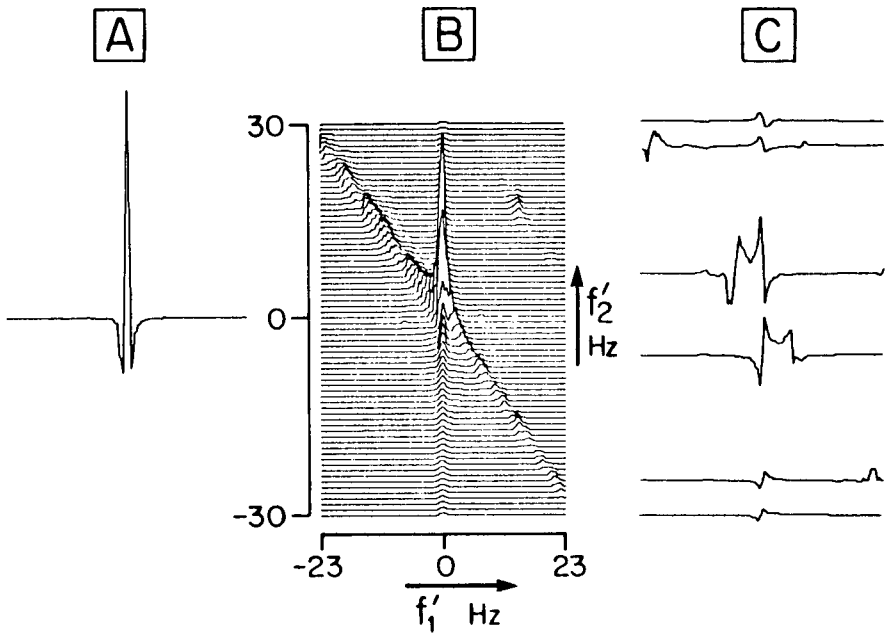

Figure 3.25: Experimental 2D J plots of a singlet. The multi-trace plot B shows the tilted spectrum in the absolute value mode; A and C are selected traces in the phase-sensitive mode (cf. Fig. 3.23).

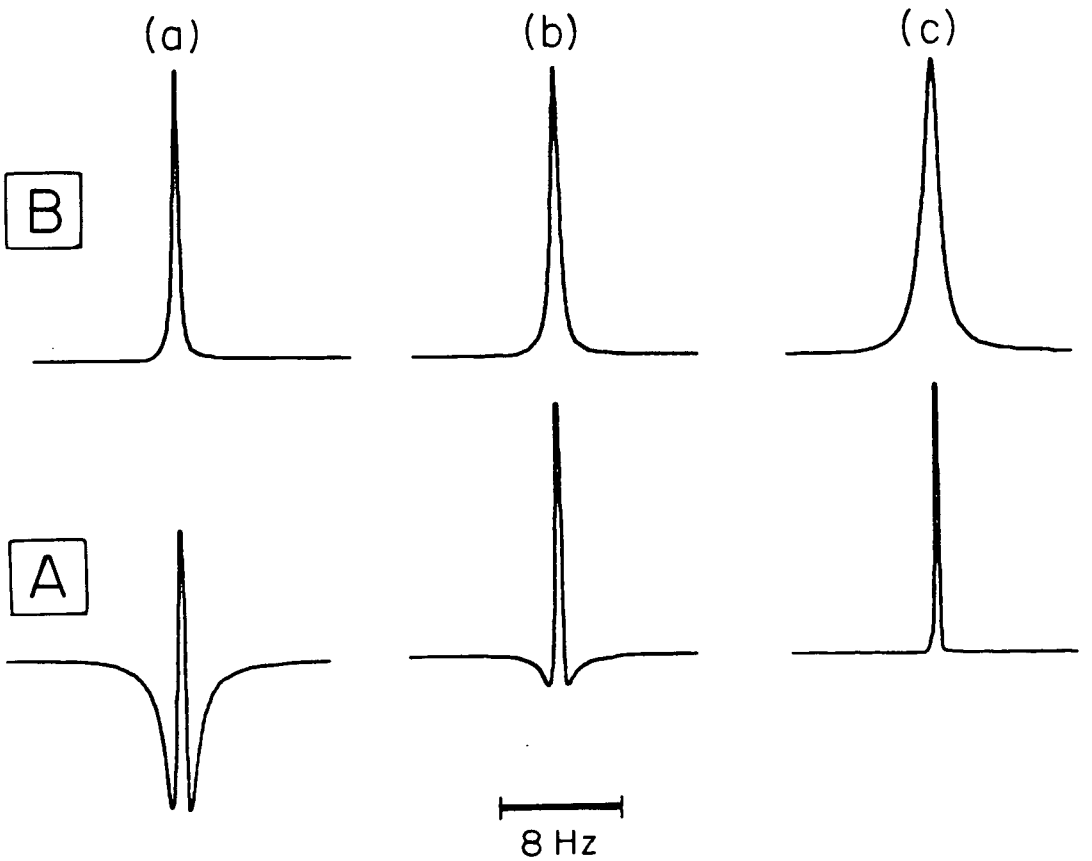

Figure 3.26: Simulated, phase-sensitive, tilted J spectra (A) and normal 1D spectra (B). a, b, and c correspond to T_2 values of 1.5, 1.0 and 0.5 s respectively. The digital resolution for the 2D traces were taken as DR_1=0.05 and DR_2=0.5 Hz. The listing of the BASIC programme which was used for calculating B is given in Appendix B.

Figure 3.27 illustrates the influence of neighbouring lines in a multiplet (see Fig. 3.20). Figure 3.27A is an experimental sub-spectrum of a doubleted doublet, showing the interference from the dispersive tail of a methyl resonance located 20 Hz away. The lower trace was obtained by simulation, using the same frequencies as the experimental plot, but with arbitrary T_2 values as indicated. Direct comparison between the experimental and simulated traces is not possible, both because the experimental data were obtained with limited digital resolution and include unresolved long-range couplings and also because it is difficult to measure with precision the T_2-values in both dimensionswhich are necessary for the simulation. However, Figure 3.27 helps to illustrate the undesireable interference of (intense) neighbouring resonances; as mentioned earlier the f_1 tail will also carry a band of noise which could further distort the sub-spectra of interest.

A comparison of the cross-sections obtained by the various methods are given in Figure 3.28. Although the three partial J spectra (Fig. 3.28B, C and D) show a significant improvement in resolution as compared with the normal spectrum (Fig. 3.28A), the distortions towards the base of the peaks in the absolute value mode (Fig. 3.28D) display become apparent when overlapping peaks are involved. The lineshapes are considerably improved using the power mode display (Fig. 3.28C) and phase-sensitive cross-sections (Fig. 3.28B). The lineshape characteristic of the latter is as expected, as was noted earlier in the simulated cross-sections (eg. Fig. 3.27B). The baseline distortion, however, does not affect the measurement of coupling constants.

In demonstrating the display of the proton-decoupled proton spectrum we draw attention to the characteristic line broadening associated with the

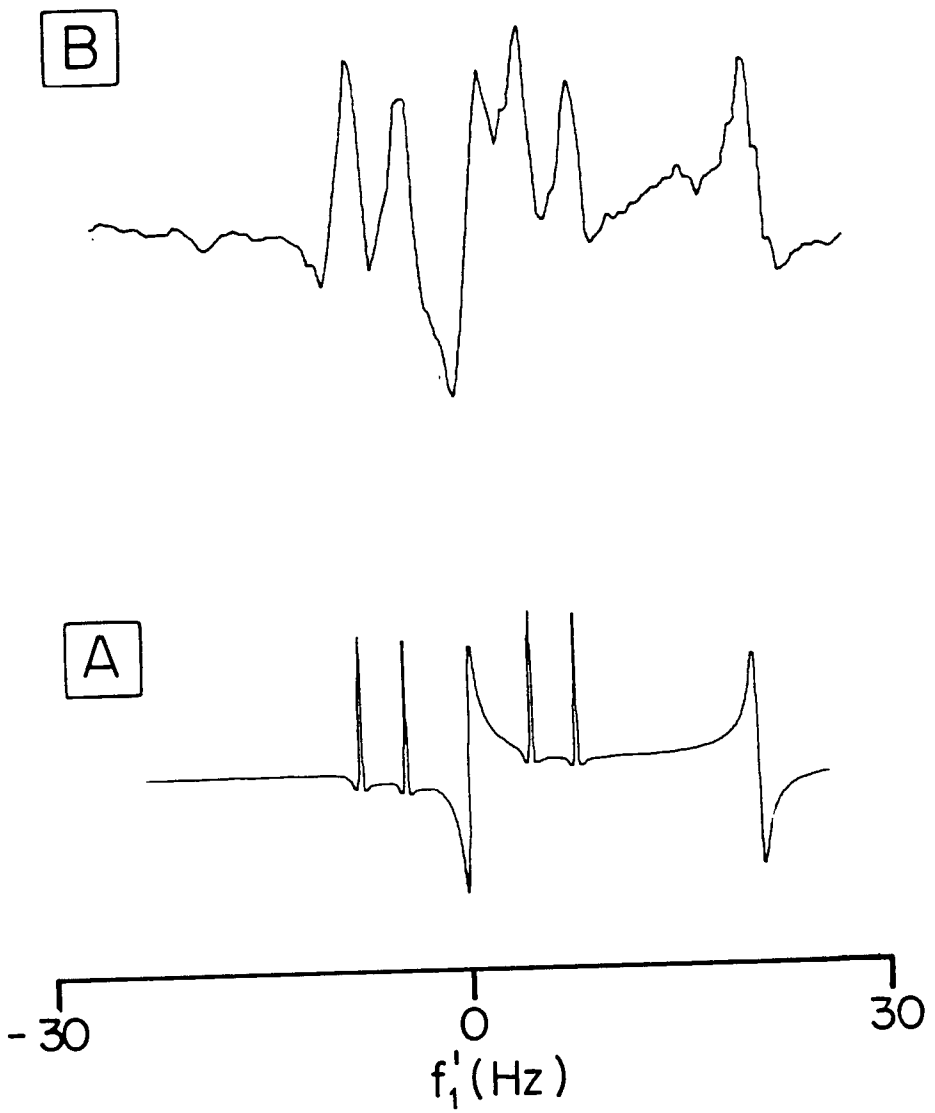

Figure 3.27: B is an experimental sub-spectrum of a doubleted doublet (J=3 and 11.6 Hz) showing the interference from an intense singlet (three times the total intensity of the multiplet) located 20 Hz away. The centre component is the f_2 tail and the outer dispersive component is the f_1 tail (note the noise on the latter). A was simulated using T_2 and T^*_2 values of 1.1 s and 0.8 s for the multiplet, and 1.6 s and 1.3 s for the singlet respectively. (Note: the simulation was not meant to reproduce the exact lineshape characteristics of B; see text).

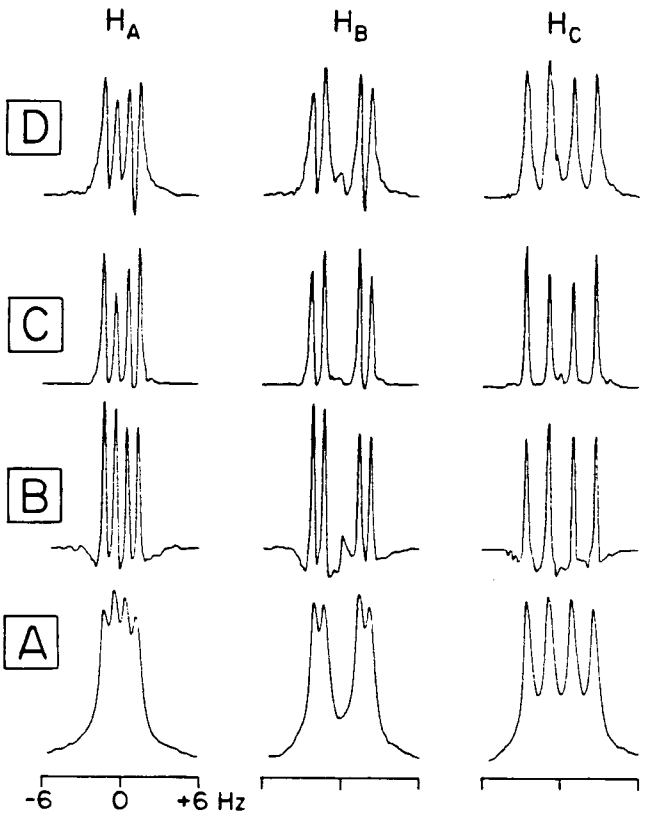

Figure 3.28: (A) The three proton multiplets of furoic acid (11) from a conventional 270 MHz spectrum. B, C and D are sections of the partial J spectra were obtained from phase-sensitive, power and magnitude mode 2D J spectra, respectively. All data processing was done on the same original time-domain signals with exponential multiplication in both time dimensions.

absolute mode in Figures 3.29C and D which represent the integral or summed projection and the "maximal" projection (profile), respectively (Sec. 3.1.3). In the latter mode only the maximum point corresponding to each f_2' value is plotted, thereby representing a profile of the 2D J spectrum, as viewed perpendicular to f_2'. The analogous projections from the power spectrum are illustrated in Figures 3.29E and F, and shows the drastic change in relative peak heights since the intensities are now equal to the square of their normal values. Although the integral projection from a phase-sensitive 2D J spectrum cannot be used to obtain a proton-decoupled proton spectrum due to the net cancellation of all signals (23), the "maximal" projection can be satisfactorily used to represent this spectrum, and is illustrated in Figure 3.29B.

3.3.4 Generalized acquisition of spin-echo data - Integrated NMR experiments

The various experiments discussed so far, namely the SEFT, SEAS and 2D J, all utilize the same basic spin-echo pulse sequence of Carr and Purcell; only the time at which the data is acquired and the subsequent data processing routines determine the final outcome of these experiments. With these close similarities in mind it is apparent that it should be possible to acquire a "general" data matrix which could then be "selectively" processed in various ways to provide a number of different experimental results such as (half-)SEFT, SEAS, 2D J and delayed 2D J spectra. The utility of this experiment will be discussed using as an illustrative example, a sample containing a mixture of 10% (0.01M) dextran (M.Wt. ca. 10,000 a 1→6 linked polymer of D-glucopyranose,3) and 0.1M methyl β-D-xylopyranoside.

The pulse sequence for this "generalised" experiment is represented by,

$$\{90^\circ - n.T - 180^\circ - \text{Acquisition}\}$$

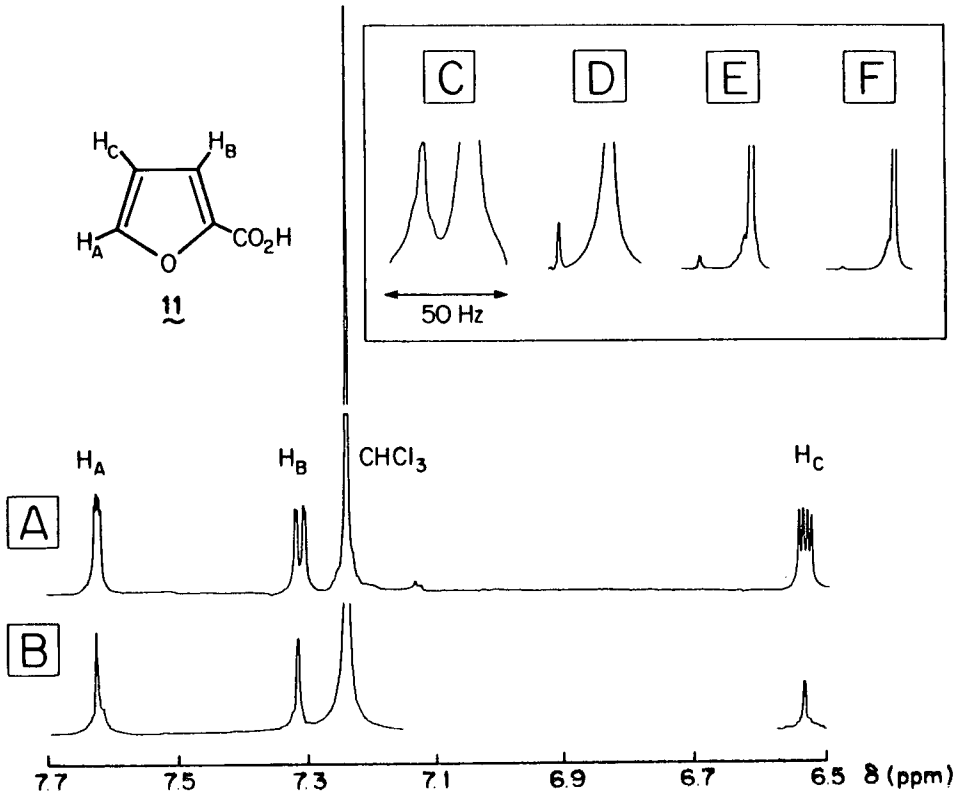

Figure 3.29: (A) The conventional 270 MHz proton spectrum of a mixture of furoic acid (11) and chloroform in $CDCl_3$ solution. (B) The corresponding proton-decoupled proton spectrum derived from a phase-sensitive 2D J spectrum $S(f'_1,f'_2)$ by taking a "maximal" projection (see text) onto the f_2 axis. Similarly (C) and (D) show the summed and maximal projections respectively of the H_B and $CHCl_3$ region derived from a magnitude spectrum; the corresponding power-mode displays are shown in (E) and (F), respectively. All processing was done on the same original data and all the spectra are scaled with respect to the $CHCl_3$ peak. Note the line broadening effect of the magnitude mode and the drastic change in the relative intensities in the power mode.

analogous to the 2D J pulse sequence, where n = 0, 1, 2, ..., N-1 (N in this case may not be a binary number). The acquired whole-echo data matrix is represented in Figure 3.30, showing every twelfth free induction decay (or echo-envelope).

The initial trace (T = 0 ms) is equivalent to a conventional FID signal obtained with a 270^{o} flip angle and on Fourier transformation it yields the conventional 1D spectrum. The half-echoes (-----) when subjected either individually to single, or collectively to double, Fourier transformations will provide either a series of SEFT spectra or the "standard" 2D J spectrum.[1] It is apparent from the conventional spectrum of the sample under consideration that no useful information concerning the monomer can be extracted from the 2D J spectrum due to the dynamic range problem; this makes it essential to obtain a partially relaxed 2D J spectrum of methyl β-D-xyloside after a suitable initial delay time T_i, as discussed in Section 3.3.1. Whole-echo Fourier transformation provides 1D partially relaxed SEAS spectra for spectral simplification and also approximate T_2 values for semi-qualitative spectral analysis as discussed in Section 2.3.

The experimental procedure described here offers a number of advantages over conventional experimental routines which are usually accomplished by subjecting a spin system to a predetermined pulse sequence and data processing cycle. The obvious advantage of the "integrated experiments" approach is the potential saving of data acquisition time; clearly this saving is dependent on the total number of separate experiments which would have to be performed to obtain the same total information, and may be considerable for complex systems

[1]Since the algorithms for the various data processing steps are generally written for data arrays with a size equal to the power of two, the 1D or 2D data arrays created in this experiment may have to be appropriately zero-filled to generate a suitable data size.

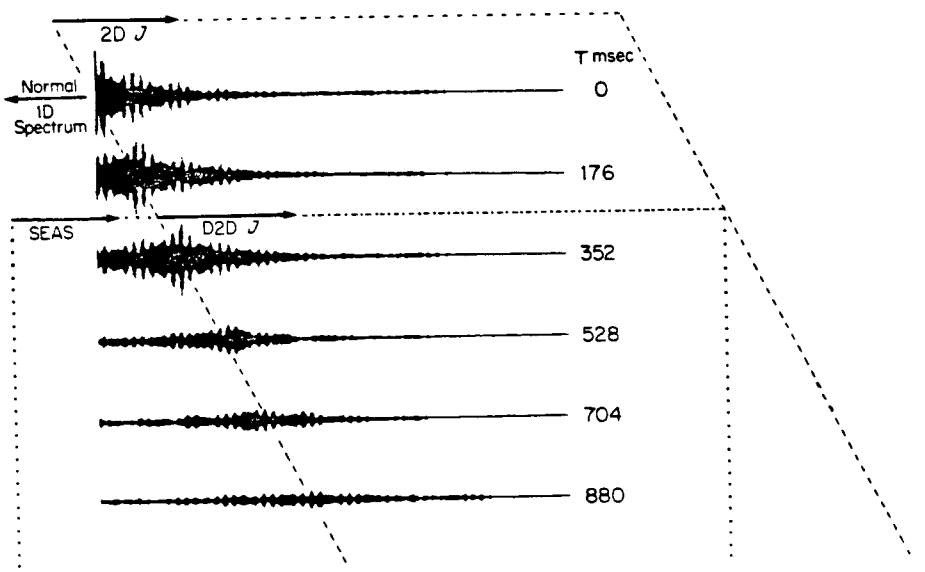

Figure 3.30: The first, and subsequently every twelfth, spin-echo signal acquired on 4K word-size data blocks with a constant increment in t_1 of 16 ms for the solution described in the text. Data processing of the half-echoes (-----) acquired from T=0 onward gives the conventional 2D J spectrum; processing of those after T_i (·····) gives a partially relaxed 2D J spectrum. Fourier transformation of individual whole echoes (·····) give SEAS information as a function of various delay times.

when studied at high dilution; this advantage is even more obvious when handling relatively unstable substances. However, an equally important advantage is that this integrated approach also provides the experimentalist with "independent" methods for analysing spectra which can be chosen after the data acquisition has been completed. In practice it is often found that the less complicated regions of the spectrum can be analysed by the 1D experiments described earlier, and it is advantageous to process only the complex regions of the spectrum by the 2D techniques if data processing time is to be minimised.

The type of experiments mentioned above requires computer systems with relatively large data storage and flexible data processing capabilities. The half-echoes can be extracted from the whole data matrix by simply left-shifting the time-domain echo-envelope signals by nT/DW number of points (DW = dwell time). The suitable initial delay, T_i, for the D2D J experiment may be obtained directly by observing the corresponding SEAS traces such as those shown in Figure 3.30.

References (Chapter III)

1. Jeener, J. Ampere International Summer School, Basko Polje, Yugoslavia, April, 1971.
2. Ernst, R. Chimi (1975) 29, 179.
3. Muller, L., Kumar, A., Ernst, R.R. J. Chem. Phys. (1975) 63, 5490.
4. Aue, W.P., Bartholdi, E., Ernst, R.R. J. Chem. Phys. (1976) 64, 2229.
5. Hester, R.K., Ackerman, J.L., Cross, V.A., Waugh, J.S. Phys. Rev. Lett. (1975) 34, 993.
6. Alla, M., Lippmaa, E. Chem. Phys. Lett. (1976) 37, 260.
7. Kumar, A., Welti, D., Ernst, R.R. J. Magn. Reson. (1975) 18, 69.
8. Wokaun, A., Ernst, R.R. Chem. Phy. Lett. (1977) 52, 407.
9. Pouzard, G., Sukumar, S., Hall, L.D. J. Am. Chem. Soc. (1981), in press.
10. Maudsley, A.A., Ernst, R.R. Chem. Phy. Lett. (1977) 50, 368.
11. Maudsley, A.A., Muller, L., Ernst, R.R. J. Magn. Reson. (1977) 28, 463.
12. Bodenhausen, G., Freeman, R. J. Magn. Reson. (1977) 28, 471.
13. Bodenhausen, G., Freeman, R., Turner, D.L. J. Chem. Phys. (1976) 65, 839.
14. Muller, L., Kumar, A., Ernst, R.R. J. Magn. Reson. (1977) 25, 383.
15. Hoffman, R.A., Forsen, S. "Progress in NMR Spectroscopy:, Emsley, J.W., Feeney, J., Sutcliff, L.H. Eds.; Pergamon Press: Oxford, 1966; Vol. 1, Chapter 2.
16. Freeman, R., Morris, G.A. Bull. Magn. Reson. (1979) 1, 5.
17. Morris, G.A. Ph.D. Dissertation, Oxford University, Oxford, 1979.
18. Carr, H.Y., Purcell, E.M. Phys. Rev. (1954) 94, 630.
19. Freeman, R., Hill, H.D.W. "Dynamic Nuclear Magnetic Resonance Spectroscopy", Jackman, L.M., Cotton, F.A. Eds.; Academic Press: New York, 1975; Chapter 5.

20. Rabenstein, D.L., Nakashima, T. Anal. Chem. (1979) 51, 1465.

21. Bodenhausen, G., Freeman, R., Niedermeyer, R., Turner, D.L. J. Magn. Reson. (1977) 26, 133.

22. Freeman, R., Hill, H.D.W. J. Chem. Phys. (1971) 54, 301.

23. Nagayama, K., Bachmann, P., Wuthrich, K., Ernst, R.R. J. Magn. Reson. (1978) 31, 133.

24. Hall, L.D., Sukumar, S. J. Magn. Reson. (1980) 38, 555.

25. Aue, W.P., Karhan, J., Ernst, R.R. J. Chem. Phys. (1976) 64, 4226.

26. Hall, L.D., Sukumar, S., Sullivan, G.R. J. Chem. Soc. Chem. Commun. (1979) 292.

27. Nagayama, K., Wuthrich, K., Bachmann, P., Ernst, R.R. Naturwissenschaften (1977) 64, 581.

28. Nagayama, K., Wuthrich, K., Bachmann, P., Ernst, R.R. Biochem. Biophys. Res. Commun. (1977) 78, 99.

29. Hall, L.D., Manville, J.F., Tracey, A. Carbohydr. Res. (1967) 4, 514.

30. Bachmann, P., Aue, W.P., Muller, L., Ernst, R.R. J. Magn. Reson. (1977) 28, 29.

31. Freeman, R., Kempsell, S.P., Levitt, M.H. J. Magn. Reson. (1979) 34, 663.

32. Levitt, M.H., Freeman, R. J. Magn. Reson. (1979) 34, 675.

33. Bax, A., Mehlkopf, A.F., Schmidt, J. J. Magn. Reson. (1980) 40, 213.

34. Hall, L.D., Sukumar, S. J. Magn. Reson. (1980) 38, 555.

35. DeMarco, A., Wuthrich, K. J. Magn. Reson. (1976) 24, 201.

36. Ferrige, A.G., Lindon, J.C. J. Magn. Reson. (1978) 31, 337.

37. Hall, L.D., Sukumar, S. Carbohydr. Res. (1979) 74, C1.

38. Hall, L.D., Morris, G.A., Sukumar, S. J. Am. Chem. Soc. (1980) 102, 1745.

39. Hall, L.D., Sukumar, S. J. Magn. Reson. (1980) 40, 405.

40. Kowalewski, V.J. "Progress in NMR Spectroscopy", Emsley, J.W., Feeney, J., Sutcliff, L.H. Eds.; Pergamon Press: Oxford, 1979; Vol. 5, Chapter 1.

41. Feeney, J., Partincton, P. J. Chem. Soc. Chem. Commun. (1973) 611.

42. Noggle, J.H., Schirmer, R.E. "The Nuclear Overhauser Effect", Academic Press: New York, 1971.

43. Hall, L.D., Sanders, J.K.M. J. Am. Chem. Soc. (1980) 102, 5703.

44. Hall, L.D., Morris, G.A., Sukumar, S. Carbohydr. Res. (1979) 79, C7.

45. Hall, L.D., Hunter, B.K., Sanders, J.K.M., Sukumar, S. to be published.

46. Freeman, R., Morris, G.A., Turner, D.L. J. Magn. Reson. (1977) 26, 373.

47. Bodenhausen, G., Freeman, R., Morris, G.A., Turner, D.L. J. Magn. Reson. (1977) 28, 17.

48. Bodenhausen, G., Freeman, R., Morris, G.A., Turner, D.L. J. Magn. Reson. (1978) 31, 75.

49. Reuben, J. "Progress in NMR Spectroscopy", Emsley, J.W., Feeney, J., Sutcliff, L.H. Eds,; Pergamon Press: Oxford, 1973; Vol. 9, Part 1.

50. Shaw, D. "Fourier Transform NMR Spectroscopy", Elsevier: Amsterdam, 1976.

51. Martin, M.L., Martin, G.J., Delpuech, J.J. "Practical NMR Spectroscopy", Heyden: London, 1980.

52. Patt, S.L., Sykes, B.D. J. Chem. Phys. (1971) 56, 3182.

53. Demco, D.E., Van Hecke, P., Waugh, J.S. J. Magn. Reson. (1974) 16, 467.

54. Jessen, J.P., Meakin, P., Kneissel, G. J. Chem. Phys. (1973) 59, 1775.

55. Hall, L.D., Sanders, J.K.M., Sukumar, S. J. Chem. Soc. Chem. Commun. (1980) 366.

56. J.K.M. Sanders, unpublished data.

CHAPTER IV

ASSIGNMENT OF NMR SPECTRA BY 2D FOURIER TRANSFORM METHODS

4.1 Introduction

Methods for assigning complex proton spectra contribute an important element in the structural elucidation of molecules using NMR spectroscopy. Simple molecules or spectra (which are usually weakly coupled and well dispersed) are generally assigned on the basis of chemical shifts, coupling constants and relative line intensities. Spin-lattice relaxation times of individual groups of protons may also be used to assign spectra of complex molecules since they are related in most cases to (dipole-dipole) relaxation contributions from neighbouring protons. The differential in relaxation properties may also be used to simplify spectra (eg. ^{1}H or ^{13}C) via the use of partially relaxed spectra (1). One of the most useful and widely used assignment techniques is selective, spin-decoupling which is available as a standard feature in most modern high-resolution spectrometers. The success of this technique is to a great extent dependent on the relative dispersion of the signals, which must be sufficient so that the irradiation frequencies can be applied selectively to just one chosen resonance. Although spectra complicated by overlap such as that shown in Figure 3.13 may be analysed by the INDOR technique (2), this cannot yet be regarded as a routine experiment mainly because it is demanding in terms of time and instrumental stability. However, it is worthwhile noting that the improved sensitivity and stability of modern high-field spectrometers does enable nuclear Overhauser enhancement (NOE) effects to be observed conveniently and accurately, and to provide structural information on molecules; because proton NOE and spin-lattice relaxation studies are related to interproton interactions "through space", they provide information on interproton distances and hence the stereochemistry of complex molecules (3,4).

Recently, novel assignment techniques based on homonuclear (5,6,7) and heteronuclear (8,9) 2D Fourier transform spectroscopy have been reported. The resulting 2D spectra provide in a rather unique way correlation between two frequencies, analogous to information obtained by double resonance techniques. In the present study, just two of these double Fourier transform techniques have been evaluated namely carbon-13-proton (^{13}C- ^{1}H) chemical shift correlation spectroscopy (9) and zero-quantum transition (2D) spectroscopy (10,11,12). The latter will be presented in the next chapter and includes ZQT spectral analysis based on the density matrix formalism. The ^{13}C- ^{1}H shift correlation experiment provides a 2D spectrum in which the f_2 and f_1 dimensions represent carbon-13 chemical shifts and the corresponding directly bonded proton chemical shifts, respectively. The (homonuclear) proton zero-quantum transition 2D spectrum represent in the f_1 dimension, ZQT frequencies which are related to the frequency "differences" of scalar coupled protons. A method based on homonuclear 2D J spectroscopy which distinguishes between peaks that arise from homo- and heteronuclear scalar couplings is also presented later in this chapter.

4.2.1 ^{13}C- ^{1}H chemical shift correlation (2D) spectroscopy

Maudsley and Ernst (8) have described an experiment to indirectly detect carbon-13 resonances using a spectrometer which is designed to detect proton resonance frequencies; this is based on the "coherent transfer of transverse magnetization" between carbon-13 and proton spin-systems and utilises the concept of double Fourier transformation. The main disadvantage of this technique for practical applications arises because the resulting 2D spectrum contains positive and negative lines which results in the net cancellation of

signals when the whole 2D spectrum is integrated (or projected onto the f_1 or f_2 axis). The ^{13}C- ^{1}H shift correlation experiment described here is that of Freeman et al. (13) and is based on a publication by Maudsley et. al. (9); the final display is a 2D spectrum with the f_1 and f_2 axes representing "decoupled" proton, and carbon-13 spectra, respectively. Although the features of chemical shift correlation experiments such as intensities and frequencies of lines can be predicted by using the density matrix approach, it may be convenient to understand the experiment in terms of a "semiclassical" approach (14,15), which is presented in the next section.[1] In these discussions the magnetization vector model is used in conjunction with the energy levels and spin population description for a simple explanation of the resulting 2D spectrum.

4.2.2 The experiment

The pulse sequence used in this study to obtain carbon-13-proton chemical shift correlation maps is given in Figure 4.1A. The features and the modifications of this experiment are best understood by first considering the original experiment of Maudsley and Ernst (8) as represented in Figure 4.1B. The initial 90° pulse applied to the proton spin system creates a transverse magnetization in a reference frame rotating at the proton transmitter frequency. During the evolution period the proton magnetization accumulates a phase angle with respect to the y' direction equal to $2\pi f_o t_1$ (rad.), where f_o is the offset frequency with respect to the proton transmitter. The second 90° proton pulse flips the y' component of this magnetization onto the longitudinal axis; the component thus created will be a function of the

[1]Such semiqualitative arguments cannot be used in the case of homonuclear shift correlation experiments.

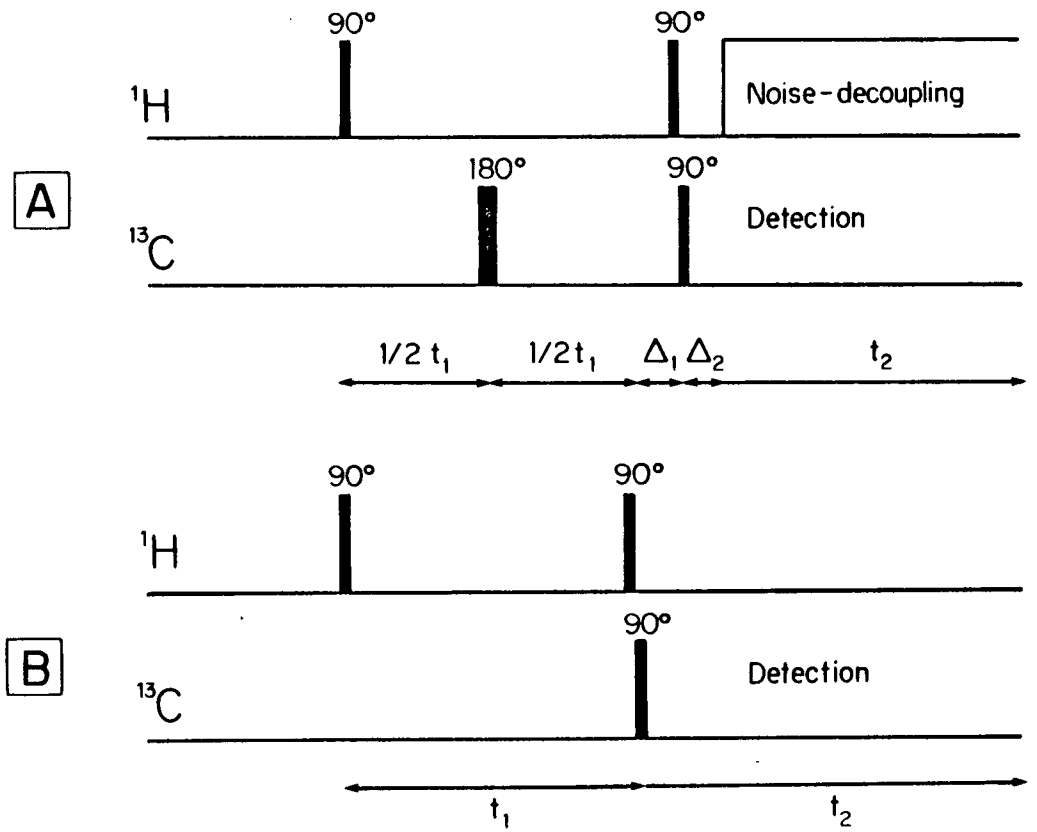

Figure 4.1: (A) The pulse sequence used for obtaining ^{13}C- ^{1}H correlation maps (Δ_1=3.3 ms; Δ_2=2.2 ms). (B) The original pulse sequence by Maudley and Ernst (8) for coherent transfer of transverse magnetization in heteronuclear systems.

evolution period t_1, and is given by $\cos 2\pi f_o t_1$. It will be recalled from Chapter I that the longitudinal magnetization is related to the population difference between two energy levels; hence the effect of the two proton pulses is to perturb the proton spin populations in a coherent fashion, related to the (proton) frequency f_o. Since carbon-13 nuclei share a common energy level with the protons (assuming they are scalar coupled), the spin populations across the carbon levels will be indirectly changed from their equilibrium values by the proton pulses. The net effect therefore is a coherent transfer of (proton) transverse magnetization into the carbon-13 system. This is analogous to population transfer experiments in 1D NMR (16). These experiments provide an improvement in sensitivity of nuclei with low gyromagnetic ratio (INEPT, Insensitive Nuclei Enhanced by Polarization Transfer).

This coherent perturbation of spins across the carbon-13 energy levels can be monitored by detecting the carbon signals, which causes <u>amplitude modulation</u> as a function of t_1.[1] The modulation frequencies are revealed by an experiment performed in accordance with 2D spectroscopy. The f_2 axis of the resulting 2D spectrum represents the conventional proton-coupled carbon-13 spectrum and the f_1 axis will represent the carbon-13 satellite proton spectrum. Although such an experiment provides all connectivity information regarding the carbon-13-proton sub-systems it may often be difficult to extract this information for complex molecules for the following reasons:

[1]The ^{13}C longitudinal magnetization prior to the, 90°, ^{13}C sampling pulse is proportional to the amplitude of the detected signal; hence the latter will be amplitude modulated as a function of t_1. This behaviour should be compared with the (^1H) 2D J experiment where the evolution of the transverse magnetization is monitored, producing a <u>phase</u> modulated signal as a function of t_1.

a) for each (proton-coupled) carbon-13 resonance in f_2, the f_1 trace represents a carbon-13 satellite proton spectrum; this complicates the 2D spectrum by introducing many overlapping lines,

b) the intensities of the multiplet components deviate from the conventional patterns with half the signals along an f_1 trace being positive and the rest negative,

c) additional lines due to long range $^{13}C-^{1}H$ couplings may also appear in the 2D spectrum.

Clearly for chemical application purposes it is desireable to simplify such a 2D spectrum by, for example, by (some sort of) decoupling in both dimensions; this should provide a simple correlation map between proton and carbon chemical shifts. Unfortunately, decoupling during either the detection period (eg. broad band noise decoupling of protons), or the evolution period (eg. by applying a 180^{o} carbon pulse at $\frac{1}{2}t_1$) causes the positive and negative signals to coincide, thereby leading to their cancellation. Solutions to these problems were suggested, and realized in practice, by Maudsley et al. (9) and by Bodenhausen et al. (14).

The variation of Freeman et al. (13) which appears to be more suitable for chemical applications is given in Figure 4.1A. The principle behind this experiment is to introduce suitable phase shifts in both time domains in order to reinforce the signals (arising from one-bond spin-spin couplings), rather than cancel them. The high- and low-frequency carbon components (due to C-H coupling) in the detected signal using the pulse sequence shown in Figure 4.1B have opposite phase; the delay Δ_2 (=1/2J) introduces a phase shift between the corresponding high- and low-frequency components so that they are brought together in phase. As a result, the noise decoupling which is subsequently

employed during the detection period does not cancel the signal. Similarly, a phase-shift is introduced in the t_1 domain by the delay Δ_1 in order to prevent signal cancellation. In practice Δ_1 is optimised for the one-bond carbon-13-proton spin-spin couplings; as a result, the signals due to long-range ^{13}C-^{1}H couplings are cancelled, which results in further simplification of the 2D spectrum. In the example chosen in this study, compromise settings of Δ_1=3.3 ms and Δ_2=2.2 ms were used.[1] (The one-bond coupling constants in the examples chosen were 130-150 Hz).

4.2.3 Experimental results

It will be recalled from Chapter III that although chemical shifts and coupling constants of multiplets can be easily measured from complex spectra by 2D J spectroscopy, assignment of these resonances may be practically impossible by conventional methods. ^{13}C- ^{1}H shift correlation spectroscopy offers a convenient means of assigning these resonances. Thus in the case of the anomeric mixture of cellobiose (Fig. 3.13) the previously assigned carbon-13 spectrum was used to assign the correlated protons (Table 4.1).

The <u>combination</u> of proton 2D J spectroscopy and ^{13}C- ^{1}H shift correlated spectroscopy provides a powerful method for resolving and assigning complex proton spectra. Since the ^{13}C- ^{1}H shift correlated spectroscopy is essentially a low resolution technique, the main purpose of the experiment is to obtain the approximate (<u>ca.</u> $\pm$ 0.01-0.02 ppm) values for of the chemical shifts of those protons which are associated with individual carbons by a one-bond ^{13}C- ^{1}H coupling.

[1]It should be noted that increasing Δ_2 results in the loss of initial points of the detected signal resulting in a loss of sensitivity.

Table 4.1 Proton and Carbon-13 NMR Parameters for Cellobiose

		1	2	3	4	5	6	
Carbon-13 shift[a]	β-D-glucopyranosyl	103.37	73.97	76.31	70.28	76.80	61.41	
	β-D-glucopyranose	96.56	74.70	75.10	79.43	75.60	60.87	
	α-D-glucopyranose	92.63	72.04	72.15	79.56	70.92	60.74	
Proton shift[b]	β-D-glucopyranosyl	4.52	3.33,3.32[c]	3.52	3.41	3.51	3.93,3.74	
	β-D-glucopyranose	4.67	3.29	3.63[d]	3.63[d]	3.59[d]	3.96,3.81	
	α-D-glucopyranose	5.23	3.58	3.83	3.65	3.96	3.88[d]	
		$J_{1,2}$	$J_{2,3}$	$J_{3,4}$	$J_{4,5}$	$J_{5,6A}$	$J_{5,6B}$	$J_{6A,6B}$
Proton coupling[e] constant	β-D-glucopyranosyl	7.9	9.5	8.8	9.9	2.4	5.8[f]	12.5
	β-D-glucopyranose	7.9	9.5	g	g	2.3	4.8[f]	12.3
	α-D-glucopyranose	3.8	9.8	8.6	g	g	g	g

[a] ±0.02 ppm, referred to external TMS *via* internal dioxane at 67.40δ [b] ±0.02 ppm, referred to internal TSP. [c] α,β forms respectively. [d] approximate shift; strongly coupled. [e] ±0.3 Hz, signs not determined. [f] assignment of reference 21 reversed. [g] strongly coupled multiplet. All values are reported for a 0.3M solution in D_2O at 22±2°C.

In a second example, 5epi-sisomycin (12), the proton spectrum shows ten out of the total seventeen "multiplets" well dispersed at 400 MHz. Therefore in this case, conventional homonuclear spin-decoupling and NOE studies provided most of the proton spectral assignments. A point of interest is the symmetry of the central cyclohexane ring. As expected, H-4 and H-6 (although they have different chemical shifts) are almost identically oriented in relation to the neighbouring protons to which they are coupled; similarly, H-1 and H-3 also show identical spatial relationship with the rest of the protons in the ring. This feature makes it impossible to assign these protons by spin-decoupling techniques. Nuclear Overhauser enhancement studies can be used to assign the H-4 and H-6 multiplets, by establishing the spatial relationship (eg. using molecular models) of these protons with those of the two neighbouring rings (see the structure of 12 given in Figure 4.4). Thus irradiation of H-1" induced an NOE in H-6; similarly the H-4 resonance was assigned by H-1'. With H-4 and H-6 assigned, spin decoupling of H-4 (because it is well dispersed, see Fig. 4.3) gave the assignment of H-3, and hence H-1. The total assignment of the proton resonances are simplified to a great extent by analysing the results from both double resonance and 2D J spectroscopy (Table 4.2).

With the completed assignment of the proton resonances it was a trivial matter to assign the carbon-13 spectrum by the use of ^{13}C- ^{1}H shift correlation spectroscopy. Figure 4.2 shows the normal carbon-13 spectrum obtained at 68 MHz together with traces corresponding to the proton spectrum associated with each carbon obtained from the shift correlation spectrum. In this example, the wide spectral width of the carbon-13 spectrum (ca. 6300 Hz from the transmitter, in the ^{13}C- ^{1}H correlation experiment) exceeded the

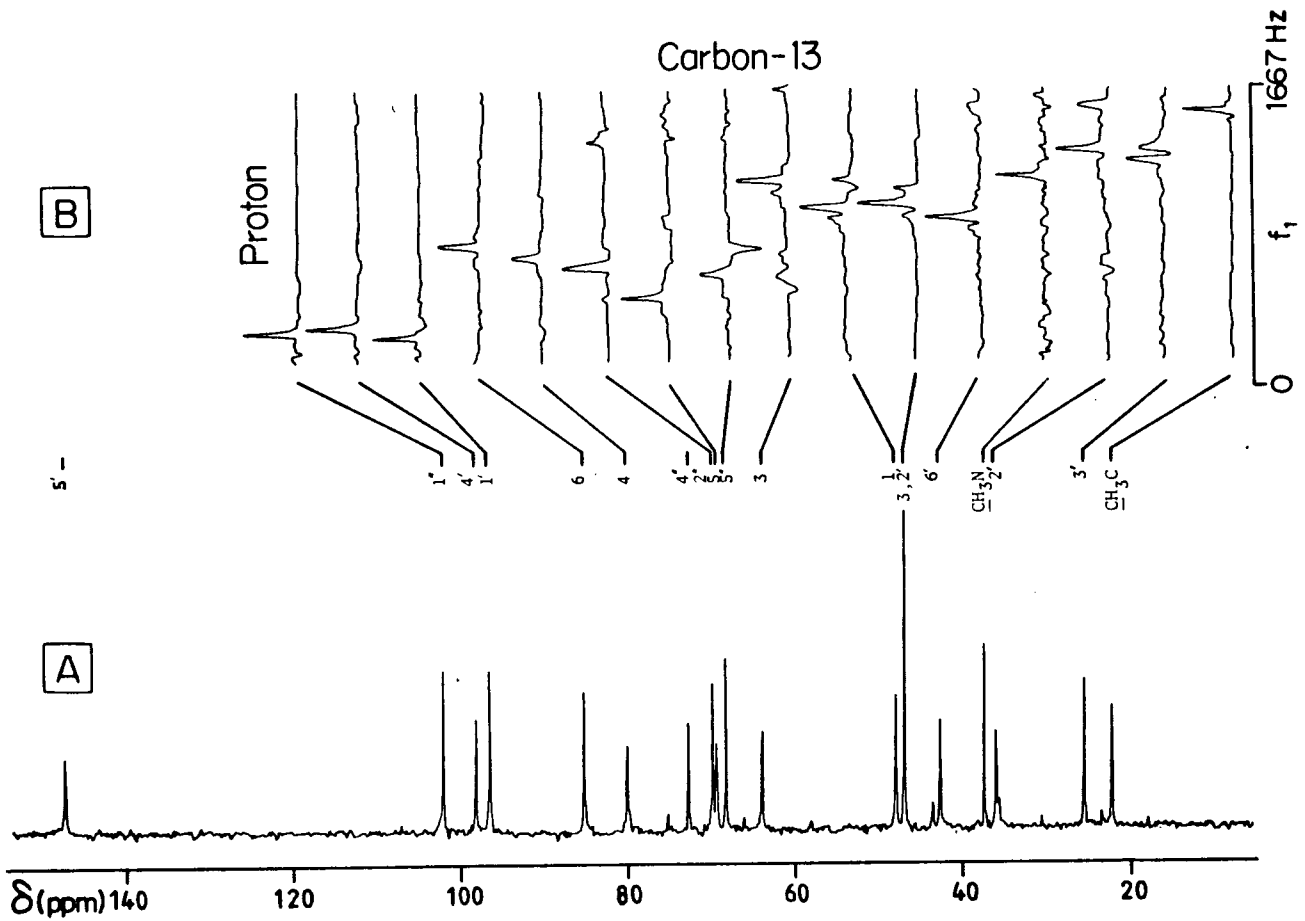

Figure 4.2: (A) The 68 MHz ^{13}C spectrum of 5,epi-sisomycin (12). (0.26M in D_2O). (B) The zero-filled individual traces obtained from the 2D spectrum, corresponding to the proton spectrum are shown above; the f_1 scale represents the frequency offset with respect to the transmitter. The trace corresponding to a CH_2 sub-system with non-equivalent protons show peaks representing both the geminal protons. Some of the distortions in lineshapes and artifacts in some of the central traces are due to imperfections in the 180° pulse on carbon. Experimental parameters: DR_1=13 Hz; DR_2=6.2 Hz; t_1 increment=150 μs; size of data matrix (t_2xt_1)=2048x256; SW_2=6300 Hz; SW_1=±1667 Hz.

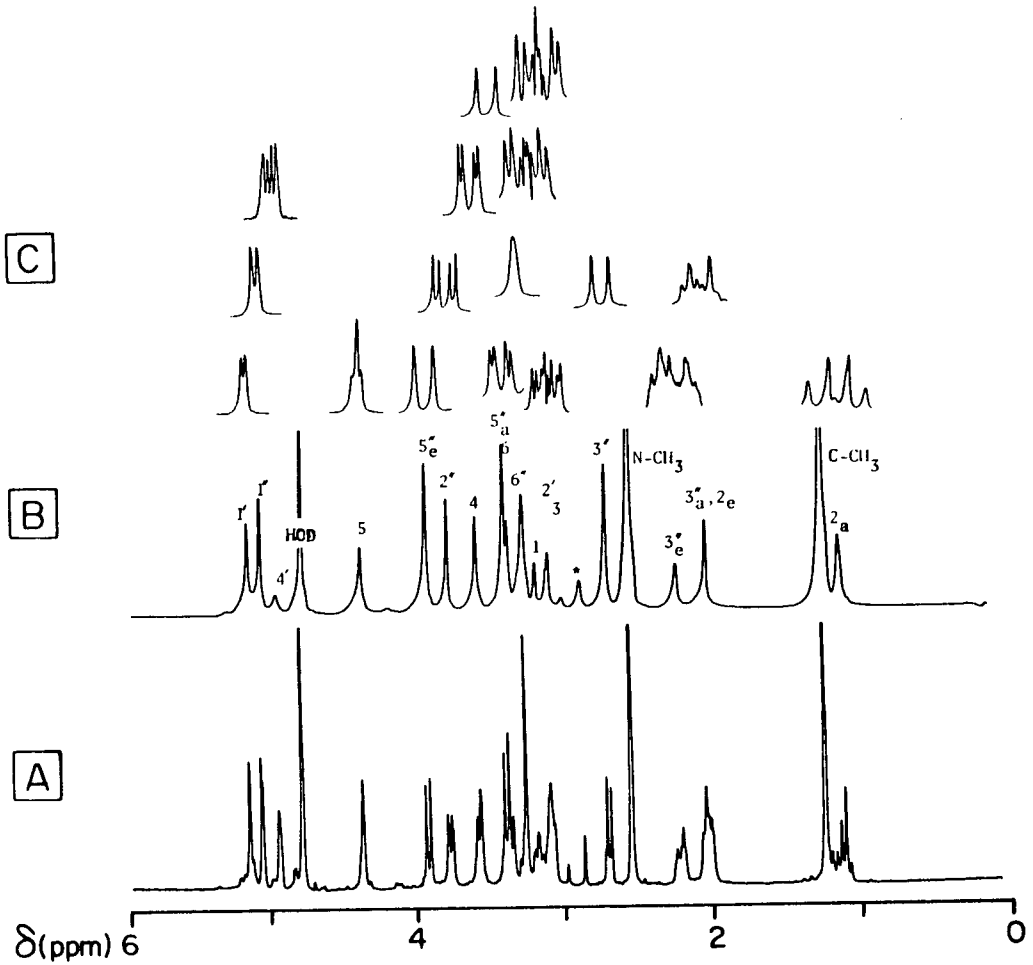

Figure 4.3: (A) The 400 MHz proton spectrum of 5,epi-sisomycin (0.1M D_2O). (B) The proton-decoupled proton spectrum and (C) the cross-sections corresponding to each proton multiplet. Note that H-2_e and H-$3'_a$ have identical chemical shifts. Digital filtering was used in both dimensions to narrow the lines in the absolute mode display. DR_1=0.15 Hz; DR_2=1.17 Hz; t_1 increment=13.33 ms; size of data matrix (t_2xt_1)=4096x128; SW_1=2400 Hz; SW_1=±18.7 Hz. (* correspond to spikes from the transmitter).

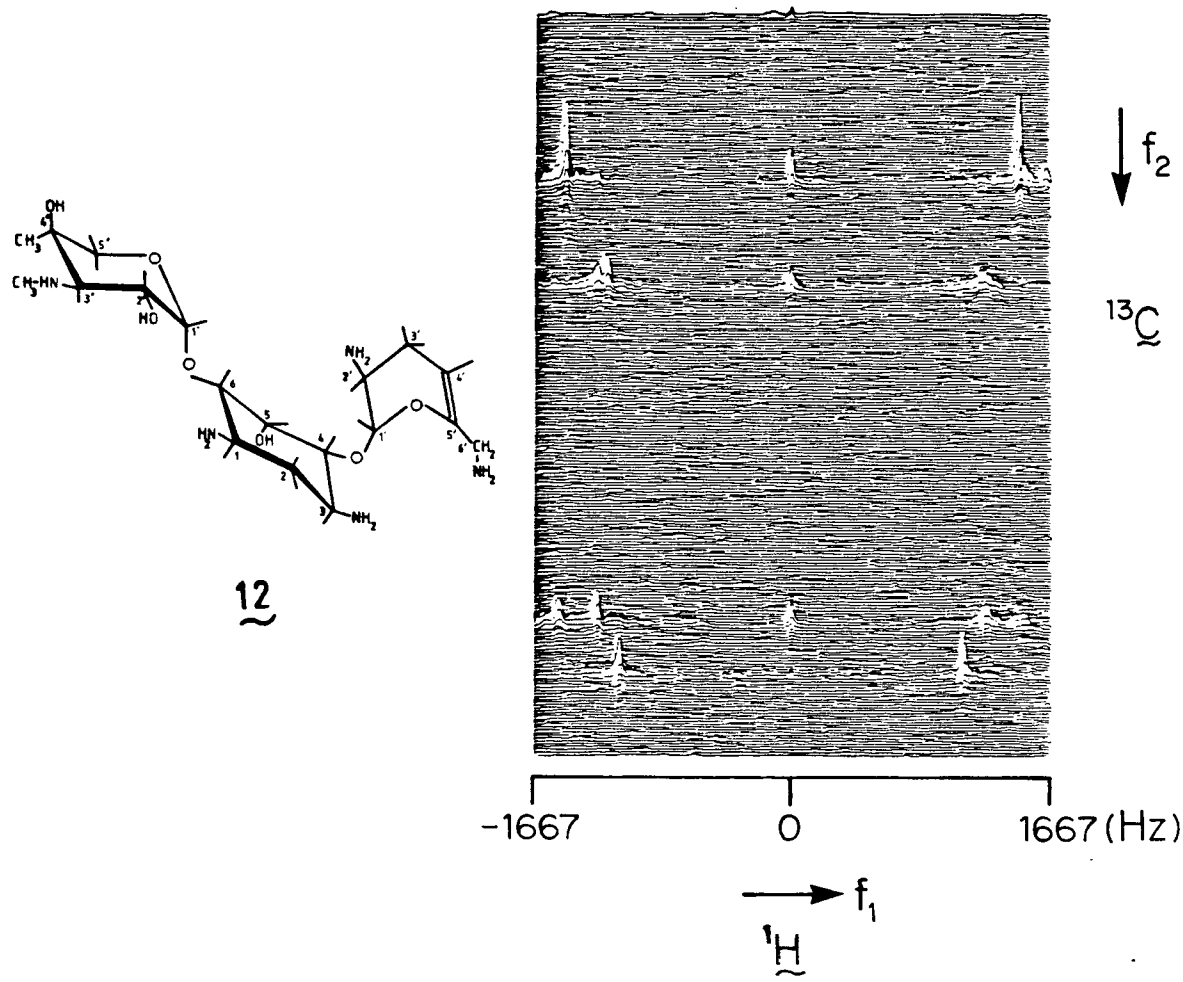

Figure 4.4: The ^{13}C- ^{1}H shift correlation 2D spectrum of the high-field region of 5,epi-sisomycin (12) plotted in the absolute value mode. The zero-frequency in f_1 corresponds to the proton transmitter frequency; the signals along this frequency correspond to the unmodulated carbon-13 component. Some of the asymmetry of the two halves may be due to inadequate digital resolution (cf. Fig. 4.2) and imperfections in the 180° pulse.

Table 4.2: Proton and Carbon-13 NMR parameters for 5,epi-sisomycin.

Carbon shifts[a]		Proton shifts[b]		Coupling constants[c]	
C-1"	102.49 δ	H-1"	5.05 δ	1"-2"	4.2 Hz
C-2"	69.95	H-2"	3.78	2"-3"	10.8
C-3"	64.07	H-3"	2.70	$5"_a$-$5"_e$	12.5
C-4"	73.02	--			
C-5"	68.40	$H-5"_a$	3.40		
		$H-5"_e$	3.92		
$^{13}CH_3$-C	22.33	CH_3-C	1.25		
$^{13}CH_3$-N	37.59	CH_3-N	2.56		
C-1'	96.79	H-1'	5.17	1'-2'	2.6
C-2'	47.06	H-2'	3.10	$2'-3'_a$	10.4
C-3'	25.70	$H-3'_a$	2.05[d]	$2'-3'_e$	6.4
		$H-3'_e$	2.24[d]	$3'_a-3'_e$	16.6
C-4'	98.89	H-4'	4.98	$3'_a-4'$	1.9
C-5'	147.65	--		$3'_e-4'$	6.4
C-6'	42.72	H-6'	3.27		
C-1	45.1	H-1	3.19	$1-2_a$	12.5
C-2	35.97	$H-2_a$	1.15	$1-2_e$	4.5
C-3		$H-2_e$	2.05	2_a-2_e	12.5
C-3	47.06	H-3	3.11	2_e-3	4.6
C-4	80.30	H-4	3.58	2_a-3	12.5
C-5	69.51	H-5	4.36	3-4	10.4
C-6	85.5	H-6	3.37	4-5	2.8
				5-6	3.0
				6-1	10.1

[a] 68 MHz data; ref. external TMS via internal dioxane. [b] 400 MHz data; ref. TSP. [c] ca. ±0.2 Hz. [d] Strongly coupled.

ability of our spectrometer[1] to apply a uniform 180° pulse to all carbon-13 spins (17) this introduced artifacts in the 2D spectrum corresponding to the resonances about 3000 Hz away from the transmitter. The traces from the 2D spectrum in Figure 4.2 were obtained from two separate experiments, with the transmitter placed on either side of the spectrum (the low-field quarternary carbon was ignored in this experiment since it does not show any response in f_1). Even so, the effect of imperfections can be noticed in some of the f_1 traces corresponding to the carbon-13 signals in the central region of the spectrum. It should be mentioned here that phase alternation of the 180° pulse, which is generally used in the spin-echo sequence to suppress imperfections cannot be applied in the $^{13}\underset{\sim}{C}$- ^{1}H experiments (18).

Based on the above experiments we infer that the advantages of the $^{13}\underset{\sim}{C}$- ^{1}H shift correlation for the application in chemistry are summarised below:

a) Unlike its 1D equivalent, selective spin-decoupling (19), the 2D, $^{13}\underset{\sim}{C}$- ^{1}H shift correlation experiment is not limited by overlap of proton resonances. Insofar that it can be performed using a <u>single</u> instrumental setting to provide simultaneously <u>all</u> the correlated frequencies.

b) For molecules such as carbohydrates, for example, where most of the proton chemical shifts are similar, the wider dispersion of the carbon-13 resonances can be advantageously used to improve the effective chemical shift

[1]Work is nearing completion on the present spectrometer to provide: a) quadrature detection of the signals so that the transmitter could be placed in the centre of the spectrum, thereby doubling the band width of the carbon-13 pulse, b) single-, rather than double-tuning of the carbon observe-coil, which could improve the efficiency of the probe, c) computer control of the transmitter frequency, so that the 180° carbon pulse can be applied at the centre of the spectrum. These features when implemented should produce ^{13}C pulses of adequate homogeneity to perform correlation experiments with compounds such as "natural products" which have resonances spread over wide spectral widths.

separation, often by a factor of about fifty (20); this is much greater than any increase in dispersion likely to become available in the foreseeable future from an increase in magnetic field strength. Providing that the carbon-13 resonances are resolved, protons which have identical chemical shifts can be resolved and identified (eg. $H\text{-}2_e$ and $H\text{-}3'_a$ in Fig. 4.2).

c) Prior to analysing a complex proton 2D J spectrum, a ^{13}C- ^{1}H correlation experiment can provide approximate chemical shifts of both weakly and strongly coupled protons; this could help in analysing proton spectra with strong coupling (see Sec. 3.2.6).

d) Because H_2O and protons that are not directly bonded to carbon atoms do not give responses in the shift correlation experiment, proton chemical shifts can be measured in aqueous solution; this can be particularly useful in biological studies.

e) It can be used to assign either proton or carbon resonances providing the chemical shift of one or of the other is known.

f) Although the spectrometer is tuned to detect carbon-13 resonances, the relaxation of the excited system is governed by spin-lattice relaxation of the protons and the sensitivity of the method is governed by population differences between the proton energy levels; as a result the overall sensitivity of the experiment is substantially greater than of an experiment designed to excite and observe carbon-13 signals.

4.3 Distinction between homonuclear and heteronuclear couplings: the use of 2D J spectroscopy to achieve broad-band heteronuclear decoupling

It has already been clearly established that a major advantage of 2D J spectroscopy in chemistry is that separation of chemical shifts and coupling

constants onto two axes increases the ease with which analysis of complex molecules can be effected. The basic phenomenon on which this approach depends is due to J modulation of signals as a function of t_1, as for example when a homonuclear spin system is subjected to non-selective pulses as described in Sections 2.3 and 3.1.

Consider now a different system, in which the pulses are applied selectively to just one group of spins (A), as for example in a heteronuclear AX system. The course of the spins in the x-y plane of the rotating frame is as illustrated in Figure 2.3a-d,g,h. Since the X nuclei do not experience the effect of the 180° pulse, the "identity" of the A magnetization vectors remains unchanged and they continue to precess at their original precession frequencies and are refocussed at the end of the evolution period. It follows from this that in a homonuclear 2D J experiment, the chemical shifts and all the heteronuclear spin-spin couplings will be simultaneously refocussed; this will be reflected in the f_1 domain of the 2D J spectra which will show only the frequencies corresponding to homonuclear spin-spin couplings. This feature may be used to distinguish between homo- and heteronuclear spin-spin couplings, without the need for any broad-band spin-decoupling apparatus such as those used in double resonance studies.

Figure 4.5 shows regions from 1D and 2D J spectra of a bicycloheptenol derivative (13)[1] in benzene-d_6; the normal spectrum indicates the complexity of the spectrum particularly when the homo- and heteronuclear couplings are of similar order of magnitude. The proton 2D J experiment performed on this compound would yield partial J spectra in the f_1 domain, showing only the proton-proton couplings. This procedure therefore allows one

[1]The IUPAC name for this compound is 1,2,3,4,7,7-hexachloro-6-exo-fluoro-bicyclo[2.2.1] hept-2-ene.

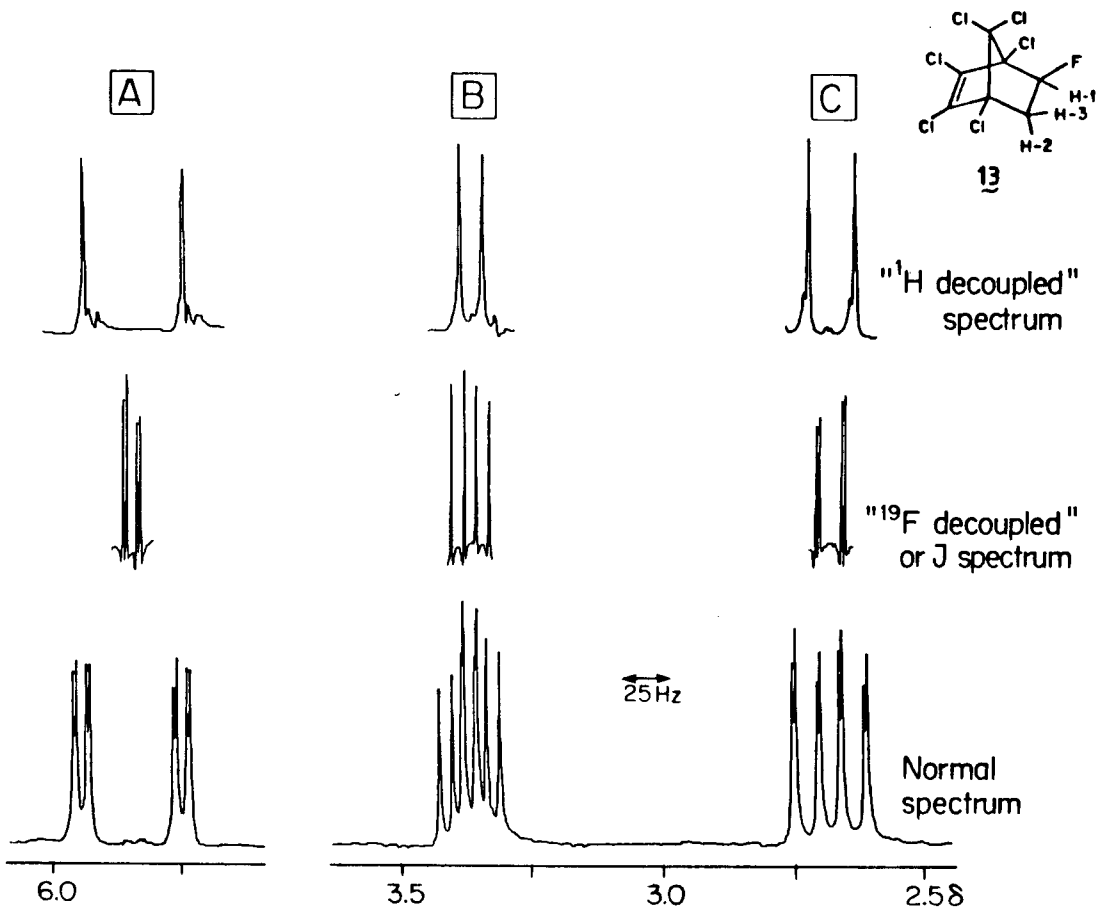

Figure 4.5: A, B and C correspond to H-1, H-2 and H-3 protons of 13 (0.1M in C_6D_6) respectively. The partial J spectra and the proton decoupled spectra were obtained from a phase-sensitive, tilted 2D J spectrum, but taking cross-sections along f'_1- and f'_2-directions respectively (SF=270 MHz).

to easily separate the homonuclear spin-spin couplings in this example. Although one could now obtain the heteronuclear couplings by comparing the normal spectrum with that of the partial J spectra, a more elegant procedure would be to measure these couplings directly from the proton-decoupled proton spectrum as shown in Figure 4.5. ($J_{H1,F}$=54.2; $J_{H1,H2}$=7.15; $J_{H1,H3}$=1.7; $J_{H2,F}$=12.3; $J_{H2,H3}$=13.5; $J_{H3,F}$=25.5 Hz). The partial J spectra were obtained by taking cross-sections parallel to the f_1 axis from a phase-sensitive 2D J spectrum; note the resolution enhancement and line shapes (Sec. 3.3.3). The "proton-decoupled" proton spectra were obtained by taking traces parallel to the f'_2 axis at the appropriate f'_1 frequencies; the line shapes in this case will be pure Lorentzian.

The results for a second example, the difluoro-sugar, 3,4,6-tri-O-acetyl-2-deoxy-2-fluoro-β-D-glucopyranosyl fluoride (14) are illustrated in Figure 4.6; although the large geminal ^1H-^{19}F couplings (~50 Hz) are obvious in the normal spectrum (Fig. 4.6B), distinction between the vicinal ^1H-^1H and ^{19}F-^1H couplings is less clear. As can be seen the partial J spectra obtained by projection of the appropriate regions of the 2D spectrum onto the f_1 axis, gives the ^1H-^1H couplings; the 45° summed projections give the ^1H-^{19}F couplings. An important practical point to note is that the equivalent information cannot be simultaneously obtained by the conventional decoupling procedures because of the large chemical shift separation between the two fluorine resonances. ($J_{F1,H1}$=55.7; $J_{F1,H2}$=13.5; $J_{F2,H1}$=4.1; $J_{F2,H2}$=51.7; $J_{F2,H3}$=16.6; $J_{H1,H2}$=6.9; $J_{H2,H3}$=9.0, $J_{H3,H4}$=9.7; $J_{H4,H5}$=9.7 Hz).

Another example which demonstrates the characterization between ^1H-^1H and ^1H-^{31}P splittings is shown in Figure 4.7, using 4,4-dideuterio-2-oxo-2-phenoxy-5-phenyl-1,3,2-dioxaphosphorinane (15). As expected, the 45° skew

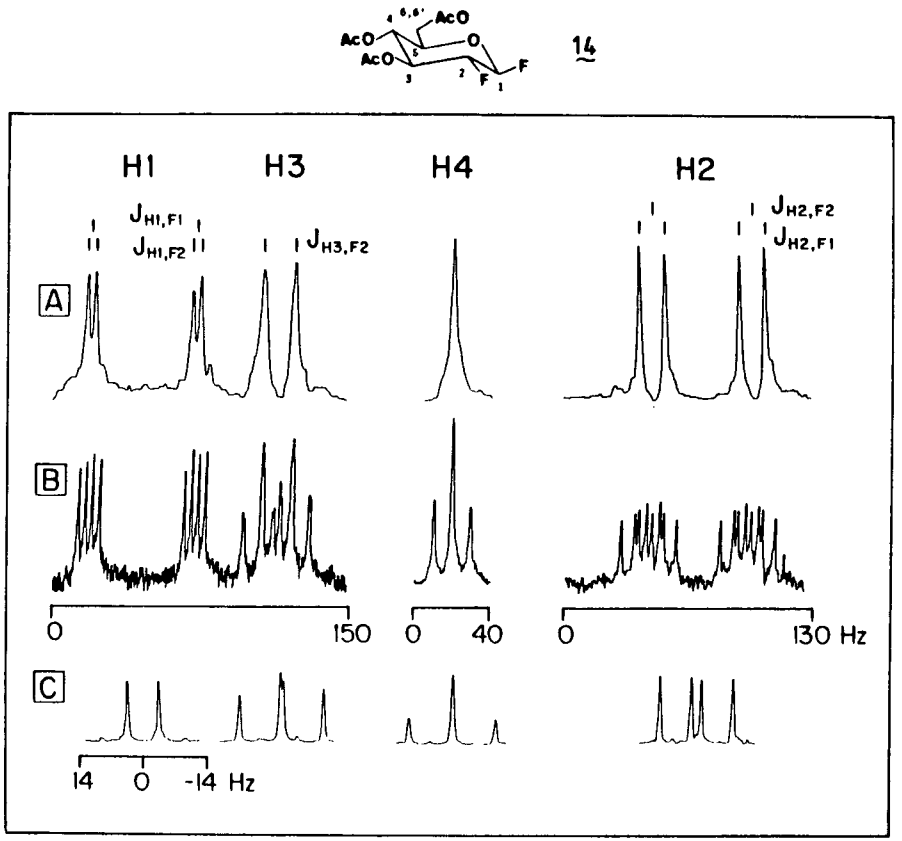

Figure 4.6: (B) Region of a normal proton spectrum 14 (0.1M in C_6D_6) at 270 MHz. A and C are respectively the proton-decoupled spectra and partial J spectra obtained by projecting the absolute value (untilted) 2D J spectrum onto the diagonal and F_1 axes. Sine-bell resolution enhancement was used in the t_2 domain. The high-field methyl peaks were suppressed by using an analog filter.

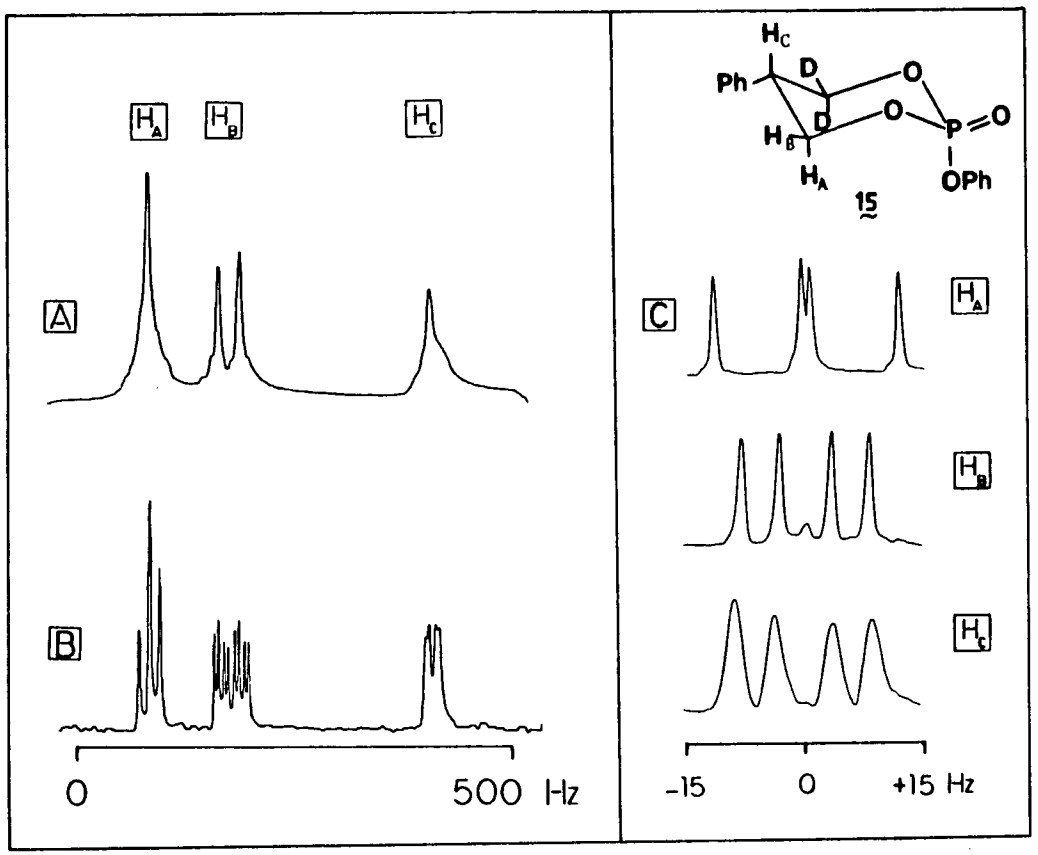

Figure 4.7: (B) The 270 MHz proton spectrum of 15 (0.1M in C_6D_6). (A) The proton decoupled and (c) the partial J spectra of the respective protons obtained by projecting regions of a (untilted) 2D J spectrum in the absolute value mode. Note the broad "tails" in the 45° skew projection, (A).

projection (Fig. 4.7A) and the partial J spectra (Fig. 4.7C) enables the easy distinction between $^{1}H-^{1}H$ and $^{1}H-^{31}P$ couplings ($J_{A,B}$=11.1; $J_{A,C}$=12.0; $J_{B,C}$=4.8; $J_{P,A}$=ca. 1; $J_{P,B}$=12.5 Hz).

As mentioned earlier, the projections from the last two examples were derived from the absolute value spectra; the indesirable features of this display mode are evident in the skew integral projections which show characteristic line-broadening effects. Obviously these may lead to the same limitations described in Section 3.2.3; in contrast the cross-sections obtained from the phase-sensitive display illustrated for the first example are clearly superior, particularly when attempting to resolve closely spaced lines in the f'_2 domain.

Another interesting application of this procedure is illustrated in Figure 4.8 using diphenyl-1,1,1-trifluoro-isopropyl-phosphate (16), in which the homonuclear couplings are separated from the heteronuclear $^{1}H-^{19}F$ and $^{1}H-^{32}P$ couplings. The limitations of the absolute value mode and the 45^{o} summed projection mode are illustrated in Figure 4.9; the many closely spaced lines and the dynamic range of the peaks within the multiplet of H-2 causes the interference of neighbouring lines causing a distortion of the resulting projection (Fig. 4.9). In contrast the Lorentzian line-shape characteristics of the phase sensitive f'_2 traces yield desirable line-shapes from which the two overlapping quartets may be easily identified for the measurement of the heteronuclear couplings ($J_{H,H}$=6.1; $J_{F,H}$=6.4; $J_{P,H}$=9.2 Hz).

The technique described above in effect provides "complete decoupling" over an infinite band-width simultaneously for all heteronuclear species. The very general nature of this experiment may prove invaluable for simplifying

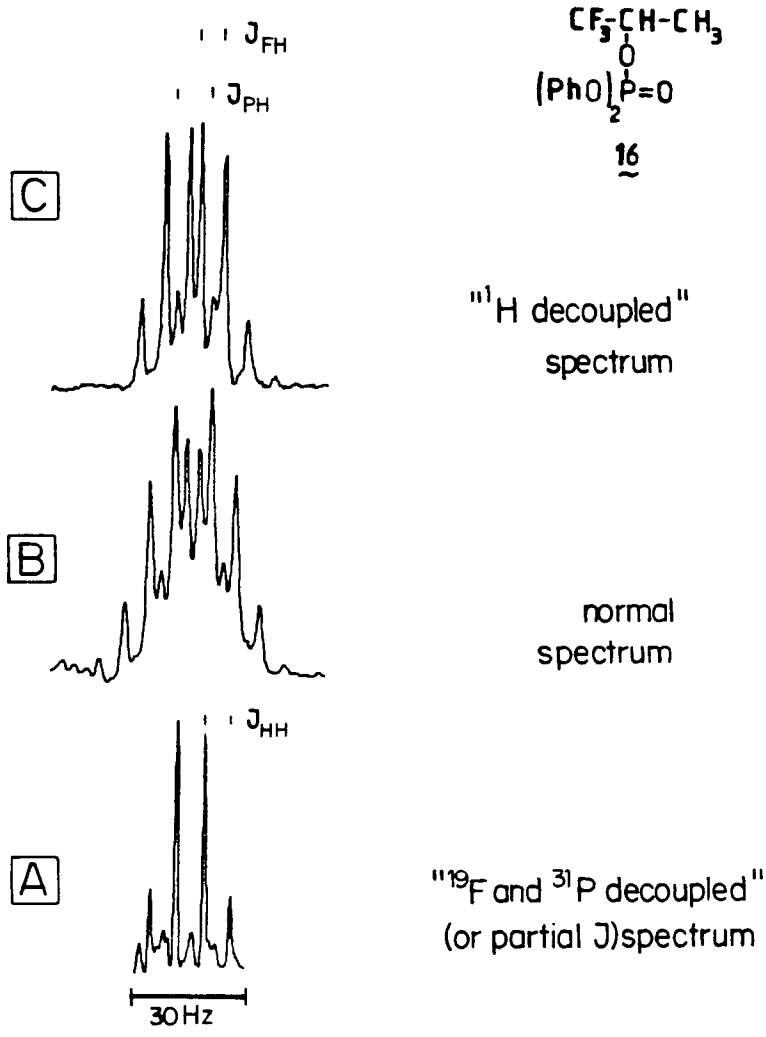

Figure 4.8: (B) The normal 270 MHz spectrum of the proton attached to C-2 of 16 (0.1M in C_6D_6). The partial J spectrum (sub-spectrum), A, gives the proton-proton coupling constants and the cross-section along f'_2 (C) gives both the ^{31}P-^1H and ^{19}F-^1H couplings. A and C are phase-sensitive traces.

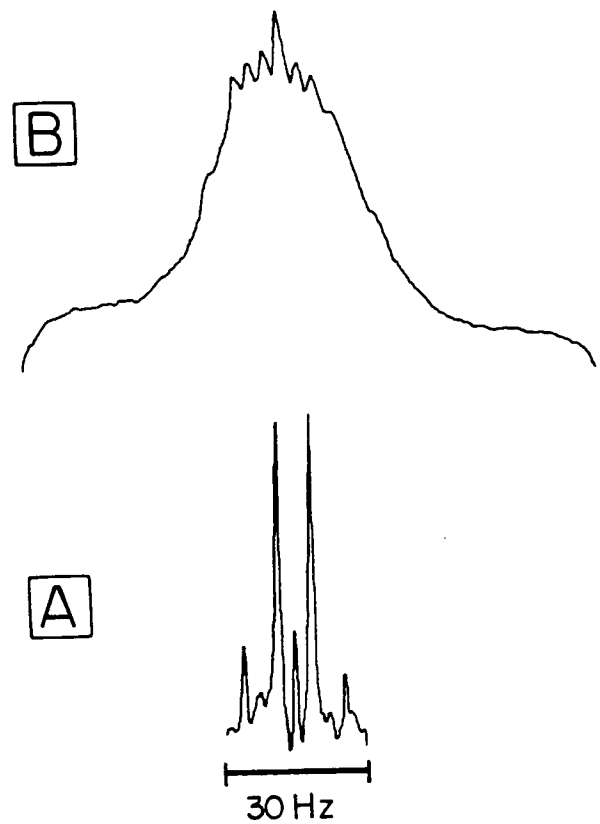

Figure 4.9: A and B were obtained from the absolute value 2D J spectrum for the sample 16. The interference of neighbouring lines makes it impossible to obtain useful information from the 45° skew projection, B. A is the partial J spectrum of H-2. Compare the phase-sensitive traces in Figure 4.8.

spectra and for measuring and assigning coupling constants, particularly because it avoids the hardware restrictions based on decoupling power and frequencies; furthermore the experiments can be performed using a conventional, single frequency proton probe and without the need for any spin-decoupling apparatus. Probably the most useful application of this technique is in organometallic chemistry, where it is not uncommon to have spin systems with many different nuclei.

References (Chapter IV)

1. Preston, C.M., Hall, L.D. Carbohydr. Res. (1974) 37, 267.
2. Moniz, W.B., Gutowsky, H.S. J. Chem. Phys. (1963) 38, 1155.
3. Noggle, J.H., Schirmer, R.E. "Nuclear Overhauser effect", Academic Press: New York, 1971.
4. Wong, K.F. Ph.D. Dissertation, The University of British Columbia, Vancouver, Canada, 1979.
5. Aue, W.P., Bartholdi, E., Ernst, R.R. J. Chem. Phys. (1976) 64, 2229.
6. Nagayama, K., Wuthrich, K., Ernst, R.R. Biochem. Biophys. Res. Commun. (1979) 90, 305.
7. Bain, A.D., Bell, R.A., Everett, J.R., Hughes, D.W. J. Chem. Soc., Chem. Commun. (1980) 256.
8. Maudsley, A.A., Ernst, R.R. Chem. Phys. Lett. (1977) 50, 368.
9. Maudsley, A.A., Muller, L., Ernst, R.R. J. Magn. Reson. (1977) 28, 463.
10. Wokaun, A., Ernst, R.R. Chem. Phys. Lett. (1977) 52, 407.
11. Wokaun, A., Ernst, R.R. Mol. Phys. (1978) 36, 317.
12. Pouzard, G., Sukumar, S., Hall, L.D. J. Amer. Chem. Soc. in press.
13. Freeman, R., Morris, G.A. J. Chem. Soc., Chem. Commun. (1978) 684.
14. Bodenhausen, G., Freeman, R. J. Magn. Reson. (1977) 28, 471.
15. Freeman, R., Morris, G.A. Bull. Magn. Reson. (1979) 1, 5.
16. Morris, G.A., Freeman, R. J. Amer. Chem. Soc. (1979) 101, 760.
17. Meakin, P., Jesson, J.P. J. Magn. Reson. (1973) 10, 296.
18. Morris, G.A. Ph.D. Dissertation, University of Oxford, Oxford, England, 1978.

19. Hoffman, R.A., Forsen, S. "Progress in NMR Spectroscopy", Emsley, J.W., Feeney, J., Sutcliff, L.H. eds.; Pergamon Press: Oxford, 1966; Vol. 1, Chapter 2.

20. Hall, L.D., Morris, G.A., Sukumar, S. J. Amer. Chem. Soc. (1980) 102, 1745.

CHAPTER V

HIGH RESOLUTION, ZERO QUANTUM TRANSITION (2D) SPECTROSCOPY

5.1 Introduction

Thus far, the principal thrust of the discussion has been towards the use of two-dimensional NMR experiments for resolving and subsequent assignment, of individual proton resonances. All of the experiments have had in common the fact that the observed transitions have involved (observable) single quantum transitions, as for example, 2D J or ^{13}C- ^{1}H chemical shift correlation spectroscopy. These experiments were described in Chapters III and IV using a "semiclassical" model for an understanding of the principles and features involved.

One of the more exciting new opportunities associated with two-dimensional NMR spectroscopy (1-5) is the possibility of observing, for weakly coupled systems, transitions which would otherwise be "forbidden", such as combination lines or multiple quantum transitions (6,7). For example, it has recently been demonstrated that zero- and multiple quantum transitions (ZQT and MQT) of simple spin systems can be selectively detected (6,8) or, even, excited (9).

Study of ZQT spectra, and their explicit analysis is of particular interest for many reasons; thus, such spectra can provide additional information on the spin system of interest which does not appear in the conventional single quantum transition (SQT) spectrum. ZQT spectra generally exhibit fewer lines than either conventional SQT spectra (7) or 2D chemical shift correlated spectra (10,11) and furthermore, the widths of the resulting lines are independent of magnetic field inhomogeneity effects. Perhaps the most appealing feature for the practicing chemist is that all of the frequency information encoded in a ZQT spectrum is correlated via <u>differences</u> in both chemical shifts and coupling constants; the latter includes information concerning the relative signs of coupling constants. As will be now shown,

these features can be recognised in the ZQT proton spectra of complex organic molecules and provide a potentially useful method for assigning the resonances of a conventional spectrum.

Although the properties of MQT spectra (more specifically, those involving double quantum transitions) have been described previously (12,13), no explicit analysis of ZQT spectra has appeared in the literature. Because it should be of general interest, that analysis for spin ½ nuclides is presented and a demonstration is given of how it can be applied, in the form of a type of sub-spectral analysis, to a more complex spin system. It is appropriate to preface that analysis with a brief reminder of how ZQT (or MQT) are created and observed in a multiple pulse Fourier transform (FT) experiment.

As we have previously mentioned, most NMR experiments involve single quantum transitions and can be simply understood in terms of the effect of pulses on classical magnetization vectors and subsequent precession (and relaxation) of these vectors in the rotating frame of reference. In contrast, ZQT (and MQT) cannot be visualized in the same sense, mainly because they are not observed directly in an FT experiment, and their creation and detection are best explained using the density matrix formalism, as summarised in the next section.[1]

5.2 Creation and observation of ZQT's in pulsed NMR

The two spin (½) systems can be conveniently represented as a 4x4 matrix (σ) written in the eigenbasis of the Zeeman hamiltonian (and F_z) (ie. ++, +-, -+, --); Table 5.1 gives the energy levels and all the possible transition frequencies for the AB case. The effect of a strong radiofrequency (RF) pulse

[1]The reader is referred to any standard text (eg. Ref. 15) on NMR for the basic equations and definitions on quantum mechanics.

Table 5.1: The energy level representation and the possible n-quantum transition frequencies for a weakly coupled AB spin 1/2 system.

M	Level	Energy[a]	Δ M	Transition	Frequency
-1	4 - -	$(f_A+f_B)/2 + J/4$	0	2 → 3	f_A-f_B
0	3 - +	$(f_A-f_B)/2 - J/4$	1	1 → 2	$f_B- J/2$
0	2 + -	$-(f_A-f_B)/2 - J/4$	1	3 → 4	$f_B+ J/2$
			1	1 → 3	$f_A- J/2$
+1	1 + +	$-(f_A+f_B)/2 + J/4$	1	2 → 4	$f_A+ J/2$
			2	1 → 4	f_A+f_B

[a] Expressed in frequency units.

of angle α applied along the x axis of the rotating frame of reference can be described by the rotation operation which transforms the matrix σ into $[\sigma]_+$ such that

$$[\sigma]_+ = \exp(-i\alpha F_x)\sigma\exp(i\alpha F_x) \qquad [5.1]$$

where the angular momentum operator projection $F_x = F_x^A + F_x^B$. Expanding the exponential form of the rotation operator yields explicit expressions for the elements of the new matrix $[\sigma]_+$ (14). It should be noted however that the new elements will also depend on the phase, ϕ, of the RF pulses, and hence the rotation operator should be written for a general case as,

$$R(\alpha,\phi) = \exp(-i\phi F_z)\exp(i\alpha F_x)\exp(i\phi F_z) \qquad [5.2]$$

For the present arguments a zero pulse phase (along the x axis) is assumed for convenience, but it will be noted later that for selective detection of n-quantum transitions it will be necessary to vary the phase, ϕ, of the RF "excitation" pulses (6,8) as shown in Figure 5.1.[1]

The NMR observable along the y axis of the rotating frame is given by

$$\langle M_y \rangle = i/2[(\sigma_{12}-\sigma_{21})+(\sigma_{13}-\sigma_{31})+(\sigma_{24}-\sigma_{42})+(\sigma_{34}-\sigma_{43}]_+ \qquad [5.3]$$

indicating that the detected signal contains only SQC's of the density matrix. However, the ZQT information is contained in the non-diagonal ZQC's of the density matrix; thus to detect ZQT (or MQT) spectra it is not only necessary to create ZQC's (or the MQ equivalent), but that information has to be transferred into the observable SQT by means of suitable pulse sequences (6,16). Of the methods available for creation and detection of ZQC's (6,16-19), the pulse sequence shown in Figure 5.1 has proven to be both convenient and of general applicability and will be described here on a weakly coupled AB spin system.

[1]The first two pulses in Figure 1 are necessary to "excite" or create ZQC.

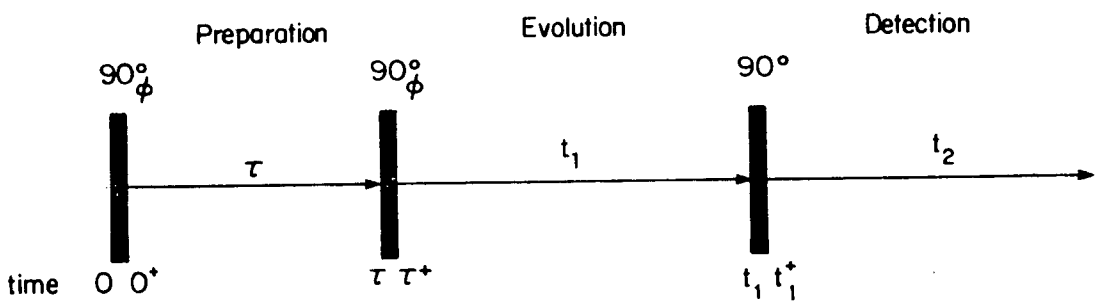

Figure 5.1: The basic pulse sequence for creation and detection of n-quantum transition spectra. The phase ϕ of the "excitation" pulses can be varied for selective detection of ZQT spectra (see text). The notation on the time-scale is used in Table 5.2.

In order to understand the creation and detection of ZQC's one can express just two elements, σ_{12}(SQC) and σ_{23}(ZQC), of the density matrix and follow the consequences of the RF pulses and the evolution of those matrix elements at various stages of the pulse sequence (Table 5.2).

The initial (Boltzmann) state of the density matrix contains only the diagonal elements (σ_{nn}) corresponding to the equilibrium populations. The intial 90° pulse equalises all diagonal elements and creates only SQC, and no ZQC (or MQC), as indicated by the $[\sigma]_{o+}$ elements in Table 5.2; the explicit expressions for the corresponding elements may be derived from equation [5.1] (14). The non-diagonal SQC's when allowed to develop during the preparation period τ, give elements of the form,

$$\sigma_{nm}(\tau) = \sigma_{nm}(0^{+})\exp(-i\sigma_{nm}\tau)\exp(-\tau/T_{2nm}) \qquad [5.4]$$

σ_{nm} is the angular velocity of the oscillating σ_{nm} coherence, with an exponential decay due to transverse relaxation (T_{2nm}); the damping term of the coherences have been omitted in Table 5.2 for convenience, since it does not contain frequency information. It can be seen from Table 5.2 that the second pulse can create ZQC (and MQC) and that these elements can now be non-zero and can evolve during the evolution period, t_1, each at their appropriate ZQT (or MQT) frequencies. Since the signal observable during the detection period (t_2) can arise only from the single quantum coherences (eq. [5.3]) it is necessary to transfer the ZQC (or MQC) information into these elements by a third (mixing) pulse. This can be seen in the final expression for the $[\sigma_{12}]_{t_2}$ element in Table 5.2 which contains terms of the type

$$a(\tau) \cdot b(t_1) \cdot \exp(-i\sigma_{12}t_2) \qquad [5.5]$$

The amplitude of each line in the final 2D spectrum will be governed by the function $a(\tau)$, which is critical for the practical applications of this

TABLE 5.2: σ_{12} and σ_{23} elements of the (4x4) density matrix of an AB system, following the pulse sequence shown in Figure 5.1. Energies are expressed in terms of angular velocities $\omega(=2\pi f)$ and $J'(=2\pi J)$. The relaxation (T_2) terms have been omitted for convenience (see text).

Time	Expressions for the matrix elements, σ_{12} and σ_{23}
0 [a]	$[\sigma_{12}]_o = 0$
	$[\sigma_{23}]_o = 0$
0^+	$[\sigma_{12}]_{o+} = i[(\sigma_{11}-\sigma_{22})+(\sigma_{33}-\sigma_{44})]_o/4 = i\Delta P/2$ [b]
	$[\sigma_{23}]_{o+} = 0$
τ	$[\sigma_{12}]_\tau = [\sigma_{12}]_{o+}\exp(-i\omega_{12}\tau) = i\Delta P\{\exp-i(\omega_B-J'/2)\tau\}/2$
	$[\sigma_{23}]_\tau = [\sigma_{23}]_{o+}\exp(-i\omega_{23}\tau) = 0$
τ^+	$[\sigma_{12}]_{\tau+} = [(\sigma_{12}+\sigma_{21})+(\sigma_{34}+\sigma_{43})-(\sigma_{13}-\sigma_{31})+(\sigma_{24}-\sigma_{42})]_\tau/4$ $= \Delta P\{\sin(\omega_B\tau/2).\cos(J'\tau/2)+i\sin(\omega_A\tau/2).i\sin(J'\tau/2)\}/2$
	$[\sigma_{23}]_{\tau+} = i[(\sigma_{12}+\sigma_{21})-(\sigma_{34}+\sigma_{43})-(\sigma_{13}+\sigma_{31})+(\sigma_{24}+\sigma_{42})]_\tau/4$ $= i\Delta P\{\sin(J'\tau/2).\sin((\omega_A+\omega_B)\tau/2).\sin((\omega_A-\omega_B)\tau/2)\}$
t_1	$[\sigma_{12}]_{t_1} = [\sigma_{12}]_{\tau+}\exp(-i\omega_{12}t_1)$ $= \Delta P\{\sin(\omega_B\tau/2).\cos(J'\tau/2)+i\sin(\omega_A\tau/2).i\sin(J'\tau/2).\exp(-i\omega_{12}t_1)\}/2$
	$[\sigma_{23}]_{t_1} = [\sigma_{23}]_{\tau+}\exp(-i\omega_{23}t_1)$ $= i\Delta P\{\sin(J'\tau/2).\sin((\omega_A+\omega_B)\tau/2).\sin((\omega_A-\omega_B)\tau/2).\exp(-i\omega_{23}t_1)\}$
t_1^+ [c]	$[\sigma_{12}]_{t_1+} = \{[(\sigma_{12}+\sigma_{21})+(\sigma_{34}+\sigma_{43})-(\sigma_{13}+\sigma_{31})+(\sigma_{24}-\sigma_{42})]_{t_1} + i[(\sigma_{14}-\sigma_{41})+(\sigma_{23}-\sigma_{32})]_{t_1}\}/4$
t_2	$[\sigma_{12}]_{t_2} = [\sigma_{12}]_{t_1+}\exp(-i\omega_{12}t_2)$ [d]

[a] Boltzmann equilibrium state. [b] $\Delta P = [(\sigma_{11}-\sigma_{22})]_0=[(\sigma_{33}-\sigma_{44})]_0$
[c] At this stage it is only necessary to know the explicit form of the observable. [d] Form of the detected signal.

experiment. The function $b(t_1)$ will contain terms involving zero, single and multiple quantum transition frequencies and will show a complex amplitude modulation of the detected signal as a function of t_1. The form of $[\sigma]_{t_2}$ indicates that a double Fourier transformation with respect to t_2 and t_1 will show only the observable SQT in the f_2-domain while the f_1-domain includes, in addition, all "forbidden" transitions. Thus the τ-domain (preparation period) and the t_1-domain (evolution period) respectively influence the amplitudes and frequencies of the n-quantum transitions studied by a 2D NMR experiment. The present work deals specifically with the ZQT spectral analysis (ie. the f_1 domain) and will be discussed for weakly coupled AB, ABC, AB_2 ABCD and AB_3 spin systems.

5.3 Spectral analysis of zero quantum transitions

5.3.1 Generalization

ABCD... refers to a weakly coupled spin ½ system having energies f_A, f_B, ..., ($f_A > f_B > \ldots$ is assumed) respectively expressed in frequency units with respect to the transmitter frequency, and coupling constants J_{AB}, J_{AC}, ...

The basic product functions and corresponding energy levels are described in standard NMR texts (15,20,21), usually in the context of analysis for the allowed single quantum transitions. These basic analyses are easily extended to predict the frequencies of the ZQT spectra. The "selection rule" for ZQT is $\Delta M = 0$ where M is the projection of the total spin angular momentum in the z direction. Spin functions will be represented by standard + and - symbols in non-degenerate systems (α and β will be used in the case of degeneracy).

It has already been noted by Wokaun and Ernst (17) that different types of ZQT can be defined, depending on whether one or several pairs of spins are involved in a transition for which $\Delta M = 0$. For the purpose of the present discussion the terms "transition of the first-kind" will refer to the ZQT involving only one pair of spins (the other spins being unchanged), ZQT of the second-kind will refer to a change of two pairs of apins, and so on. The following transition notation, which is convenient for predicting the frequencies involved, is also introduced: for example, a transition of the first kind in an ABCD system,

$$+-++ \rightarrow ++-+$$

will be denoted by $(A^+)B^-C^+(D^+)$, where the parentheses around the A and D nuclei imply that the + spins corresponding to these nuclei remain unchanged, while the B and C spins, which are involved in the transition, change from - to + and + to - respectively. The signs in the above notation refer to the initial states.[1]

5.3.2 AB system

This is the simplest case of a coupled spin ½ system which will be expected to show a single ZQT, as can be seen in Table 5.1. Since ZQT appear as a complex amplitude modulation of the NMR observable (ie. SQC in the density matrix), the frequencies corresponding to both 2→3: A^+B^- and 3→2: B^+A^- (opposite in sign) are expected in the ZQT spectrum, but for convenience only the positive (absolute) frequencies will be presented in the following discussions. The ZQT, A^+B^-, in this example will appear with the frequency $(f_A - f_B)$ and is independent of J_{AB}. It can be noted from Table

[1]A different nomenclature is used when equivalent groups of nuclei are involved, as will be seen later for the AB_2 and AB_3 case.

5.1 that the double quantum transition (DQT) appearing at (f_A+f_B), corresponds to a higher frequency than the ZQT. In this simple case, the ZQT spectrum will not provide more information than the conventional SQT spectrum.

5.3.3 ABC system

Table 5.3 gives the energy levels for the ABC system and the possible ZQT frequencies, which are centred at the chemical shift difference between each pair of nuclei. The ZQT spectrum will show three doublets centred at (f_A-f_B), (f_A-f_C), and (f_B-f_C), the splittings being $(J_{AC}-J_{BC})$, $(J_{AB}-J_{BC})$ and $(J_{AB}-J_{AC})$ respectively. Inspection of these ZQT frequencies will indicate that the chemical shift difference between two nuclei, for example A and B, is associated with the coupling constants J_{AC} and J_{BC} but not their mutual coupling, J_{AB}. This feature is quite general to ZQT's of the first kind and can be easily extended to other systems which show multiplets of the form,

$$(f_A-f_B)\pm(J_{AC}-J_{BC}\pm(J_{AD}-J_{BD})\pm \cdots\cdots$$

The appearance of chemical shift and coupling constant <u>differences</u> in ZQT spectra is very different from conventional NMR spectroscopy and it is this feature which provides a technique for correlating chemical shifts and coupling constants. Because the coupling constant terms appear as <u>differences</u>, their relative signs have significance in the ZQT spectra and hence can be evaluated by intercomparison between the normal (SQT) and ZQT spectra.

The AB_2 system is a special case of a three spin system, and the corresponding energy levels are given in Figure 5.2, in which the functions of nuclei B are separated according to their symmetry. ZQT's will be expected only within each of the $M=\pm\frac{1}{2}$ submanifolds and, since elements of different

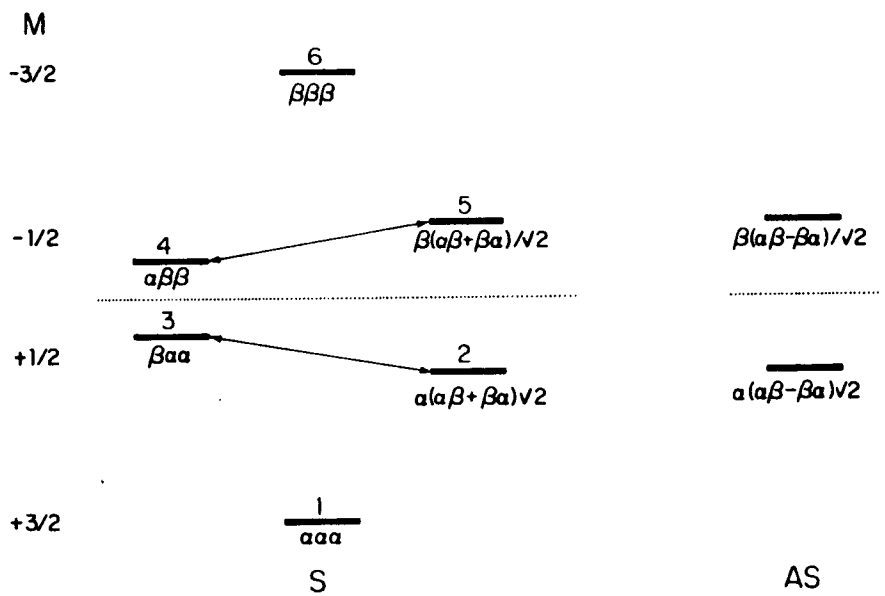

Figure 5.2: Energy level representation for an AB_2 spin ½ system; S and AS refer to the symmetric and anti-symmetric functions respectively. The possible ZQT's are indicated by the arrows.

TABLE 5.3: The energy levels and the ZQT frequencies for an ABC system.

M	Level	Energy[a]	ZQT	Frequency
-3/2	8 - - -	$(f_A+f_B+f_C)/2 + (J_{AB}+J_{AC}+J_{BC})/4$		
	7 - - +	$(f_A+f_B-f_C)/2 + (J_{AB}-J_{AC}-J_{BC})/4$	$(A^-)B^+ C^-$: 6 → 7	$(f_B-f_C) - (J_{AB}-J_{AC})/2$
-1/2	6 - + -	$(f_A-f_B+f_C)/2 - (J_{AB}-J_{AC}+J_{BC})/4$	$A^+(B^-)C^-$: 5 → 7	$(f_A-f_C) - (J_{AB}-J_{BC})/2$
	5 + - -	$-(f_A-f_B-f_C)/2 - (J_{AB}+J_{AC}-J_{BC})/4$	$A^+ B^-(C^-)$: 5 → 6	$(f_A-f_B) - (J_{AC}-J_{BC})/2$
	4 - + +	$(f_A-f_B-f_C)/2 - (J_{AB}+J_{AC}-J_{BC})/4$	$A^+ B^-(C^+)$: 3 → 4	$(f_A-f_B) + (J_{AC}-J_{BC})/2$
+1/2	3 + - +	$-(f_A-f_B+f_C)/2 + (J_{AB}-J_{AC}+J_{BC})/4$	$A^+(B^+)C^-$: 2 → 4	$(f_A-f_C) + (J_{AB}-J_{BC})/2$
	2 + + -	$-(f_A+f_B-f_C)/2 + (J_{AB}-J_{AC}-J_{BC})/4$	$(A^+)B^+ C^-$: 2 → 3	$(f_B-f_C) + (J_{AB}-J_{AC})/2$
+3/2	1 + + +	$-(f_A+f_B+f_C)/2 + (J_{AB}+J_{AC}+J_{BC})/4$		

[a] Expressed in frequency units.

symmetry do not mix in the density matrix, only elements belonging to the same irreducible representation within a given M submanifold will give rise to ZQT lines. Therefore in this case we would expect the ZQT's 2↔3 and 4↔5 at frequencies $(f_A-f_B)\pm\frac{1}{2}J_{AB}$. Note that the coupling J_{AB} appears in the above term but not J_{BB}.

5.3.4 ABCD system

Table 5.4 gives the levels and their corresponding energies, in frequency units, for an ABCD case, including all possible ZQT frequencies. If we first consider the transitions within the M=+1 submanifold, six ZQT's are expected (due to the six possible chemical shift differences), each of the form,

$$(f_C-f_D)+\tfrac{1}{2}[(J_{AC}-J_{AD}) + (J_{BC}-J_{BD})] \qquad (A^+)(B^+)C^+D^-:2\leftrightarrow3$$

The corresponding transitions in the M = -1 submanifold will be of the form,

$$(f_C-f_D)-\tfrac{1}{2}[(J_{AC}-J_{AD}) + (J_{BC}-J_{BD})] \qquad (A^-)(B^-)C^+D^-:14\leftrightarrow15$$

Taken together, these twelve transitions correspond to the six doublets in the ZQT spectrum only positive frequencies being considered, arising from the M = ±1 levels.

Similarly one can expect fifteen ZQT's arising from the M = 0 level, of these, three are ZQT's of the second-kind, involving the simultaneous change of two pairs of spins, namely $A^+B^+C^-D^-$, $A^+B^-C^+D^-$ and $A^+B^-C^-D^+$ andoccurring at frequencies $(f_A-f_B) + (f_C-f_D)$, $(f_A-f_C) + (f_B-f_D)$ and $(f_A-f_D) + (f_B-f_C)$; note that the transitions appear at relatively higher frequencies and are singlets. The remaining twelve ZQT's are of the first-kind, and the transitions involving the chemical shift differences, for example between C and D nuclei, will be of the form,

TABLE 5.4A: The energy levels for an ABCD system, expressed in frequency units.

M	Level		Energy
-2	16	- - - -	$(f_A+f_B+f_C+f_D)/2 + (J_{AB}+J_{AC}+J_{AD}+J_{BC}+J_{BD}+J_{CD})/4$
-1	15	- - - +	$(f_A+f_B+f_C-f_D)/2 + (J_{AB}+J_{AC}-J_{AD}+J_{BC}-J_{BD}-J_{CD})/4$
	14	- - + -	$(f_A+f_B-f_C+f_D)/2 + (J_{AB}-J_{AC}+J_{AD}-J_{BC}+J_{BD}-J_{CD})/4$
	13	- + - -	$(f_A-f_B+f_C+f_D)/2 - (J_{AB}-J_{AC}-J_{AD}+J_{BC}+J_{BD}-J_{CD})/4$
	12	+ - - -	$-(f_A-f_B-f_C-f_D)/2 - (J_{AB}+J_{AC}+J_{AD}-J_{BC}-J_{BD}-J_{CD})/4$
0	11	- - + +	$(f_A+f_B-f_C-f_D)/2 + (J_{AB}-J_{AC}-J_{AD}-J_{BC}-J_{BD}+J_{CD})/4$
	10	- + - +	$(f_A-f_B+f_C-f_D)/2 - (J_{AB}-J_{AC}+J_{AD}+J_{BC}-J_{BD}+J_{CD})/4$
	9	- + + -	$(f_A-f_B-f_C+f_D)/2 - (J_{AB}+J_{AC}-J_{AD}-J_{BC}+J_{BD}+J_{CD})/4$
	8	+ - - +	$-(f_A-f_B-f_C+f_D)/2 - (J_{AB}+J_{AC}-J_{AD}-J_{BC}+J_{BD}+J_{CD})/4$
	7	+ - + -	$-(f_A-f_B+f_C+f_D)/2 - (J_{AB}-J_{AC}+J_{AD}+J_{BC}-J_{BD}+J_{CD})/4$
	6	+ + - -	$-(f_A+f_B-f_C-f_D)/2 + (J_{AB}-J_{AC}-J_{AD}-J_{BC}-J_{BD}+J_{CD})/4$
+1	5	- + + +	$(f_A-f_B-f_C-f_D)/2 - (J_{AB}+J_{AC}+J_{AD}-J_{BC}-J_{BD}-J_{CD})/4$
	4	+ - + +	$-(f_A-f_B+f_C+f_D)/2 - (J_{AB}-J_{AC}-J_{AD}+J_{BC}+J_{BD}-J_{CD})/4$
	3	+ + - +	$-(f_A+f_B-f_C+f_D)/2 + (J_{AB}-J_{AC}+J_{AD}-J_{BC}+J_{BD}-J_{CD})/4$
	2	+ + + -	$-(f_A-f_B-f_C+f_D)/2 + (J_{AB}+J_{AC}-J_{AD}+J_{BC}-J_{BD}-J_{CD})/4$
+2	1	+ + + +	$-(f_A+f_B+f_C+f_D)/2 + (J_{AB}+J_{AC}+J_{AD}+J_{BC}+J_{BD}+J_{CD})/4$

TABLE 5.4B: The ZQT frequencies for an ABCD case.

Transitions of the first-kind	Transitions of the second-kind
$(f_A-f_B) \pm \frac{1}{2}\{(J_{AC}-J_{BC})\pm(J_{AD}-J_{BD})\}$	$(f_A-f_B) + (f_C-f_D)$
$(f_A-f_C) \pm \frac{1}{2}\{(J_{AB}-J_{BC})\pm(J_{AD}-J_{CD})\}$	$(f_A-f_C) + (f_B-f_D)$
$(f_A-f_D) \pm \frac{1}{2}\{(J_{AB}-J_{BD})\pm(J_{AC}-J_{CD})\}$	$(f_A-f_D) + (f_B-f_C)$
$(f_B-f_C) \pm \frac{1}{2}\{(J_{AB}-J_{AC})\pm(J_{BD}-J_{CD})\}$	
$(f_B-f_D) \pm \frac{1}{2}\{(J_{AB}-J_{AD})\pm(J_{BC}-J_{CD})\}$	
$(f_C-f_D) \pm \frac{1}{2}\{(J_{AC}-J_{AD})\pm(J_{BC}-J_{BD})\}$	

$(f_C-f_D)+\frac{1}{2}[(J_{AC}-J_{AD}) + (J_{BC}-J_{BD})]$ $(A^+)(B^-)C^+D^-$: 7→8

$(f_C-f_D)+\frac{1}{2}[(J_{AC}-J_{AD}) + (J_{BC}-J_{BD})]$ $(A^-)(B^+)C^+D^-$: 9→10

Thus the final ZQT spectrum will contain 27 lines (Table 5.4) composed of six quartets (doublets of doublets), one centred at each of the six possible frequency differences Δ_{AB},... with the splitting pattern $\pm(J_{AC}-J_{BC}) \pm (J_{AD}-J_{BD})$,... and three singlets corresponding to the ZQT's of the second-kind. (Note that the corresponding SQT spectrum consists of 56 lines, 24 of which are combination lines).

Another four-spin system of interest is the AB_3 case; three of the nuclei are equivalent and hence the B_3 sub-system may be represented according to the C_3 symmetry group. The basic symmetry functions may be classified with respect to the A_1 or E irreducible representations as shown in Table 5.5 (the subscripts refer to the M values). The ZQT's originating from the various levels are indicated in Table 5.6. The ZQT spectrum will show signals at frequencies, $(f_A-f_B)\pm J_{AB}$ and (f_A-f_B).[1]

The above discussions can be easily extended to more complicated spin systems to predict the ZQT spectra by following procedures similar to those of conventional NMR spectral analysis. First, the stationary state wave functions should be determined and their energies calculated; then the frequencies of the ZQT's can be predicted by considering only the transitions between states of a given M sub-manifold ($\Delta M=0$) and function of same symmetry, as discussed earlier.

[1]It is interesting to note that although for molecules in isotropic solution ZQT's occur only between levels belonging to the same irreducible representation, Tang and Pines have recently demonstrated how this rule can be broken in the case of an "oriented" CH_3 group (22),

TABLE 5.5: Energies and basic (symmetry) functions corresponding to an AB_3 system. The A and E states of the C_3 symmetry group are indicated in the left hand column; the subscripts here indicate the M values. The E states are doubly degenerate but only one of the functions is represented.

State	Basic function	Energy[a]
A_{-2}	$\beta\beta\beta\beta$	$(f_A+3f_B)/2 + 3J/4$
$1A_{-1}$	$\beta\{\beta\beta\alpha + \beta\alpha\beta + \alpha\beta\beta\}/\sqrt{3}$	$(f_A+ f_B)/2 + J/4$
$2A_{-1}$	$\alpha\beta\beta\beta$	$-(f_A-3f_B)/2 - 3J/4$
$1A_0$	$\beta\{\alpha\alpha\beta + \alpha\beta\alpha + \beta\alpha\alpha\}/\sqrt{3}$	$(f_A- f_B)/2 - J/4$
$2A_0$	$\alpha\{\beta\beta\alpha + \beta\alpha\beta + \alpha\beta\beta\}/\sqrt{3}$	$-(f_A- f_B)/2 - J/4$
$1A_1$	$\beta\alpha\alpha\alpha$	$(f_A-3f_B)/2 - 3J/4$
$2A_1$	$\alpha\{\alpha\alpha\beta + \alpha\beta\alpha + \beta\alpha\alpha\}/\sqrt{3}$	$-(f_A+ f_B)/2 + J/4$
A_2	$\alpha\alpha\alpha\alpha$	$-(f_A+3f_B)/2 + 3J/4$
E_{-1}	$\beta\{\beta\beta\alpha - \beta\alpha\beta\}/\sqrt{2}$	$(f_A+ f_B)/2 + J/4$
$1E_0$	$\beta\{\alpha\alpha\beta - \alpha\beta\alpha\}/\sqrt{2}$	$(f_A- f_B)/2 - J/4$
$2E_0$	$\alpha\{\beta\beta\alpha - \beta\alpha\beta\}/\sqrt{2}$	$-(f_A- f_B)/2 - J/4$
E_1	$\alpha\{\alpha\alpha\beta - \alpha\beta\alpha\}/\sqrt{2}$	$-(f_A+ f_B)/2 + J/4$

[a] J refers to J_{AB}.

TABLE 5.6: The ZQT's and their energies given in frequency units for an AB_3 case (see Table 5.5).

ZQT	Energy
$2A_1 \rightarrow 1A_1$	$(f_A-f_B) - J_{AB}$
$2A_0 \rightarrow 1A_0$	(f_A-f_B)
$2A_{-1} \rightarrow 1A_{-1}$	$(f_A-f_B) + J_{AB}$
$2E_0 \rightarrow 1E_0$	(f_A-f_B)

5.4 Applications of ZQT spectroscopy in chemistry

It might have been anticipated that explicit analysis of the ZQT-spectrum of the multiple spin-systems of a typical, complex organic molecule would be both cumbersome and time-consuming. However, it will be noted from the above formalism that since ZQC can only be created between spins which have mutual spin-spin coupling, a type of sub-spectral analysis is invariably possible.... long-range couplings (across four, or more, bonds) are frequently of small- or zero-magnitude and so it is generally possible to consider in isolation only those spins which have a vicinal or geminal coupling; as will be seen, this substantially simplifies analysis of ZQT spectra in practical cases. We shall illustrate this point, and hence some of the diagnostic potential of ZQT spectroscopy in organic chemistry, by a study of trideuteriomethyl 2,3,4,6-tetra-O-trideuterioacetyl-α-D-glucopyranoside (6), which is a seven spin system (Figure 5.3; Table 5.7).

The 2D spectrum resulting from the three-pulse experiment (Fig. 5.1) described earlier will contain the conventional SQT frequencies in the f_2 domain and all possible n-quantum transition frequencies in the f_1 domain. However by use of suitable phase-shifted sequences it is possible to selectively observe only the ZQT spectrum in f_1 (6). This point is illustrated in Figure 5.4 which shows transitions, corresponding to the H1 proton (in f_2). Spectrum A, is an f_1 trace obtained using the basic pulse sequence ($\phi=0^\circ$) and shows the responses due to zero, single and multiple (double) quantum transitions. Figure 5.4B shows that phase shifting the two excitation pulses by 180° (eg. $\phi=90^\circ$ and 270°) results in cancellation of the SQT's (odd-n-quantum transitions) while retaining the zero and double (even-n-) quantum transitions in the final spectrum. In this particular case,

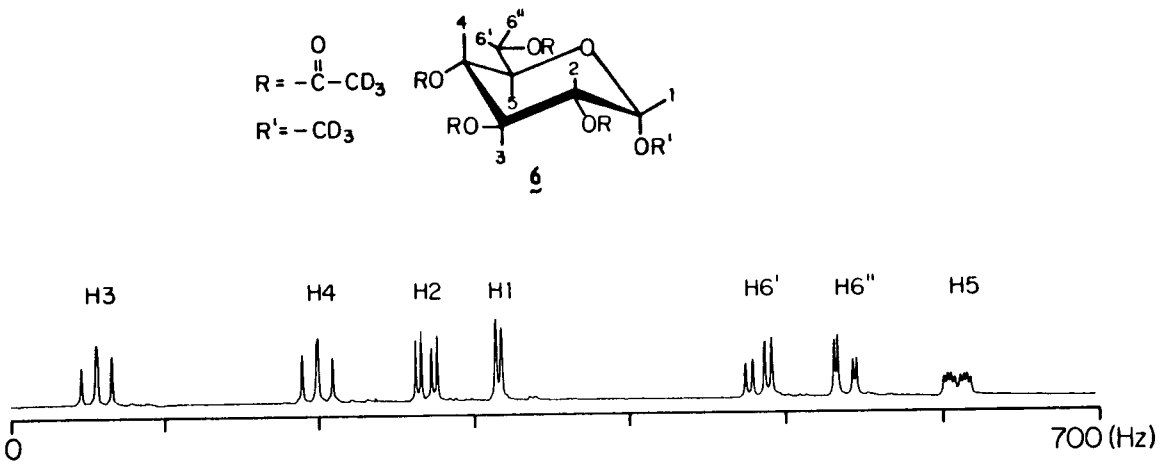

Figure 5.3: The normal 270 MHz FT NMR spectrum of trideuteriomethyl 2,3,4,6-tetra-O-trideuteriomethyl-α-D-glucopyranoside (6) in benzene-d_6 (0.1M); the scale represents the offset from the transmitter frequency.

TABLE 5.7: The conventional and ZQT spectral data for trideuteriomethyl 2,3,4,6-tetra-O-(trideuterioacetyl)-α-D-glucopyranoside (6).

Frequency[a]	Coupling constants[b]	Shift separations[c]	ZQT results[d]
f_1 = 316 (Hz)	J_{12} = 3.8 (Hz)	Δ_{12} = 41 (Hz)	J_{12} = 4 (Hz)
f_2 = 275	J_{23} = 10.6	Δ_{23} = 219	J_{23} = 10.5
f_3 = 56	J_{34} = 9.5	Δ_{34} = 144	J_{34} = 9.5
f_4 = 200	J_{45} = 10.6	Δ_{45} = 411	J_{45} = 10.5
f_5 = 611	$J_{56'}$ = 4.7	$\Delta_{56'}$ = 127	$\lvert(J_{56'} - J_{6'6''})\rvert$ = 16.5
$f_{6'}$ = 484	$J_{56''}$ = 2.5	$\Delta_{56''}$ = 72	$\lvert(J_{56''} - J_{6'6''})\rvert$ = 14
$f_{6''}$ = 539	$J_{6'6''}$ = 12.5	$\Delta_{6'6''}$ = 55	$\lvert(J_{56'} - J_{56''})\rvert \approx 2$ [e]

[a] Offset from the transmitter frequency. [b] From reference 23.
[c] The chemical shift differences obtained from the conventional spectrum; a direct comparison of these separations between the protons can be made by matching the conventional spectrum with the ZQT traces (eg. (f_1-f_2) in Figure 5.3 is equel to the separation between the Δ_{23} multiplets in Figure 5.5B. [d] Obtained from ZQT spectra with 1.5 Hz digital resolution.
[e] Not well resolved due to limited resolution and overlap. (See Fig.5.5C).

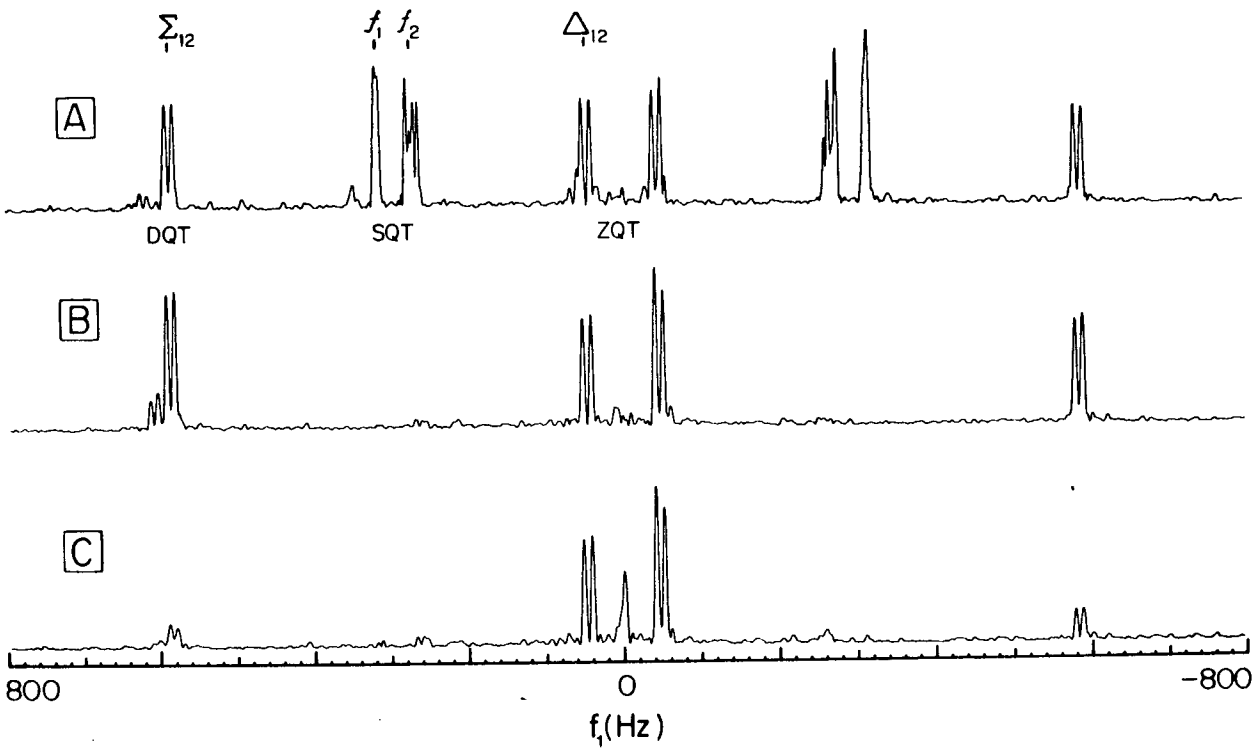

Figure 5.4: Trace (A) was obtained using the basic pulse sequence 90°- τ-90° -t_1-90°- Acquisition, (τ=200 msec., φ=0°) and represents the f_1 domain corresponding to the H1 proton. (B) shows the selective suppression of the SQT's, achieved by shifting the phase of the two initial pulses by 180°. The DQT were suppressed, as seen in trace (C), by co-adding signals from two separate experiments in which the initial pulses were phase shifted from 90° to 270°. The incomplete cancellations are probably due to pulse (phase) imperfections, and long-term instabilities (see Experimental section).

suppression of the double-quantum transitions, and hence the selective detection of the ZQT spectrum can be obtained by shifting the pulse phase by 0^{o}, 90^{o}, 180^{o} and 270^{o} and is shown in Figure 5.4C.[1]

The ZQT spectrum corresponding to the H1 proton[2] gives a simple pattern because H-1 is coupled to only one other proton, H2(J_{12}=3.8 Hz). The ZQT spectrum is expected to show a multiplet centred at the chemical shift difference $\pm(f_1-f_2)$ (which is denoted by Δ_{12}). The structure of this multiplet can be predicted by considering these transitions as arising from and ABC "sub-spin system" (see Table 5.3), involving H1, H2 and H3:

$$\Delta_{12}\overset{+\frac{1}{2}}{-}(J_{13}-J_{23})$$

The multiplet is observed as a doublet, separated by J_{23}=10.6 Hz (23); the transitions corresponding to Δ_{13} do not appear in the ZQT spectrum since there is no appreciable spin-spin coupling between H1 and H3.[3]

Similar arguments may be used to predict the possible ZQT's corresponding to the H3 proton. Since H3 is coupled to H2 (J=10.5 Hz) and H4 (J=9.5 Hz), two multiplets centred at Δ_{23} and Δ_{34} will be in the ZQT spectrum, arising from the sub-spin systems, H1, H2, H3, H4 and H2, H3, H4, H5 respectively.

[1]In this instance the trace C in Figure 5.4 was obtained by adding the time domain signals (interferograms) from two separate experiments ($\phi=0^{o}$, 180^{o} and 90^{o}, 270^{o}). After completion of this work, we have acquired a 293B pulse programmer which enables the above experiment to be performed in a single experiment; the long term instabilities in this case are minimised, which gave better cancellation of higher order transitions (cf. Fig. 5.4).

[2]"ZQT spectrum of the H1 proton", refers to the (ZQT) traces in the f_1 domain corresponding to the H1 frequencies in f_2. The ZQT spectrum may be obtained as a single trace from the 2D spectrum or an integral projection of the selected (H1) region onto f_1.

[3]Long-range, four-bond couplings (ca. 0.8 Hz) can be detected in these type of molecules between 1,3-axial, equatorial protons, however the choice of the preparation delay τ ($\simeq$200-300 msec) is generally too short to allow for any significant contribution from protons more than three bonds away. The limited digital resolution and line-broadening in f_2 further decrease the detection of the ZQT's associated with these couplings.

The multiplet patterns for these signals are given by (Table 5.4),

$$\Delta_{23}{}^{\pm\frac{1}{2}}[(J_{12}-J_{13}) \pm (J_{24}-J_{34})] = \Delta_{23}{}^{\pm\frac{1}{2}}(J_{12}{}^{\pm}J_{34})$$

and,

$$\Delta_{34}{}^{\pm\frac{1}{2}}[(J_{23}-J_{24})\pm(J_{35}-J_{45})] = \Delta_{34}{}^{\pm\frac{1}{2}}(J_{23}{}^{\pm}J_{45})$$

These multiplets are illustrated in the ZQT traces in Figure 5.5B. The above examples demonstrate a potential use for ZQT spectra in structural analysis namely by establishing connectivities between weakly coupled protons. In addition, the splitting patterns provide a method for indirectly obtaining coupling constants; for example, it should be possible in principle, to determine the coupling constants J_{12}, J_{45} by analysing the ZQT spectrum of H3 (J_{34} and J_{23} will appear in the f_2 domain, corresponding to the conventional SQT's).

The H6" proton is part of the H6', H6", H5, H4 sub-spin system, and is coupled to H6' (J=12.5 Hz) and H5 (J=2.5 Hz). Following the earlier discussion the ZQT spectrum corresponding to the H6" proton would be expected to show the signals

$$\Delta_{56"}{}^{\pm\frac{1}{2}}[(J_{45}-J_{46"})\pm(J_{56'}-J_{6'6"})] = \Delta_{56"}{}^{\pm\frac{1}{2}}[(J_{45})\pm(J_{56'}-J_{6'6"})]$$

and

$$\Delta_{6'6"}{}^{\pm\frac{1}{2}}(J_{56'}-J_{56"})$$

In addition to these chemical shift differences, another multiplet centred at $\Delta_{56'}$ is seen in Figure 5.5C with the frequency pattern,

$$\Delta_{56'}{}^{\pm\frac{1}{2}}[(J_{45}-J_{46'})\pm(J_{56"}-J_{6'6"})] = \Delta_{56"}{}^{\pm\frac{1}{2}}[(J_{45})\pm(J_{56"}-J_{6'6"})]$$

This multiplet, unlike in the previous examples, would be expected when observing H6" since there is a finite coupling ($J_{56'}$=4.7 Hz) between H5 and H6' protons, which are also coupled to H6".

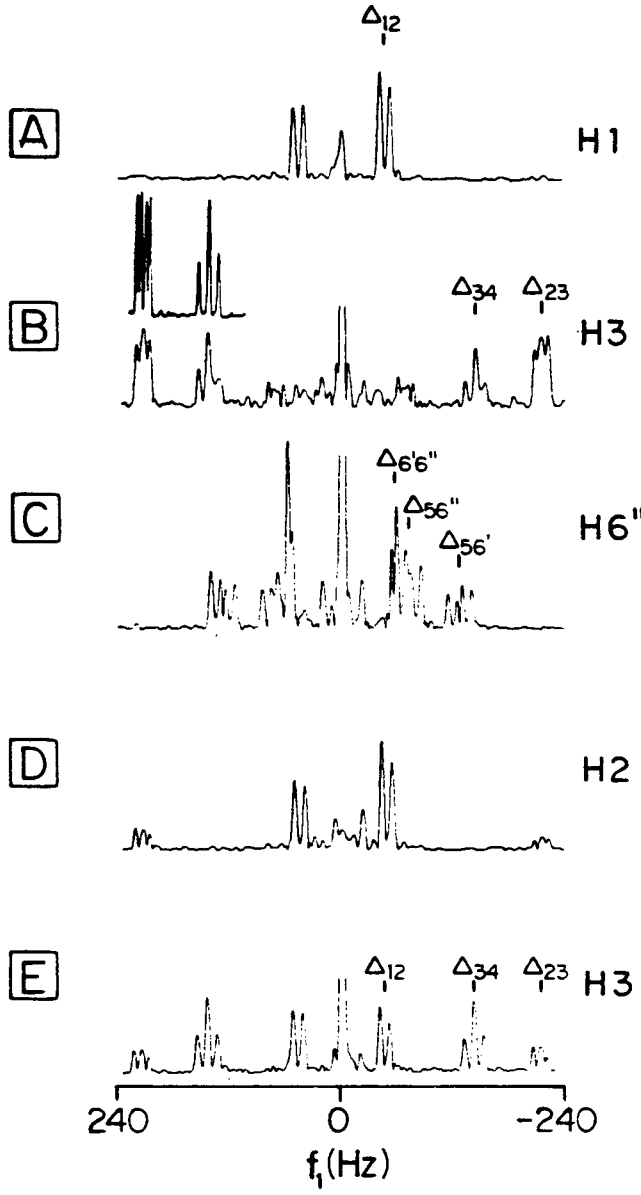

Figure 5.5: ZQT (absolute value) spectra for the protons indicated, each corresponding to a single trace in f_1. The appropriate "interferograms" (512x2 words) were zero-filled, and apodised to improve the effective resolution. The trace shown as an inset was obtained for H3 by halving the f_1 width to achieve higher digital resolution. The experimental parameters were: digitization in f_2, 0.68 Hz; increment in t_1, 625 μsec; number of acquisitions, 8; preparation delay (τ), 200 msec. (except trace B, 260 msec.)

An interesting feature in the ZQT spectrum of H6" is the appearance of the geminal (negative) coupling $J_{6'6''}$, as a difference. This enables the distinction to be made between positive and negative coupling constants,[1] which is rarely used in conventional spectral analysis mainly because of the difficulty in obtaining this information. This could help in distinguishing between the geminal (negative) and trans-diaxial (positive) couplings of steroids, which are of similar magnitude (24).

The delay times τ(200, 260 and 200 msec respectively) used to obtain the ZQT spectra shown in Figure 5.5A, B and C were selected to give optimum signal intensities to illustrate the expected spectral patterns. However, it should be noted that the ZQT signal intensity is a rather complicated function of both coupling constants and chemical shift frequencies, which makes it difficult to simultaneously optimise conditions for all protons in the spectrum. For example, the ZQT spectra (Fig. 5.5D and E) corresponding to the H2 and H3 protons for τ=200 msec show relatively weak signals for the multiplet Δ_{23} (cf. Trace B), indicating the significance of the preparatory delay in these experiments for optimum signal intensities. Although in all the previous discussions only the protons with vicinal or geminal relationship were considered, Figure E, which corresponds to the H3 proton, shows a doublet at Δ_{12}; this reflects the fact that H3 is indirectly connected to H1 via H2. Such responses from the indirectly connected protons were generally found to be weak in the present study and hence they have not been emphasised. (This should be compared with the earlier discussion on the (absence of) signals at Δ_{13} due to small long-range couplings.)

[1]For example the multiplet at $\Delta_{56'}$, shows two large couplings of about 10 and 14 Hz, the latter arising from the J difference [2.5-(-12.5)].

Although we have deliberately chosen a weakly coupled multi-spin system, with relatively simple sub-spin systems, it is evident from Table 5.4 that ZQT of the second kind could well give rise to additional peaks for more complicated spin systems. In general these lines may be expected to appear at relatively higher frequencies in f_1 than those of the first kind and they should therefore, be easily identified.

In this chapter a preliminary study regarding a two-dimensional correlation (or assignment) technique was presented which involves forbidden transitions in a homonuclear (proton) system. It was evident from the discussions in the previous chapters that more versatile and convenient assignment techniques are needed for the study of complex molecules. The relative merits and limitations of the various assignment techniques are discussed in the final chapter.

References (Chapter V)

1. Aue, W.P., Bartholdi, E., Ernst, R.R. J. Chem. Phys. (1976) 64, 2229.
2. Alla, M., Lippmaa, E. Chem. Phys. Lett. (1976) 37, 260.
3. Hester, R.K., Akerman, J.L., Neff, B.L., Waugh, J.S. Phys. Rev. Lett. (1976) 36, 1081.
4. Vega, S., Shattuk, T.W., Pines, A. Phys. Rev. Lett. (1976) 37, 43.
5. Bodenhausen, G., Freeman, R., Niedermeyer, R., Turner, D.L. J. Magn. Reson. (1977) 26, 133.
6. Wokaun, A., Ernst, R.R. Chem. Phys. Lett. (1977) 52, 407.
7. Wokaun, A., Ernst, R.R. Mol. Phys. (1978) 36, 317.
8. Bodenhausen, G., Vold, R.L., Vold, R.R. J. Magn. Reson. (1980) 37, 93.
9. Warren, W.S., Sinton, S., Weitekamp, D.P., Pines, A. Phys. Rev. Lett. (1979) 43, 1791.
10. Nagayama, K., Wuthrich, K., Ernst, R.R. Biochem. Biophys. Res. Commun. (1979) 90, 305.
11. Bain, A.D., Bell, R.A., Everett, J.R., Hughes, D.W. J. Chem. Soc. Chem. Commun. (1980) 256.
12. Kaplan, J.I., Meiboom, S. Phys. Rev. (1957) 106, 499.
13. Yatsiv, S. Phys. Rev. (1958) 113, 1522.
14. Schaublin, S., Hoehner, A., Ernst, R.R. J. Magn. Reson. (1974) 13, 196.
15. Slichter, C.P. "Principles of Magnetic Resonance", 2nd ed., Spinger-Verlag: Berlin, 1978.
16. Maudsley, A.A., Wokaun, A., Ernst, R.R. Chem. Phys. Lett. (1978) 55, 9.
17. Vega, S., Pines, A. J. Chem. Phys. (1977) 66, 5624.
18. Hatanaka, H., Terao, T., Hashi, T. J. Phys. Soc. Japan (1975) 39, 835.

19. Stoll, M.E., Vega, A.J., Waughan, R.W. J. Chem. Phys. (1977) 67, 2029.

20. Emsley, J.W., Feeney, J., Sutcliff, L.H. "High resolution Nuclear Magnetic Resonance Spectroscopy", Vol. I; Pergamon Press: London, 1966.

21. Pople, J.A., Schneider, W.G., Bernstein, J. "High resolution Nuclear Magnetic Resonance", McGraw-Hill: New York, 1969.

22. Tang, J., Pines, A. J. Chem. Phys. (1980) 72, 3290.

23. Hall, L.D., Sukumar, S., Sullivan, G.R. J. Chem. Soc., Chem. Commun. (1979) N6, 292.

24. Hall, L.D., Sanders, J.K.M.; J. Amer. Chem. Soc. (1980) 102, 5703.

CHAPTER VI

SUMMARY AND DISCUSSION

5.1 Summary and Discussion

In this Section, an attempt will be made to briefly summarize the principal findings of this study, to place them into a chemical context, and to speculate about future possibilities with the numerous recent advances in high-field, superconducting magnet technology and (mini)-computer technology. NMR has proven to be an increasingly powerful and widely used analytical tool in chemistry. In addition to the conventional (single-pulse) NMR experiment, the literature describes a wide range of NMR techniques which have potential for solving chemical problems, either by providing more information on molecular properties (eg. relaxation time measurements) or by simplifying spectral analysis. The main thrust of this thesis has dealt with the latter aspect and it should be clear from the examples chosen that several versatile and convenient NMR techniques now exist for resolving and assigning NMR spectra.

Although NMR spectroscopy is used extensively in chemistry, particularly in synthetic organic chemistry, relatively less work has been done in biochemistry. Proton NMR spectra of biological (or macromolecular) systems are usually too complicated to be analysed by conventional means; however some simplification can be achieved by studying, for example, carbon-13 or phosphorous-31 resonances which exhibit a wider range of chemical shifts than protons. One method of simplifying proton NMR spectra of biomolecular systems is by selective suppression of signals, for example by SEFT methods. However the major limitation of the method arises from the phase and intensity anomalies as discussed in Chapter II. SEAS offers a convenient solution to this problem, by providing essentially a high resolution proton spectrum, independent of the phase problem encountered in SEFT spectroscopy. The first

applications of SEAS in chemistry and biology have been presented in this thesis (Sec. 2.5 and 2.6) and serve to demonstrate the potential use of this method in biology. Since the above technique is more suitable for studying the more slowly relaxing (high resolution) components in the spectrum, mobile units of a macromolecule or small molecules in a biological system, for example, can be used as "probes" to study aspects of the system under consideration.

Most of this thesis has dealt with an exploration study of the use of double Fourier transform methods for solving NMR spectral analysis; these techniques, in a rather unique way, provide methods to resolve and assign complex spectra and could well revolutionize the use of NMR spectroscopy in many areas of chemistry.

Chapter III dealt with proton 2D J spectroscopy mainly from an experimentalist's point of view. Most of the limitations in displaying the 2D J spectral data arise from the complex 2D lineshapes associated with each signal. In the past these spectral traces were displayed in the absolute value mode; however, in the presence of large differences in signal intensities this can cause distortion in a 2D J spectrum and can often lead to loss of information. Several methods were suggested in Chapter III to alleviate this problem such as by selective suppression of unwanted signals and by displaying phase-sensitive (tilted) traces or sub-spectra.

Since both chemical shift and coupling constant information of a resonance are contained in the appropriate 45° cross-section of a 2D J spectrum the tilt routine is a vital step in the 2D J data processing procedure. It is suggested that the phase-sensitive tilt routine provides a means of manipulating the (sub-) spectrum of each <u>individual</u> multiplet, at the

final stage after the double Fourier transformation, thus optimising the display of each multiplet separately.

2D J spectroscopy provides a method of obtaining effectively "broad-band homonuclear-decoupled" spectrum in one dimension and homonuclear spin-spin coupling constants in the other dimension. This principal can be used to achieve "broad-band heteronuclear decoupling" and thus distinguish homonuclear and heteronuclear spin-spin coupling constants (Sec. 4.3), without the limitations imposed by high-power irradiating frequencies.

Usually proton NMR spectral assignments have been achieved via various 1D methods including spin-decoupling and related double resonance techniques such as NOE studies and INDOR techniques. Although in principle these techniques should provide all connectivity information between the spin system of interest, their success is critically dependent on the relative dispersion of the proton chemical shifts, which can be a serious limitation when dealing with complex spectra. Furthermore, the decoupling power or the band-width of the irradiating field may have to be individually optimised for each resonance or multiplet to achieve the selectivity needed.

Assignment techniques based on two-dimensional Fourier transform spectroscopy have a major advantage over these double resonance methods because they are not limited by the spectral dispersion or the irradiating field. Although these experiments simultaneously provide, usually in a single experiment, all connectivity information their general potential in chemistry remains to be fully explored.

^{13}C- ^{1}H shift correlated spectroscopy is an elegant assignment technique which uses the wider dispersion of the carbon-13 spectrum to resolve and correlate the proton chemical shifts. This work has shown for the first

time that, in conjunction with 2D J spectroscopy, this provides a powerful tool for spectral analysis and structural elucidation (Sec. 4.2).

The first application of zero-quantum transition (2D) spectroscopy for NMR spectral assignment was demonstrated in Chapter V, along with an explanation of the features involved, based on the density matrix approach. ZQT spectroscopy is unique in that it provides a 2D correlation information based on chemical shifts and coupling constants, and also that the ZQT frequency information cannot be directly obtained by conventional methods. Further discussions on the application of the various assignment techniques are given in the latter part of this chapter.

Given that most practicing chemists have restricted access to the type of sophisticated instruments required for these experiments it is clear that "time" considerations are crucial to the extent to which these experiments will be used. Accordingly, the next few paragraphs will be concerned with this situation. For studies of complex organic molecules, the main practical limitation of most 2D NMR experiments arises from the time required for the large data matrix that has to be generated and processed to yield the final 2D spectrum. For example, the sample of 0.1M 5,epi-sisomycin (12) used in this study (Sec. 4.2) required a 4096 by 128 word-size data matrix, corresponding to the t_2 and t_1 domain respectively for the 2D J experiment (the experimental parameters are given along with the figure caption in Fig. 4.4), and required about an hour for data acquisition. The ^{13}C- ^{1}H shift correlation experiment on 0.26M solution of the compound was performed on a 2048 by 256 data matrix corresponding to the two domains, t_2 and t_1 respectively, which required about 4½ hours for data acquisition (see experimental parameters listed with Fig. 4.2). Data processing for the 2D J

and shift correlation experiments took about 3 and 1½ hours respectively. Furthermore the time spent in plotting and obtaining frequency measurements was also substantial; it is not possible to generalize these times because it is determined by the complexity of the molecule. For example, the 2D J spectrum shown in Figure 3.7 took about two hours.

Although the experimental times are not substantial, it must be remembered that for better digitization, particularly in the f_1 domain, it will be necessary to increase both the data acquisition and processing times. On the other hand if it is only necessary to obtain approximate chemical shifts for spectral assignments as in the ^{13}C- ^{1}H shift correlation experiments, poor digitization can be used in both dimensions.

The experimental times given above are for processing the whole data matrix. In practice, however, only the regions bearing the signals need to be processed, and the frequency information obtained from the appropriate traces (note, for example, most regions of the 2D spectrum in Fig. 4.4 consists of noise).

Although 2D NMR experiments are rather time consuming and complex, considering the immense quantity and variety of information that they provide, usually in a single experiment, the time scale of these experiments should not be regarded as prohibitive. Furthermore these techniques can provide information that is unique, and which is otherwise often tedious or impossible by conventional means; thus ZQT spectroscopy and "wide-band" homonuclear and heteronuclear decoupling are experiments which have no equivalent in conventional NMR spectroscopy.

For any chosen experiment, the total data acquisition time is governed principally by the sensitivity of the spectrometer and concentration of the

sample. Present day, high-field spectrometers have considerably eased this problem.[1] Data processing times depend to a great part on the type of computer system (eg. memory size) available and on the efficiency of the computer program (soft-ware). With the rapid growth of computer technology data handling and processing may be expected to be performed more rapidly and efficiently in the future.

A new method for effectively increasing the overall efficiency of certain NMR experiments was suggested in Section 3.3.4; this involves the concept of an "integrated" NMR experiment. In the example chosen, several different sets of NMR spectral information were obtained from a single experimental data matrix; portions of the original data matrix were appropriately processed to yield SEFT, SEAS, 2D J and D2D J spectral information. Similar procedures can be adapted for selective detection of n-quantum transition spectra. It seems likely that further extensions of this concept could substantially decrease the total time required for a complete NMR study of complex molecules.

It should also be possible to improve the overall efficiency of 2D NMR experiments by performing data processing simultaneously with data acquisition ("foreground-background operation") or by automating the whole experimental procedure.

It was evident from this study that versatile, new techniques for assigning proton resonances are necessary to complement the high resolving power of proton 2D J spectroscopy. One such technique is ^{13}C- ^{1}H shift correlation spectroscopy; this provides a simple method for assigning or correlating resonances providing that either the proton or carbon-13 signal is previously known. A new assignment technique that was described in this

[1]The sensitivity is proportional to the static magnetic field.

thesis was that based on ZQT (2D) spectroscopy. In contrast to the ^{13}C- ^{1}H shift correlation experiment ZQT- and "conventional" homonuclear (^{1}H-^{1}H) shift correlation (1,2,3) 2D-spectroscopy may be regarded as "high resolution" experiments; for both the homonuclear techniques the f_1 domain represents frequencies of the order of chemical shifts (or "differences") and hence this domain must be sufficiently digitized which invariably leads to a larger data matrix. In either experiment, handling of large data arrays should be given serious consideration, both from the viewpoint of signal acquisition times and data processing capabilities.

The use of ZQT spectra to obtain connectivities appears to have the following advantages over the homonuclear (^{1}H) shift correlation methods:

a) the ZQT's are independent of field inhomogeneity, enabling one to obtain high-resolution spectra (in f_1) which are limited mainly by "natural" line-widths (cf. J spectra; Ref. 4),

b) the transition frequencies (of the first-kind) appear as chemical shift differences, which may considerably reduce the spectral width in the f_1 domain; this has a number of practical advantages - since the size of the data matrix can now be reduced to achieve the suitable digitization in the final 2D spectrum (cf. Ref. 1, 2 and 3), this could in turn lead to significant time saving in data acquisition and processing, and also minimise the problems associated with the handling of large data assays,

c) it should be possible, as described in the previous section, to indirectly determine the relative signs of coupling constants,

d) ZQT spectra generally exhibit fewer lines than the corresponding SQT spectra, which could help simplify spectral analysis, and

e) it is known that in 2D correlation spectroscopy there is no net magnetization transfer (Sec. 4.2) and that it results in multiplets which have

both positive- and negative-going signals; it is conceivable that limited digital resolution in either dimension could result in cancellation of these signals, however, in spite of the limited digital resolution used to obtain the traces in Figure 5.5 all ZQT's show finite intensities.

Since ZQT's are independent of magnetic field inhomogeneity effects, the higher order n-quantum transitions may be eliminated by applying a field gradient pulse during the evolution period (5), thereby obviating the need for elaborate phase cycling procedures. On the other hand if one needs to selectively study, for example, SQT's or DQT's it is only necessary to add or subtract signals resulting from the appropriate phase shifting of the excitation pulse.

Although DQT's also contain connectivity information, the relatively higher frequencies in f_1 (sums of chemical shifts) and the greater sensitivity to field inhomogeneity effects makes DQT spectra less desirable for practical applications.

A potential limitation of ZQT spectroscopy is the dependence of the intensity of the signals in the final 2D spectrum on the preparation delay, τ. For example, it was necessary in this study of 6 to perform several individual experiments to select suitable values of τ to maximise ZQT signal intensities, and thus obtain high resolution information. On the other hand it may be that this τ-dependence of signal intensities can be used to simplify ZQT spectra by reducing the total number of lines in a complex 2D spectrum. In either event it will be necessary to have more experience of the experimental practice of ZQT spectroscopy and a deeper theoretical understanding of the signal intensity dependencies.

At the time the author started the studies described in this thesis, the three different NMR techniques namely 2D J- ^{13}C- ^{1}H shift correlated- and n-QT-spectroscopy were already described in the literature, however their diagnostic potential in the context of studies by a practicing chemist of complex molecules was less obvious. Although 2D NMR spectroscopy is still not widely used, the work included in this thesis has demonstrated the potential of 2D NMR techniques is exciting. Ernst's group in Switzerland have described a 2D NMR technique for studying NOE (6) and also a method for studying chemical exchange (7), which appear to have many useful practical advantages over the conventional 1D methods for obtaining the same information. These techniques are yet to be fully explored for the study of chemical systems.

References (Chapter VI)

1. Aue, W.P., Bartholdi, E., Ernst, R.R. J. Chem. Phys. (1976) 64, 2229.

2. Nagayama, K., Wuthrich, K., Ernst, R.R. Biochem. Biophys. Res. Commun. (1979) 90, 305.

3. Bain, A.D., Bell, R.A., Everett, J.R., Hughes, D.W. J. Chem. Soc., Chem. Commun. (1980) 256.

4. Freeman, R., Hill, H.W. J. Chem. Phys. (1971) 54, 301.

5. Wokaun, A., Ernst, R.R. Mol. Phys. (1978) 36, 317.

6. Kumar, A., Ernst, R.R., Wuthrich, K. Biochem. Biophys. Res. Commun. (1980) 95, 1.

7. Jeener, J., Meier, B.H., Bachman, P., Ernst, R.R. J. Chem. Phys. (1979) 71, 4546.

CHAPTER VII

EXPERIMENTAL SECTION

7.1 The spectrometer

The spectrometer used in this study was assembled at U.B.C. from components which originally comprised a Nicolet TT-23 (100 MHz) console, and a narrow bore superconducting solenoid (6.3T) from Oxford instruments. The initial experiments were performed using a 293A pulse controller, which was later updated to a 293A' unit. The spectrometer is controlled by a Nicolet 1180 computer (40K); the standard NTCFT (NMR) programme was used for data acquisition and processing. Data processing and storage of large (2D) data arrays was facilitated by two Diablo disk drives (model-30), each with a disk capable of storing one megawords of information.

In its recently updated configuration, the spectrometer is fitted with a Nicolet 293B pulse programmer. In addition to the 1180 computer used for the basic data-acquisition and processing an independent data processing system comprising another Nicolet 1180 (40K) computer, a disk drive and a digital plotter has been installed. Although each of the Nicolet computers has capabilities for simultaneous "foreground-background" operation, the two-computer system described here was found to be far more versatile and substantially increased the overall efficiency of the 2D NMR experiments.

It is possible with the 293B pulse programmer to programme pulse sequences which include up to 128 steps; in contrast the 293A-series allows a maximum of only 16 steps. This confers many advantages for programming experiments which involve many pulses; it is now possible, for example, to include relatively sophisticated phase-cycling procedures into multipulse experiments for the cancellation of instrumental imperfections.

The Bruker WH-400 (9.4T) with an Aspect 2000 computer was also used in some experiments.

7.2 The chemicals used

Most of the carbohydrate derivatives used in this study were laboratory samples. The mono- and di-saccharides were obtained from standard laboratory suppliers such as Aldrich Chemical Co., or Pfanstiehl Lab. Inc. A list of the source of the rest of the chemicals are given below:[1]

Dextran T-10 -	Pharmacia Ltd.
BSA, lysozyme -	Worthington Biochemicals Co.
Compound 6 -	Laboratory sample (1)
Compound 7 and 10 -	Gifted by Prof. L. Hough
Uridine -	Pfanstiehl Lab. Inc.
Furoic acid -	Aldrich Chemical Co.
5,epi-sisomycin -	Gift from Schering Pharmaceutical Co.
1,1,1 trifluoro propan-2-ol -	PCR Research Chemicals, Inc.
Compound 13 -	Hooker Chemical Co.
Compound 15 -	Laboratory sample
Compound 16 -	1,1,1 trifluoro propan-2-ol (1 m) and

diphenylphosphorochloridate (1.2 m) were reacted in pyridine (solvent and base) according to standard procedures (2,3). The product (16) was obtained by evaporating the solvent and was used for the NMR study without further purification. Although the sample contained residual pyridine and traces of unreacted material, the spectral region of interest was not affected by the impurities.

The deuterated solvents used in the study were purchased from Merck Sharpe and Dohme. The samples when studied in aqueous medium were usually lyophilized three times in 98% D_2O and made up in 100% D_2O for proton NMR

[1]Refer to the list of compounds for the names of the respective compounds.

studies. However this procedure was not necessary in the latter part of the work since it was possible to presaturate the solvent peak in 2D J NMR experiments when using the 270 MHz spectrometer.

NMR spectra measured in aqueous solvents and organic solvents are referenced with respect to internal TSP (sodium 3-trimethylsilylpropionate-2,2,3,3-$\underline{d}_4$) and TMS (tetramethylsilane) respectively.

The 2D NMR experiments described in the following sections is an accurate but brief description of the experimental procedures and not intended to be a detailed instruction manual.

7.3 Red blood cells, sample preparation

Red blood cells (RBC) were prepared from freshly drawn venous blood (from Mr. Rob Snoek) and collected in EDTA (10.5 mg Na_2EDTA/7 ml blood; anti-coagulant). The whole blood was centrifuged and the red cells washed three times in phosphate buffered saline, with or without added glucose (10 mM). The cells were then washed in Kreb Ringer solution (4) which was made up in D_2O, with or without glucose (10 mM) at pH 7.2.

The samples that were to be exposed to glucose were incubated in Kreb Ringer solution containing 10 mM glucose in D_2O for two hours at room temperature (haematocrit ~10%). They were then centrifuged and the supernatant separated from the "pellet" (procedure B). Part of the pellet (haematocrit ~90%) was used in the SEAS studies.

Another portion of the RBC-glucose sample was lysed by adding D_2O (5 ml/1 ml blood). The sample was then centrifuged at 20,000 g and the pellet, separated from the supernatant, was used in the NMR studies.

The RBC which were not exposed to glucose were centrifuged (20,000 g) and the pellet (haematocrit ~85%) made available for NMR studies (procedure A).

Sample spinning was not employed during the NMR measurements of the RBC samples.

7.4 2D J spectroscopy

The pulse sequence used in proton 2D J spectroscopy with phase alternation of the 180° pulse is as follows:

1. Preparation delay
2. 90° pulse
3. Incremental delay
4. 180° pulse (ϕ=0°)
5. Incremental delay
6. Signal acquisition
7. Relaxation delay
8. Preparation delay
9. 90° pulse
10. Incremental delay
11. 180° pulse (ϕ=180°)
12. Incremental delay
13. Signal acquisition
14. Relaxation delay
15. Signal average by repeating (1) through (14)

The incremental delay is equal to (T_i+n.T) where T_i is an initial delay (~50 μs); n=0, 1, 2, ... (N-1).

A brief summary of the data processing procedures used in 2D J spectroscopy is:

1. FT with respect to t_2

2. Transpose either a section of, or the whole, data matrix
3. FT with respect to t_1
4. Transpose data
5. Tilt
6. Transpose data
7. "Pick-out" cross-sections (or sub-spectra)
8. Inverse Fourier transform
9. Manipulate data (eg. zero-filling, digital filtering)
10. "Forward" Fourier transform
11. Phase correct
12. Plot and take measurements

Using the Nicolet 2D NMR spectroscopy software the normalization constants for scaling the spectra were obtained by first locating the largest signal, and then setting the scaling factor with respect to this spectrum prior to Fourier transformation. Depending on the circumstances, suitable digital filtering of time-domain signals was employed.

Selective irradiation was employed during the preparation (and relaxation) delay when solvent suppression was needed. In the case of solvent nulling by inversion recovery, the preparation delay included the following sequence:

1. 180° (non-selective) pulse ($\phi=0^{\circ}$)
2. Delay (equal to the "null point")

and the 2D J pulse sequence repeated with phase alternation ($\phi=180^{\circ}$) of the 180° pulse.

For the D2D J experiment the initial delay (T_1) was set to a suitable value (Sec. 3.3.1).

In the Bruker 2D NMR spectra software, steps (1) through (7) of the data processing procedure are automated. This makes the whole operation rather more convenient than that using the Nicolet software. However, the Bruker system does not provide phase-sensitive sub-spectra, nor can it be modified for the different 2D NMR experiments described in the text; this lack of flexibility is a regrettable, serious limitation.

7.5 ^{13}C- ^{1}H shift correlation spectroscopy

The carbon-13 measurements were performed using a home built probe,[1] with the receiver coil double tuned for observing carbon-13 and deuterium "lock". The 60 watt amplifier provided a 22 μs 90° pulse. The proton pulses (and noise-decoupling) were applied using the decoupler coil; the proton 90° pulse was 45 μs using a 10 watt amplifier. It was necessary to cool the probe (because of the heat generated by noise-decoupling) by passing air through it at ambient temperature (~20°C).

The pulse sequence used is summarised below:

1. Preparation delay
2. 90° proton pulse
3. Incremental delay
4. 180° carbon pulse
5. Incremental delay
6. Δ_1 delay (3.3 ms)
7. 90° proton pulse
8. 90° carbon pulse

[1]The probe construction and electronics was done by Tom Markus (Electronics section, Chemistry Department, U.B.C.) based on a prototype design by Dr. G.A. Morris.

9. Δ_2 delay (2.2 ms)

10. Signal acquisition (and noise-decoupling)

11. Relaxation delay

12. Repeat (1) through (11) for signal averaging

During the preparation delay the carbon-13 signals were saturated by using two long pulses (~450°) with a delay of 150 ms between them; this minimised the unmodulated component (zero-frequency in f_1) in the 2D spectrum.

The data processing steps are summarised below:

1. FT with respect to t_2

2. Transpose

3. "Pick-out" the appropriate interferograms

4. FT (after data manipulation) with respect to t_1

5. Take measurements (eg. after plotting)

From the results in the present study it was noted that a non-ideal 180° pulse caused distortions and artifacts in the spectrum. This can be a serious limitation when dealing with carbon-13 spectra whose spectral widths are >ca. 3000 Hz. In the example chosen in Section 4.2 (SW=6000 Hz), it was necessary to perform two experiments each with the transmitter at one end or other of the spectrum to produce the f_1 traces in Figure 4.3.

7.6 Zero-quantum (2D) spectroscopy

The pulse sequence used for the selective detection of odd-n-quantum transitions is given below (where $\phi = 0^\circ$):

1. 90° pulse (phase= ϕ°)

2. Preparation delay (τ)

3. 90° pulse (phase= ϕ°)

4. Incremental delay
5. 90^{o} pulse (phase=0^{o})
6. Signal acquisition
7. Relaxation delay
8. Repeat sequence (1) to (7) with $\phi=(\phi+180)^{o}$
9. Signal average by repeating sequence (1) through (8)

The selective detection of ZQT's (Figs. 5.4 and 5.5) was achieved by adding the time-domain signals (interferograms) from a separate experiment, similar to the sequence (1) to (9), but with ϕ being equal to 90^{o}.

The signals $S(t_1,t_2)$ were acquired on 2048-word size blocks, for 512 increments (625 μsec.) in t_1. After the first Fourier transformation with respect to t_2 and transposition, individual interferograms were zero-filled and Fourier transformed with respect to t_1, to give the traces, $S(f_2,f_1)$ shown in Figures 5.4 and 5.5. The preparation delay τ was set to ca. 100-300 msec. (which is of the order of the inverse, average coupling constant) for optimum signal intensities in the final spectrum.

After the completion of the experimental work on ZQT spectroscopy described in this thesis, which used a 293A' pulse controller, the above experiment was repeated using the Nicolet 293B pulse programmer. With the latter it is possible to program the whole pulse sequence described above into a single, composite experiment and the f_1 traces thus obtained showed complete cancellation of higher order transitions. In contrast, those traces obtained from a combination of two separate experiments showed imperfect cancellation of double quantum transitions (Fig. 5.4); it seems likely that this is due to long-term instabilities in the spectrometer. A further advantage of using a composite pulse sequence or single experiment for

detecting the ZQT spectum is that it avoids the limitations (eg. time, storage, etc.) in handling two large data sets.

The data processing for obtaining the individual traces (eg. Fig. 5.4) was similar to that given in the previous section.

References (Chapter VII)

1. Wong, K.F. Ph.D. Dissertation, University of British Columbia, Vancouver, Canada, 1979.

2. Hall, L.D., Malcolm, R.B. Can. J. Chem. (1972) 50, 2092.

3. Vogel, A.I. "A text book of practical organic chemistry", 3rd ed.; Longmans: London, 1956.

4. Cohen, P.P. "Manometric Techniques", Burgess Publishing Co: New York, 1975.

APPENDICES

APENDIX A

PROGRAM TO TILT PHASE SENSITIVE 2D J DATA

```
100 DIM B1(7500),A(7500)                    /Allocate space and files
110 DIM N1$(3),N2$(3)
120 PRINT "INPUT FILE NAME------\"
130 INPUT N1$(0),N1$(1),N1$(2)
140 PRINT "OUTPUT FILE NAME-----\"
150 INPUT N2$(0),N2$(1),N2$(2)
160 CALL BDEFINE(3,N1$)
170 CALL BDEFINE(4,N2$)
180 CALL FREAD(3,B1,352)
190 CALL FWRITE(4,B1,352)                   /Write parameters onto output
200 PRINT "F2 SW = "                         file
210 INPUT W2
220 PRINT "F2 SIZE = "
230 INPUT S2
240 PRINT "CURRENT BLOCK SIZE(REAL+IMAG) = /Size of data (f2) to be tilted
250 INPUT S3
260 LET M=352
270 CALL FAINT(M,1)
280 CALL IAFLT(B1,M)
290 PRINT "F1 SIZE AFTER ZF ="
300 INPUT S1
310 LET T1=S1
320 PRINT "I8 = "
330 INPUT I8
340 LET W1=250000/I8                        /±f1 width
350 LET H1=2*W1/T1                          / f1 digitization
360 LET H2=2*W2/S2                          / f2    "
370 LET X=S3/352
380 LET T2=(1+INT(X))*352                   /Number of points to read per
390 LET M2=T2                                block
400 CALL FAINT(M2,1)
410 LET T=S3
420 CALL FDISPI(B1,T,200)                   /Display array
430 PRINT "NO. OF BLOCKS TILTED"
440 FOR B=0 TO T1-1
450 CALL FREAD(3,B1,T2)
460 CALL IAFLT(B1,M2)
470 IF B>=(S1/2) THEN    600               /Do "right"  shift
480 LET X=H1*((S1/2)-0.5-B)                 /Calculate offset and do "left"
490 LET Y=X/H2                               shift to nearest point
500 LET Z=INT(Y)
510 FOR P=0 TO T2-1
520 LET A1=P-Z
530 IF A1>=0 THEN    560
540 LET A(P)=0
550 GO TO    580
560 IF A1>=S2 THEN    540
570 LET A(P)=B1(A1)
580 NEXT P
```

```
590 GO TO    700
600 FOR P=0 TO T2-1
610 LET X1=H1*(B+0.5-(S1/2))
620 LET Y1=X1/H2
630 LET Z1=INT(X1/H2)
640 LET A1=P+Z1
650 IF A1>=S2-Z THEN    680
660 LET A(P)=B1(A1)
670 GO TO    690
680 LET A(P)=0
690 NEXT P                                  /Quadratic interpolation routine
700 FOR P=0 TO T2-1
710 LET Q=P-1
720 LET R=P
730 LET S=P+1
740 IF R=0 THEN    870
750 IF S>=S2 THEN    870
760 LET E=(Y-Z)*H2
770 LET D2=H2+E
780 LET D3=D2+H2
790 LET L1=((A(R)*D3*D3)-(A(S)*D2*D2))
800 LET L2=(D2*A(S))-(D3*A(R)*D2)
810 LET L4= (A(R)-A(Q))/D2
820 LET L3=(A(S)-A(R))*A(Q)*D2
830 LET J=((L1*L4)-L3)/(L1+L2)
840 LET K=(A(R)-A(Q)-(J*D2))/(D2*D2)
850 LET B1(P)=(A(Q))+(J*H2)+(K*H2*H2)
860 GO TO    880
870 LET B1(P)=A(R)
880 NEXT P
890 CALL FAINT(B1,T2)
900 CALL FWRITE(4,B1,T2)                    /Write tilted block
910 LET S4=B+1
920 PRINT S4,
930 NEXT B
940 CALL DISPOF
950 PRINT "TILT FINISHED"
960 END
```

APPENDIX B

PROGRAM TO SIMULATE PHASE SENSITIVE TILTED TRACES

```
100 DIM S(750)                                  /Allocate space and files
110 DIM U$(3),X$(3)
120 PRINT "INPUT FILE NAME------\"
130 INPUT U$(0),U$(1),U$(2)
140 PRINT "OUTPUT FILE NAME------\"
150 INPUT X$(0),X$(1),X$(2)
160 CALL BDEFINE(11,U$)
170 CALL BDEFINE(12,X$)
180 CALL FREAD(11,S,352)
190 CALL FWRITE(12,S,352)                       /Write parameters onto output file
200 PRINT "T1="
210 INPUT T1                                    /T2 in f1
220 PRINT "T2="
230 INPUT T2                                    /T2 in f2
240 LET K=8000                                  /Constant - unit amplitude
250 LET W1=-7                                   /f1 frequency
260 LET W2=93                                   /f2 frequency
270 LET N=512                                   /Number of points in f1
280 LET H2=0.5                                  /f2 digitization
290 LET H1=0.05                                 /f1      "
300 PRINT "M="
310 INPUT M                                     /f2 trace number
320 LET R1=1/T1
330 LET R2=1/T2
340 LET Q=352
350 LET Q2=Q
360 CALL FDISPI(S,Q2,200)                       /Display
370 LET E=6.2832
380 FOR P=0 TO Q-1                              /Calculate tilted trace
390 LET A0=(P-((N-1)/2))*H1
400 LET A1=(A0-W1)*E
410 LET V1=T1/(1+(A1*A1*R1*R1))
420 LET A2=((M*H2)+A0-W2)*E
430 LET V2=T2/(1+(A2*A2*R2*R2))
440 LET S(P)=K*((V2*V1)-(T1*T2*A1*V1*A2*V2))
460 NEXT P
470 LET Q1=Q
480 CALL FAINT(S,Q1)
490 CALL FWRITE(12,S,Q1)                        /Write onto output file
500 BENDFILE #12
510 END
```

APPENDIX C

PROGRAMME TO SIMULATE A PHASE SENSITIVE-TILTED CROSS-SECTION TO SHOW THE EFFECT OF INTENSE NEIGHBOURING SIGNALS

```
100 DIM S(1056),J(1056),I(1056),L(1056)     /Allocate space and files
110 DIM U$(3),X$(3)
120 PRINT "INPUT FILE NAME-----\"
130 INPUT U$(0),U$(1),U$(2)
140 PRINT "OUTPUT FILE NAME-----\"
150 INPUT X$(0),X$(1),X$(2)
160 CALL BDEFINE(11,U$)
170 CALL BDEFINE(12,X$)                     /Read and write parameters onto
180 CALL FREAD(11,S,352)                     output file
190 CALL FWRITE(12,S,352)
200 BENDFILE #11
210 PRINT "T1="                             /T2 of multiplet
220 INPUT T1
230 PRINT "T2="                             /T2* of multiplet
240 INPUT T2
250 LET K=16000                             /Constant
260 PRINT "T3="                             /T2 of singlet
270 INPUT T3
280 PRINT "T4="                             /T2* of singlet
290 INPUT T4
300 LET N=1002                              /Number of points in f1
310 LET M=200                               /Cross-section at 200th point in f2
320 LET H1=0.05                             /Digitization in f1
330 LET H2=0.5                              /Digitization in f2
340 LET R1=1/T1
350 LET R2=1/T2
360 LET R3=1/T3
370 LET R4=1/T4
380 LET Q=1056
390 LET Q2=Q
400 CALL FDISPI(S,Q2,200)                   /Display calculation
410 LET E=6.2832
420 LET W4=120                              /Chemical shift offset of singlet
430 LET W3=0.0
440 LET J(P)=0
450 LET W1=-7.366                           /Frequency components of the
460 GOSUB    540                             multiplet
470 LET W1=-4.318
480 GOSUB    540
490 LET W1=4.318
500 GOSUB    540
510 LET W1=7.366
520 GOSUB    540
530 GOTO    730
```

```
540 LET W2=W1+(M*H2)
550 FOR P=0 TO Q-1                          /Calculate tilted trace for each
560 LET I(P)=0                               line and sum them
570 LET L(P)=0
580 LET A0=(P-((N-1)/2))*H1
590 LET A1=(A0-W1)*E
600 LET V1=T1/(1+(A1*A1*R1*R1))
610 LET A2=(A0-W1)*E
620 LET V2=T2/(1+(A2*A2*R2*R2))
630 LET I(P)=K*((V2*V1)-(T1*T2*A1*V1*A2*V2))
640 LET A3=(A0-W3)*E
650 LET V3=T3/(1+(A3*A3*R3*R3))
660 LET A4=((M*H2)+A0-W4)*E
670 LET V4=T4/(1+(A4*A4*R4*R4))
680 LET L(P)=(K*3)*((V3*V4)-(T3*T4*A3*V3*A4*V4))
690 LET J(P)=I(P)+L(P)+J(P)
700 LET S(P)=J(P)
710 NEXT P
720 RETURN
730 LET Q1=Q
740 CALL FAINT(S,Q1)
750 CALL FWRITE(12,S,Q1)                    /Write onto output file
760 BENDFILE #12
770 CALL DISPOF
780 END
```

APPENDIX D

PROGRAMME TO SHIFT FID'S IN INTEGRATED NMR EXPERIMENTS

```
100 DIM Q(9000),R(9000)                  /Allocate space and files
110 DIM N1$(3),N2$(3)
120 PRINT "INPUT FILE NAME------\"
130 INPUT N1$(0),N1$(1),N1$(2)
140 PRINT "OUTPUT FILE NAME------\"
150 INPUT N2$(0),N2$(1),N2$(2)
160 CALL BDEFINE(11,N1$)
170 CALL BDEFINE(12,N2$)
180 CALL FREAD(11,Q,352)                 /Read and write parameters onto
190 CALL FWRITE(12,Q,352)                 output file
200 PRINT "I8(USEC)="                    /Tau value
210 INPUT I8
220 PRINT "DWELL TIME="
230 INPUT D1
233 PRINT "D8(USEC)="                    /Initial delay
240 INPUT D8
250 PRINT "SIZE="
260 INPUT S2
270 PRINT "NO. OF BLOCKS="
280 INPUT S1
290 LET T1=S1
300 LET T=(S2/352)+0.6
310 LET T2=(INT(T))*352                  /Number of points to read per block
320 LET M2=T2
330 FOR B=0 TO T1-1                      /For each block
340 LET J=(((B*I8)+D8)/D1)+0.5           /First point of new block
350 LET J4=0
360 LET J1=INT(J)
370 LET J4=J1
380 CALL FREAD(11,Q,M2)
390 CALL IAFLT(Q,M2)
400 LET J3=(T2-J1)
410 FOR P=0 TO T2-1
420 LET J5=(J4+P)
430 IF J5>=S2 THEN     460
440 LET R(P)=Q(J5)
450 GO TO     470
460 LET R(P)=0
470 NEXT P
472 CALL FAINT(R,M2)
480 CALL FWRITE(12,R,M2)                  /Write shifted block onto
490 NEXT B                                 output file
500 PRINT "END OF EXPT"
510 END
```

APPENDIX E

ABBREVIATIONS[1]

NMR	Nuclear Magnetic Resonance
CW	Continuous Wave
FT	Fourier Transform
RF	Radio Frequency
2D	Two-Dimensional
FID	Free Induction Decay
SPD	Single Phase Detection
QPD	Quadrature Phase Detection
C-P	Carr-Purcell
CPMG	Carr-Purcell-Meiboom-Gill
ZQT (or C)	Zero-Quantum Transition (or Coherence)
SQT	Single-Quantum Transition
MQT	Multiple-Quantum Transition
INDOR	Inter-Nuclear Double Resonance
NOE	Nuclear Overhauser Enhancement
B_o	Static magnetic field
B_1	Applied radio-frequency magnetic field
i	$(-1)^{\frac{1}{2}}$
$\alpha\underline{\pm}_x$, $\alpha\underline{\pm}_y$	A pulse which corresponds to a "flip-angle" of α^o; the subscript refers to the applied direction
x,y,z	The Laboratory coordinates
x',y',z'	The rotating frame coordinates
α,β	α and β nuclear spin state wave functions

[1]See also Appendix F

$[\sigma_{ij}]_t$	The ij coherence of the density matrix at time t
	Chemical shift in parts per million (ppm)
Δ_{nm}	Chemical shift separation between n and m nuclei in Hz
Σ_{nm}	Summation of the precession frequencies of the nuclei n and m in the rotating frame
h	Planck's constant
γ	Magnetogyric ratio
k	Boltzmann's constant
AT	Acquisition (sampling) time
SR	Sampling rate
$SW_{1,2}$	Spectral width; the subscripts refer to the f_1 or f_2 domain
$DR_{1,2}$	Digital resolution
BS	Block size
NA	Number of acquisitions
RD	Relaxation delay
VD	Variable delay
SF	Spectrometer frequency
RBC	Red Blood Cells

APPENDIX F

NOMENCLATURE

One-dimensional (NMR) spectroscopy -

The standard or conventional NMR experiment in which the time domain signals arising from a system which has been subjected to a pulse sequence is Fourier transformed to yield a signal intensity versus frequency spectrum.

Two-dimensional (NMR) spectroscopy -

A technique by which an NMR spectrum is displayed in two frequency dimensions. It involves the acquisition of a data matrix, $S(t_1,t_2)$, as a function of two time variables (t_1 and t_2) which when subjected to Fourier transformation with respect to t_1 and t_2 yields a 2D spectrum $S(f_1,f_2)$, with the orthogonal frequency axes f_1 and f_2 respectively. The f_2 domain corresponds to the observable NMR signals.

J modulation -

A resonance, whose amplitude or phase is modulated as a function which is related to its coupling constant, with time.

Proton 2D J spectroscopy -

A 2D NMR experiment in which the f_1 dimension represents coupling constants only (J spectrum); the chemical shifts and magnetic field effects are eliminated in the f_1 domain; the f_2 domain represents the conventional spectrum (see 45^o-tilt routine).

"Proton-flip" ^{13}C 2D J spectroscopy -

The carbon-13 2D J experiment in which a 180^o pulse is applied to the proton spins simultaneously with the carbon refocussing pulse.

"Gated-decoupler" ^{13}C 2D J spectroscopy -

The carbon-13 2D J experiment where the decoupler is gated on or off during the evolution period (t_1).

Chemical shift correlated spectroscopy -

2D NMR experiment which give a correlation between spin-spin coupled nuclei. Such experiments may involve homonuclear or heteronuclear systems, and include allowed SQT's or forbidden transitions.

MQT (2D) spectroscopy -

2D NMR experiments which enable the measurement of (forbidden) multiple quantum transition frequencies. Selective detection of transitions of a specific order is also possible. The f_1 domain represents the n-QT spectrum.

Delayed 2D J experiment -

A 2D J experiment in which the broad, rapidly relaxing components from a 2D J spectrum are eliminated.

Interferogram -

The t_1, time domain signal, $S(f_2,f_1)$. The corresponding signal obtained from the spin-echo experiment is often referred to as the echo-interferogram.

45°-tilt routine -

A transformation in frequency space, which results in a proton 2D J spectrum, $S(J,\delta)$, in which the two orthogonal axes represent coupling constants and chemical shifts respectively. In the phase-sensitive tilt routine the real and imaginary parts of the spectra are independently subjected to the tilt.

Projection -

A display procedure which is obtained by summing a 2D data matrix, along a specified direction. This should be compared with the "maximal" projection which represents the highest point along a specified direction.

Cross-section -

A trace taken along a specified direction from a 2D spectrum. Usually this refers to a 45° cross-section of a multiplet taken from a 2D J spectrum and is equivalent to a partial J spectrum.

Sub-spectrum -

A phase-sensitive cross-section, which includes both the real and imaginary parts.

Proton-decoupled proton spectrum -

A 45° projection of a proton 2D J spectrum (or a 0° projection of a tilted 2D J spectrum $S(f'_1,f'_2)$) which represents the chemical shift spectrum for a weakly coupled proton spin system.

"t_1-noise" -

A band of noise which appears along each "resonance" frequency in the f_1 dimension.

"phase-twist" -

A complex 2D lineshape resulting from double Fourier transformation

T1IR -

Refers to the inversion recovery pulse sequence used for spin-lattice relaxation time measurements.

Carr-Purcell pulse sequence (T2CP) -

The basic C-P pulse sequence which involves a 90° pulse and a 180° pulse separated by a delay, τ (method A). A modification which minimises the effect of diffusion in T_2 measurements involves a series of 180° pulses each separated by 2τ, after an initial 90° pulse (method B).

Spin-echo Fourier transform (SEFT) spectroscopy -

This involves the Fourier transformation of the half-echo signals obtained from a T2CP pulse sequence.

Spin-echo absorption spectroscopy (SEAS) -

This involves the Fourier transformation of the whole-echo signal obtained from a T2CP pulse sequence and the display of the magnitude spectrum which shows an absorption mode NMR spectrum.

Phase alternation -

The change of the phase of a pulse by 180° on every alternate pulse sequence. This is usually performed in order to minimize the effects of pulse imperfections.

Spin-echo correlated spectroscopy (SECSY) -

A homonuclear chemical shift correlated experiment, including phase-cycle of the two 90° pulses so as to obtain a 2D spectrum where the f_1 axis is represented by only "frequency differences" of correlated protons. The effective digitization in f_1 may be improved and the experimental time decreased when compared to the original experiment which uses just two 90° pulses. The pulse-sequence for SECSY is:

$$\{90^\circ - \tfrac{1}{2}t_1 - 90^\circ - \tfrac{1}{2}t_1 - \text{Acquisition}\}$$

Two-dimensional nuclear Overhauser enhancement (2D NOE) experiment -

A 2D technique for obtaining, in the f_1 domain, correlation between protons which couple via dipolar interactions. This is analogous to the NOE studies used in 1D NMR. The pulse sequence used is

$$\{90^\circ - t_1 - 90^\circ - \tau_m - 90^\circ - \text{Acquisiton}\}$$

where τ_m is the mixing period

Transposition -

A operation which "exchanges" the rows and columns of a data matrix. In 2D NMR experiments, real and imaginary components are transposed independently.

J spectrum or partial J spectrum -

A spectrum which contains only coupling constant information, eg. the projection of the whole 2D J spectrum onto the f_1 axis, is a J spectrum, and a partial J spectrum corresponds to one which contains signals corresponding to a single multiplet.

PUBLICATIONS

1. Forrest,T.P., Sukumar,S. Can. J. Chem. (1977) 55, 3686:

   "A comparison of Substituent Effects on Vicinal Proton-Proton and Carbon-Proton Coupling Constants".

2. Hall,L.D., Sukumar,S., Sullivan,G.R. J. Chem. Soc., Chem. Commun. (1979) 293:

   "Two-dimensional J Spectroscopy: ^{1}H NMR Spectra of Mono- and Di-saccharides".

3. Hall,L.D., Sukumar,S. J. Amer. Chem. Soc. (1979) 101, 3120:

   "Applications of Homonuclear Two-dimensional J Spectroscopy:an alternative to Heteronuclear and Homonuclear Decoupling".

4. Hall,L.D., Sukumar,S. Carbohydr. Res. (1979) 74, C1:

   "Nulling of residual-solvent resonance during proton Two-dimensional J NMR experiments:Uridine in water".

5. Hall,L.D., Morris,G.A., Sukumar,S. Carbohydr. Res. (1979) 76, C7:

   "Resolution of complex, proton-N.M.R. spectra of Carbohydrate derivatives by using "Tilted" Two-dimensional J spectra".

6. Hall,L.D., Morris,G.A., Sukumar,S. J. Amer. Chem. Soc. (1980) 102, 1745:

   "Resolution and Assignment of the 270-MHz Proton Spectrum of Cellobiose by Homo- and Heteronuclear Two-dimensional NMR".

7. Hall,L.D., Sukumar,S. J. Magn. Reson. (1980) 38, 559:

   "Applications of Absorption-mode Spin-Echo Spectra".

8. Hall,L.D., Sukumar,S. J. Magn. Reson. (1980) 38, 555:

   "Phase-Sensitive Displays for Proton 2D J Spectra".

9. Hall,L.D., Sukumar,S. J. Magn. Reson. (1980) 40, 405:

   "A versatile strategy for the Generalised Acquisition of Proton Spin-Echo Data:Measurement of Partially relaxed Two-dimentional J Spectra".

10. Hall,L.D., Sanders,J.K.M., Sukumar,S. J. Chem. Soc., Chem. Commun. (1980) 366:

    "Measurement of Vicinal and Geminal Proton Coupling Constants of Steroids using Proton Two-dimensional J Spectroscopy".

11. Hall,L.D., Sukumar,S. Relaxation Times, (1980) 1, 3:

    "Two-dimensional NMR for the Practising Chemist".

12. Pouzard,G. Sukumar,S. Hall,L.D. J. Amer. Chem. Soc. (1981), in press:

    "High Resolution Zero-Quantum Transition (Two-dimensional) NMR Spectroscopy: Spectral Analysis".